Experimental and Analytical Investigations into Fretting Fatigue

A thesis submitted to the Department of Engineering Science of the University of Oxford as partial fulfilment of the requirements for the degree of Doctor of Philosophy

by

James Truelove

St Hilda's College
Oxford

Trinity Term, 2023

Acknowledgements

Firstly, I would like to thank David Hills and Luke Blades for their supervision and support throughout this DPhil.

I would like to thank Rolls Royce and ESPRC for their award of iCASE ref 17000027, which allowed me to perform this work.

Finally, I would like to thank my friends and family for their help and support throughout my time as a postgraduate student.

Abstract

Fretting fatigue is a damage process that occurs in contacts subjected to oscillatory loading. It is complex and involves many processes such as wear and slip: predicting the life of fretting contacts analytically is challenging. One of the primary methods of achieving this, therefore, remains experimental investigation.

In this thesis, several pieces of research are presented that contribute towards the overall aim of improving methods available to design fretting fatigue experiments. The ultimate objectives are that future experiments better match prototypical contacts, and also allow experimental investigation of the fundamental causes of fretting fatigue.

The first paper examines whether the stress fields at the edge of a fretting contact has similarities with the stresses present at a crack tip, as has been suggested in earlier literature. It is shown that they do not, implying that it would not be appropriate to model fretting fatigue as a crack turning problem.

Two papers focus on the effect of moments in fretting fatigue experiments. It is shown that significant moments can occur due to the design of test apparatus. Then, a method of finding equivalence between normal and moment loadings is derived and applied to remove the effect of coupled moments.

A series of experiments using single crystal pads were performed, with the goal of investigating a previously identified trend in fretting fatigue life. This was motivated by an experimental study previously reported that indicated an effect but considered too few specimens to be regarded as conclusive. In the current work, it is shown that there is no evidence for orientation of the crystal structure affecting the life of the contact.

Several papers are then presented that cover the effect of load path on the behaviour of a fretting contact, in which it is demonstrated that it is possible to design experiments to investigate novel behaviours, such as slipping in only one direction. These allow for future investigation of the fundamental causes of fretting fatigue damage.

The work presented provides several methods of improving the design of fretting fatigue experiments. Also discussed are potential avenues for follow up work, such as the design of further load paths to investigate other properties of the fretting contact.

Contents

1 Introduction **1**

2 Literature Review **5**

2.1 Contact Fundamentals 5

2.2 Tangential Loading 6

2.3 Asymptotic Methods 7

2.4 The Effect of Crystal Orientation in Fretting Fatigue Experiments 8

3 Plasticity and the Crack Analogy **10**

4 Measurement of Moment Coupling in Fretting Fatigue Experiments **28**

5 Moment–Normal Load Equivalence **36**

6 Fretting Fatigue Experiments with Single Crystal Pads **44**

7 The Effect of Load Path Under P-Q Loading **58**

8 The Effect of Load Path Under P-Sigma Loading **76**

9 The State of Stress Under P-Sigma Loading **100**

10 Future Work **130**

10.1 Design of Additional Load Paths 130

10.2 Finding the Shear Traction Solution Under Conditions of Full Stick 131

11 Conclusion **134**

1 Introduction

Fretting fatigue is a damage and failure process that occurs in contacts subject to oscillatory tangential loading. Understanding the causes of fretting fatigue is essential in order to predict accurately the failure of components and ensure the safety of engineered assemblies across a range of industries. Predicting the life of fretting components and modelling their behaviour is a complex problem involving a number of processes, such as wear, slip and fatigue, which is currently poorly understood.

Given the great difficulty in predicting the life of these contacts from an analytical model and the number of properties involved, one of the primary ways of predicting the fretting fatigue life of components is through experimental investigation. These experiments are typically based around matching the contact geometry and loads from a prototypical component to a much simpler test specimen, such as a pair of profiled pads in contact with a standard fatigue dog bone. This style of component testing has proven valuable for predicting the life of contacts in real components, but it limits the possibility of investigating the fundamental causes of fretting fatigue.

One industry in which fretting fatigue failures present a major problem is aerospace, specifically the manufacture and maintenance of turbofan engines. Turbofan engines have multiple stages, consisting of a fan, a compressor and a turbine, with each stage of the engine often subdivided into several substages based on the pressure of the gasses passing through them. Each stage of the engine is constructed from blades attached to a central disk; while in some sections of the engine these are combined into a single component (called a "blisk"), in many regions the blades and the central disk are separate components, with the blades being removable to aid maintenance and construction of the engine. Two main forms of attachment are typically used: a simpler dovetail arrangement, and a more complex, multi contact "fir tree" design.

When the engine is running, a number of forces act upon the blades, causing them to fret and in turn experience damage. As the engine speed varies during flight, the centripetal force acting upon blades changes, due to the angled contact surfaces this can cause the blades to slide. Gasses passing over the fan blades inside the engine impart forces upon them, which can result in the blades vibrating. In some situations, the blades can experience additional loading arising from abnormal engine conditions, such as the tips of the blades rubbing on the abradable liner inside the engine, or during bird strike events.

Fretting fatigue cracks initiating at the blade contacts can grow through both the fan blades and the central hub; once these cracks reach a critical length they can cause the fan blades to detach, often called a "blade off event". A crack growing through an individual blade will typically

cause one blade to detach, in this situation the engine housing is designed to be able to contain the debris. In contrast if a crack grows through the central hub of the engine several blades can detach simultaneously, which can lead to catastrophic failure of the engine.

For reasons of weight it is often not possible to design engines so that fretting fatigue does not occur, and in some engine designs fretting of the blades is seen as beneficial, as it helps dampen vibration via frictional damping. In order guard against component failures an inspection and replacement regime is therefore implemented, wherein engines are disassembled for maintenance at predetermined intervals. Performing these inspections represents a significant expense, so being able to maximise the life of the contacts is of paramount importance.

Subsea oil and gas extraction is another industry where fretting fatigue failures represent a serious risk and design consideration. Subsea oil wells are typically fitted with short pipe stubs, with serrated ends. When it is necessary to attach equipment to the pipe in order to operate the well a segmented ring with serrations to match the pipe is clamped onto the pipe serrations with hydraulic pressure. When an oil rig is connected to the pipe a massive amount of force can be applied to the connection, due to the length of pipe acting as a lever arm. The action of the waves on the attached equipment results in oscillatory loading, causing the contact to fret.

The growth of fretting cracks from these contacts represents a serious environmental risk, if such cracks are allowed to propagate through the wall of the pipe an oil spill will result. Being able to optimise the applied clamping force and being able to accurately predict the life of the component are therefore essential.

This thesis covers a range of work related to experimental investigation into fretting fatigue and some analysis supporting such experiments. This includes modelling of fretting fatigue experiments involving significant amounts of plasticity, measuring and modelling the effect of a moment on a fretting fatigue test, performing a set of tests investigating the effect of crystal orientation in single crystal pads on fretting fatigue life, and studying the effect of load path on fretting fatigue experiments.

The first paper, 'A Comparison of the State of Stress at an Incomplete Fretting Contact Edge with a Crack Tip', discusses the modelling of fretting fatigue experiments with a significant amount of plasticity. The experiments were designed to investigate the fretting fatigue failure of sub sea oil pipeline connectors; an application in which the contacts are subjected to very high loading. These loads result in a large region of plasticity at the contact edge, so standard analysis methods based elastic models were not applicable. Instead, a speculation that the initiation of cracks at the edge of contacts can be modelled as a crack turning or crack branching problem is investigated as a possible alternative.

The next two papers, 'Measurement of Moment Coupling in Fretting Fatigue Experiments' and 'Flat and rounded contacts - modelling the effect of a moment with application to fretting fatigue tests', investigate the effect of moments in fretting fatigue experiments, specifically those using contacts with a 'flat and rounded' geometry. The first of these papers covers moment coupling effects, the generation of a moment when shear force is applied due to the design of the test apparatus resulting in the shear force support being in a different plane to the point where the shear force is applied. Within this paper a method of measuring the magnitude of the moment coupling is derived, and the effect of the moment on the contact problem is discussed.

The second of these papers describes a method for deriving equivalent pairs of pressure-moment loading: varying the normal load applied to the contact in order to simulate the effect of a moment. This has a number of applications; it is possible to remove the effect of a coupled moment in a rig where they are present, but it is also possible to simulate the effect of a moment present in a prototype contact on a test rig that does not have independent moment control. The expressions derived are very simple and apply with a good degree of accuracy over a wide range of loading conditions and contact geometries, making them ideal for direct integration into test load calculations or test design.

The next paper, 'Fretting Fatigue Experiments with Single Crystal Pads', describes a series of experiments designed to investigate the effect of crystal orientation in single crystal pads on the life of fretting contacts. Previous experiments performed at the University of Oxford have indicated that the crystal orientation in the pads plays a dominant role in determining the life of the contact. These previous experiments had a number of shortcomings, however, as the effect of crystal orientation was not the main feature being investigated – in one case the main aim of the experiments was to investigate the effect of changing the contact geometry. In another test program the experiments were investigating the effect of varying load ranges at high temperatures. This makes it difficult to isolate the effect of the crystal orientation from the results, as there are very few pairs of tests that are directly comparable. The experiments described in the paper, here, were therefore designed to isolate the effect of the crystal orientation. Approximately 100 tests were performed, split into two sets, with each set of tests having the crystal structure oriented in a different axis. The contact geometry, loads and material treatment were kept constant so that the only thing varying between tests was the crystal orientation, allowing its effect to be isolated.

The final three papers of this thesis, 'Half-Plane Contact Problems in partial Slip with varying Normal and Tangential Loads', 'Frictional Half Plane Contacts Subject to Varying Normal Load and Bulk Tension Under Various Load Paths with Application to Fretting Fatigue Experiments' and 'The State of Stress in Fretting Contacts Under Varying Load Paths', concern the design of

fretting fatigue experiments using different load paths. The first of these papers focuses on contacts loaded with a combination of normal and shear forces, while the latter focuses on contacts loaded with normal forces and bulk tensions, in each case under varying normal load. While contacts loaded with shear forces are easier to analyse they have a number of disadvantages when used experimentally: there is the risk of a contact sliding if the applied shear force reaches the coefficient of friction multiplied by the normal load, the application of shear forces can result in moment coupling, as discussed in previous papers, and lastly, in order to detect the presence of damage bulk tension variation is required in order to propagate cracks to a length where they may be observed.

The load paths derived in this work have a number of novel features that allow for analysis of the fundamental causes of fretting fatigue. By changing the order in which loads are applied (and therefore the path through load space) it is shown how it is possible to create experiments where the contact moves between the same force states, but where the slip behaviour of the contact differs. These ideas can be applied to create load paths moving between the same points in load space where some experience no slip, others experience reversing slip with various sizes of slip zones and some allow the possibility of imposing slip in only one direction. Performing experiments using combinations of these load paths therefore allows for detailed investigation of the effect of slip on fretting fatigue life. The surface traction distributions, state of stress in both bodies, slip displacements and energy dissipated in slip are found and compared for a variety of load paths, and it is shown how, by careful design of the experiment, the influence of each may be isolated and studied.

2 Literature Review

2.1 Contact Fundamentals

Contacts in engineered assemblies can be categorized into one of a number of groups, based on their behaviour under loading. Three of the most common types of contacts encountered in engineering are complete, incomplete and receding contacts [1], with incomplete contacts often further subdivided into conformal and non-conformal types.

The main feature of a complete contact is that the size of the contact is defined by the geometry of the contact and is independent of the applied load. An example of this type of contact would be a square block placed on a half plane - regardless of the applied normal load the contact extent is given by the size of the block.

For an incomplete contact the size of the contact is determined by both the geometry and the applied load; The contact will grow larger as more normal load is applied. If the two contacting bodies have curvature in the same direction the resulting contact is said to be conformal. An example of a contact of this type is a pin loosely located in a circular hole. If the two contacting bodies have curvature in the opposite direction they are said to be non-conformal, an example is contact between two spheres.

The final class of contact to note is receding contacts. These have the property that as the normal load applied increases the contact area gets smaller or remains at a fixed size, as it does in an incomplete contact. These contacts occur very frequently in engineering, an example would be a thin sheet placed onto a half plane and loaded with a point load or a line load - as load is applied the plate will curve, leaving only a small region of contact around the load. Bolted connections also behave in this manner, such as those found in pipe flanges.

The majority of contacts used in fretting fatigue experiments are of the incomplete type, normally having either a cylindrical or 'flat and rounded' geometry. The first detailed study of contacts of this type was performed by Hertz [2], who was interested in studying the optical properties of stacked lenses. In this pioneering work it was assumed that both contacting bodies could be modelled as semi-infinite spaces, with second order polynomial geometry representing the curvature of the contact.

A major advancement in the study of contact problems was the work of Flamant [3], who adapted the solution for a point load in a half space by Boussinesq [4] to find the stress and displacement solution for a wedge loaded with a normal and tangential force at its tip. By making the wedge angle equal to 180 degrees this solution can be used to study the problem of a line load on a half plane, a solution which, via superposition, can be used to study problems involving

distributed contact pressure, a framework known as 'half plane theory'.

While half plane theory allows for analysis of many contact problems the integral equations that it produces are often difficult to solve. A number of alternative formulations have therefore been derived, one such example being the work by Mossakovskii [5]. In this analysis the contact geometry is represented by a series of sharp ended punches, which makes the resulting integral easier to handle. Recent work by Moore et al has extended this method to handle problems where a moment is also present, leading to asymmetry of the contact, but only for the case where both edges of the contact are advancing [6].

2.2 Tangential Loading

In fretting fatigue problems it is essential to be able to find the shear traction behaviour of the contact in order to characterise fully the state of stress and slip behaviour of the problem. There are generally two approaches that can be taken in solving the tangential problem: either (a) the contact can be allowed to slide fully then a corrective term added to restore the stick behaviour in the stick zone, or (b) the contact can be solved under conditions of full stick then a distribution of dislocations added to allow for slip and redistribute shear tractions so that at no point in the contact is the friction law exceeded.

The first method, finding the fully sliding shear traction and adding a corrective term over the slip zone, was the method used in early studies. The partial slip behaviour of sequentially loaded contacts when under a shear force loading was first studied by Cattaneo [7], who showed that the shear traction for a cylindrical contact was simply given by the superposition of the full sliding shear traction distribution with a scaled and inverted copy of the same traction. This solution was found independently by Mindlin [8], who expanded the solution to include a study of the effect of loading history. The final advancement was the simultaneous discovery by Ciavarella [9] and Jager [10] that the Cattaneo-Mindlin solution was applicable to any incomplete contact geometry, not just cylindrical contacts, a principle known as the Ciavarella-Jager Theorem.

In many situations a contact will not be sequentially loaded, and will instead be subject to a much more complex loading history. In many cases the loading will be driven by some cyclic process, and as such will be oscillatory in nature. The problem of a contact being loaded by an out of phase sinusoidal normal and shear force (such that the path through load space forms an eclipse) was studied by Barber et al [11], who demonstrated how the solution can be constructed via superposition of copies of the Cattaneo-Mindlin solution with various load components. The solution for a contact loaded along a straight line between two points in load space, a common load path used in experiments, is simply the case where the phase difference between the load

components is zero, as discussed in Fleury et al [12].

In addition to exciting shear tractions by shear loads, it is also possible to create a shear traction by applying a differential bulk tension to the components. The solution to a sequentially loaded contact under this loading was first studied by Nowell and Hills [13], who solved the problem numerically and identified two distinct regions to the solution. For small amounts of bulk tension (when both slip zones are in the same direction) the problem can be solved in closed form, with the effect of the bulk tension being to introduce an 'eccentricity' into the Cattaneo-Mindlin solution. For larger amounts of bulk tension the direction of slip is different at each end of the contact.

The problem of a Hertzian contact loaded sequentially with normal load and bulk tension was solved in closed form by Ciavarella and Macina [14], and Navarro, Mugadu, Hills and Dominguez [15]. Ramesh and Barber [16] studied a Hertzian contact following an elliptical load path in P, σ space by generalising these results to cover contacts following any load path. This was done by demonstrating that a contact following an arbitrary load path where during part of the load path the contact is stuck and during another part he contact slips is equivalent to the same contact following the original load path until the size of the contact reaches the size of the permanent stick zone, followed by a sequential loading. The load paths are equivalent as the slip in the latter parts of the loading history completely erases any locked in tangential displacements from the fully stuck part of the load history that were present in the region that becomes the slip zones. The first part of the load path therefore creates the distribution of surface displacements that should be present in the sick zone, and the sequential loading represents the simplest load path that creates appropriately sized slip zones, as no knowledge of the load path is maintained in this portion of the contact.

Another method of finding the distribution of shear traction is via superposition of shear loaded flat punches, a method used by Mossakovskii [5] Spence [17] and Jager [10]. This method can be further extended to cover contacts loaded with a bulk tension and a moment, at least for the case where both contact edges are advancing, covered in the work by Hills [18].

2.3 Asymptotic Methods

The use of asymptotes is a well established principle in fracture mechanics and fatigue. The pioneering paper in this area was the work of Williams [19], whose now famous solution studied the stress fields around the tip of a notch through the use singular stress fields. By letting the wedge angle equal 180 degrees this solution can be applied to the study of crack problems, it being possible to describe the state of stress around the crack tip as a function of two stress intensity factors, K_I and K_{II}. The concept of finding a critical stress intensity factor (ΔK_{th}), along with

models such as Paris' law, are common methods of predicting plain fatigue life of engineering components.

The edge of a complete contact, where a square ended body indents upon another, has obvious geometric similarities with a sharp cornered notch, and so it is sensible to ask if it is possible to use the William's solution to describe the stress field adjacent to the contact edge. Dundurs [20] treated the frictionless problem, while Comninou [21] found solutions for the problem with friction, demonstrating that in both cases analogies do indeed exist. The applicability of these results to fretting fatigue experiments was considered by Mugadu et al [22], who studied the behaviour of the contact when subject to reciprocating shear load.

For an incomplete contact the question of representation by asymptotes is complicated by the fact that, while the shear traction remains singular under conditions of full stick, the contact pressure is bounded, and instead drops smoothly to zero. Dini and Hills [23] therefore suggested that an appropriate asymptotic representation of an incomplete contact could consist of a square root bounded pressure asymptote combined with a square root singular shear traction asymptote, work that was further expanded upon in a paper by Dini et al [24] to cover the case of reciprocating loads and frictional shakedown. Using asymptotes to represent the stress field is attractive for a number of reasons, principal among them that it allows the state of stress to be collapsed down to two variables, the square root singular shear multiplier (K_{II}) and the square root bounded pressure multiplier (L_I), regardless of the loads that are applied or the geometry of the contact.

The strong resemblance between the stress fields for complete contacts and those for a sharp notch led to suggestions that similar analogies existed for incomplete contacts. This 'crack analogy' was first proposed in a pair of papers by Giannakopolos et al [25, 26], in which he drew analogies between the state of stress at the edge of a flat and rounded punch, and those at the edge of a blunted crack. The concept of there being crack like behaviour at the edge of contacts has since been significantly expanded upon by numerous other researchers: Chambon and Journet [27] proposed a way of modelling the entire growth process of a fretting crack purely within a linear elastic fracture mechanics framework, by treating the problem as 3 stages of crack growth. Firstly the initiation of a crack due to the contact loads, secondly the growth of the crack under the influence of the contact loads and thirdly the crack growing under the influence of the bulk tension.

2.4 The Effect of Crystal Orientation in Fretting Fatigue Experiments

A unique feature of the contacts that occur in the root of gas turbines is that they involve the contact of single crystal material with polycrystaline material. In many turbines the blades are

cast as a single crystal, while the hub is a polycrystaline forging.

When single crystal materials are considered in the context of a fretting contact there are two distinct paths a crack could take; the crack can grow through the single crystal material, or the crack can grow through the polycrystalline contacting body. In a turbojet engine these would correspond to the crack growing through a blade of the engine and a crack growing through the hub of an engine. These correspond to the cases of a crack growing through the single crystal and polycrystalline material respectively.

One of the first experimental investigations into the effects of crystal orientation on crack initiation in polycrystalline material was performed unintentionally by Sarsfield [28], who was attempting to investigate the effects of switching from flat and rounded contacts to Hertzian contacts in the context of turbojet engines. The results were surprising, in that the amount of scatter in the results was so large as to mask completely any variation due to the swap from flat and rounded to Hertzian.

As part of his DPhil studies [29] Fleury investigated the cause of this variance. A conical indenter was used to measure the angle of the crystal structure in each pad, following the method devised by Huang et al [30], and the average crystal angle was plotted against cycles to failure. It was found that the results suggest an unexpectedly strong relationship between the crystal orientation and the fretting fatigue life of the contact, but these results should be taken with caution, both due to the extremely small sample size (6 tests) and the fact that the angle is averaged, a process that may not be appropriate for tests where the crystal orientation is notably different in each pad.

A further set of tests was later performed by Fleury and Paynter [31], in which the pads were matched before the tests, to ensure that the crystals were in a reasonably close orientation. Once again the results suggest that the fretting fatigue life of the contact depends upon the angle of the crystal, but since these experiments were performed at high temperature and under different loads it is almost impossible to separate out the effect of the orientation from the loading. As part of the work a series of finite element models were created, incorporating anisotropic behaviour, in order to study what effect the rotation of the crystal would have on the contact solution. It was shown that for a 2D plane model the changes due to the rotation are small, of the order less than 10%.

3 Plasticity and the Crack Analogy

The paper presented in this chapter has been published as: *Truelove, J. P. J., & Hills, D. A. (2021). A comparison of the state of stress at an incomplete fretting contact edge with a crack tip. Tribology International, 153, 106643.*

Analysis of fretting fatigue experiments is typically based on fully elastic models, any regions of plasticity are assumed to be small compared to the geometric features of the test and any other process zones and properties of the contact, such as the frictional slip zone size.

More recently a series of tests have been performed modelling the contacts present in sub-sea oil riser connections. These contacts are subjected to extremely heavy loading due to the combined action of a static force from the hydraulic clamping assembly and a cyclic loading arising from the motion of the oil platform. It was found that attempting to apply typical methods of fretting fatigue life prediction and fitting such as those based on asymptotic matching methods produced extremely poor agreement with the observed life.

It was known that when using a standard design of dogbone specimen the loads applied during the test were high enough that plastic collapse of the specimen would have occurred. The specimens were redesigned to use a thin and tall dogbone in order to add additional distance between the two contact patches and prevent complete failure of the test specimen, however even with these modifications a significant amount of plasticity was present within the contact region during the tests.

An initial investigation based on violations of the yield condition along the contact interface indicated that the plastic zones in these contacts would have been much larger than the frictional slip zones, a condition not previously seen in tests in the Oxford fretting fatigue laboratory.

In order to model the life of these contacts a new approach capable of handling plasticity was therefore required. One possibility that has been floated around the literature regards the idea of a 'crack analogue', the idea that similarities exist between the state of stress at the edge of a contact and those in a shear loaded crack. If these analogues can be shown to hold true for the problem under consideration then prediction of the life of the contact can be treated as a crack branching or crack turning problem and standard crack growth methods applied.

A Comparison of the State of Stress at an Incomplete Fretting Contact Edge with a Crack Tip

J P J Truelove and D A Hills

Department of Engineering Science, University of Oxford, Parks Road, OXFORD OX1 3PJ UK

Abstract

The similarity in implied process zones, based on violations of the plastic yield condition, between the state of stress at the edge of an incomplete contact subject to reciprocating shear and tension and a crack suffering pure mode II loading are compared. This is done for both small and large amounts of edge slip, i.e. when the frictional slip region is either enveloped by the plastic region or envelops it. The results show that for realistic coefficients of friction strong agreement is unlikely to occur, so that attempting to analyse the nucleation of fretting cracks as a form of crack branching/turning is inappropriate and the effect of normal load on crack nucleation is an important consideration.

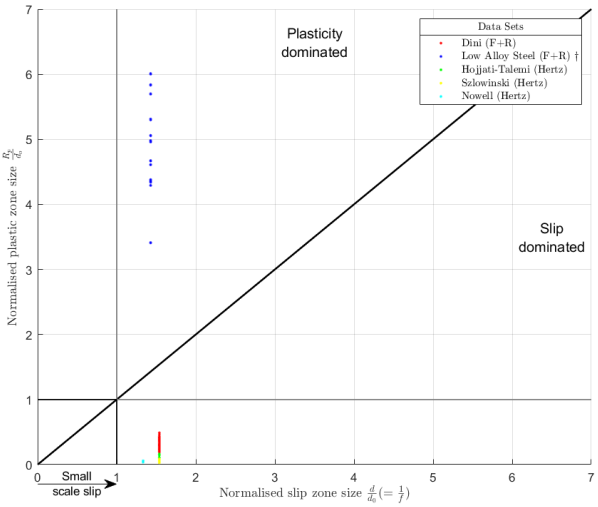


Figure 1: In this paper we demonstrate that in order for the contact edge to behave like a crack tip we require both the slip zone size, d, and the plastic radius, r_p, to be smaller than the internal length scale of the asymptote, d_0. In the figure above results for a range of tests are plotted, showing that while the plastic radius falls within the region $r_p < d_0$ for the majority of tests, there are no tests where the slip zone falls within the region $d < d_0$.

Preprint submitted to Elsevier

Keywords: Contact Mechanics, Fretting, Plastic

Nomenclature

σ_0 Bulk tension

σ_y Yield stress

a Contact half width

d Slip zone size

d_0 Internal length scale of the asymptotic stress fields

f Coefficient of friction

K_{II} Mode II stress intensity factor

L_I Asymptotic multiplier for square root bounded pressure field

L_{II} Asymptotic multiplier for square root bounded shear field

P Normal force applied to contact

Q Shear force applied to contact

r, θ Polar coordinates

r_p Plastic radius

s Distance along the line of contact, measured from the edge

x, y Cartesian coordinates

1. Introduction

Fretting fatigue is a material damage phenomenon that occurs when two bodies in contact are subjected to reciprocating shear loading. The prediction of fretting fatigue life is of great importance to a number of industries, and as such creating a model of fretting fatigue damage that encapsulates the major contributing factors has been a subject of much academic interest for a number of years. Some, such as the theory of critical distances [Zabala et al, 2020] focus on finding the state of stress in a region surrounding the edge of the fretting contact, but one model that has been the subject of much interest for many years is the "crack analogue" concept, as discussed in [Chambon and Journet, 2006], which uses concepts from linear elastic fracture mechanics to treat the growth of cracks from the edge of a contact as a crack turning or crack branching phenomenon.

In a very prescient paper published more than twenty years ago, Giannkokpoulos, [1998] argued that there was a strong equivalence between the state of stress adjacent to a contact edge and that present at a crack tip. The paper was very thought-provoking, but it was not immediately apparent whether the authors intended these ideas to be used where the contact under consideration was in the form of a flat-faced rigid punch, or whether they were to be applied to incomplete contacts. In fact, the rigid punch comparison produces only a true match of asymptotic stress fields with a crack tip if the counterbody is incompressible, whereas if the contacting bodies are made from the same material but are convex so that the resulting contact is incomplete, perhaps surprisingly the analogy may potentially be stronger. We say 'surprising' because, at the edges of incomplete contacts, the contact pressure must fall smoothly to zero, and hence the attendant shear traction is limited by friction and so it, too, must also fall to zero. Therefore one might expect the comparison with the singular field at a sharp crack tip to be poor, but this is not necessarily so.

Imagine, first, that the coefficient of friction between the bodies is extremely high, sufficient to prevent all slip, Figure 2, so that when a shear force is applied the local state of stress is necessarily square root singular. If each body is capable of being idealised as a half-plane, the spatial distribution of stress is exactly the same as a mode II crack field. The stress concentration adjacent to contact edges may be relieved by either frictional slip or plastic slip. When it is the latter then there will be a whole area (in two dimensions) of plasticity which will straddle the contact interface.

We might wish to analyse the possibilities of frictional and plastic slip separately, and to start off in an approximate way, simply by considering violations of the frictional law (assuming the pair of bodies to be stuck everywhere) and the yield condition (assuming the material to be infinitely elastic). We do not expect there to be gross plasticity, but cyclic plasticity on a small scale with attendant irreversibilities which give rise to material degradation and the nucleation of cracks. If we have a weak material and strong friction we might expect the frictional slip zone to be buried well within the plastic zone, and therefore for the contact edge to behave as a monolithic notch. If the problem is one of a half-plane (convex) contact the notch becomes a crack, albeit one where the normal dominant eigensolution is square root bounded but, more importantly, the reversing mode II solution is symmetrical and, as stated earlier, the same as that at a crack tip. Nucleation of cracks from this region - small scale slip - becomes one of crack branching - the branch being a conventional opening mode I . On the other hand if the material is strong and the coefficient of friction weak the slip zone will be bigger than the implied plastic zone and, indeed, the process zone may be significantly smeared out or modified by slip. This, then, would truly be a fretting generated crack whereas the small-slip problem becomes one of branching of an existing crack.

This paper provides an objective comparison between the plastic slip zone shape and size at a contact edge and that at a crack tip, and looks at the former with and without frictional slip.

2. Implied Plastic Zone size and Shape

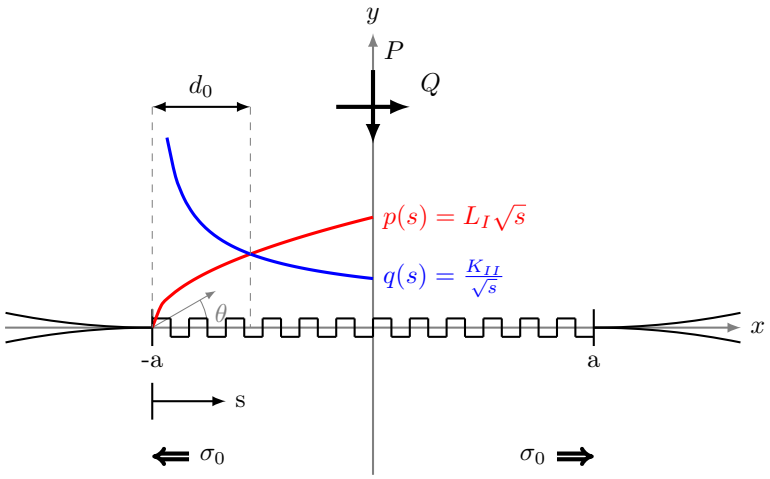


Figure 2: A diagram of the geometry for the fully stuck case showing loads and local stress asymptotes

If we have an incomplete contact between two elastically similar bodies of half width a, the shear stress, $q(x)$, along the contact interface induced by a shear force, Q, and a tension in one body of magnitude σ_0 is given by

$$q(x) = \frac{Q}{\pi\sqrt{a^2 - x^2}} \pm \frac{\sigma_0 x}{4\sqrt{a^2 - x^2}} \tag{1}$$

when all slip is prohibited. We may write down the local state of stress at the contact edge in the form

$$q(s) = \frac{K_{II}}{\sqrt{s}}, \tag{2}$$

where s is a coordinate measured inwards from the contact edge and

$$K_{II} = \frac{Q}{\pi\sqrt{2a}} + \frac{\sigma_0}{4}\sqrt{\frac{a}{2}}. \tag{3}$$

Similarly, the normal load induces a contact pressure, $p(s)$, which falls smoothly to zero at the contact edge in a square root bounded manner, i.e.

$$p(s) = L_I\sqrt{s} \tag{4}$$

where L_I is a geometry-dependent multiplier and is given by, for example

$$L_I = \frac{P}{\pi}\sqrt{\frac{8}{a^3}} \tag{5}$$

where P is the normal load, for a Hertzian contact [Hills, et al 2016].

The mode II crack tip stress field is given by (note that these equations differ by a factor of $\sqrt{2\pi}$ from the standard crack tip solutions because we don't include that factor in our definitions of the stress intensity factor)

$$\left\{ \begin{array}{c} \sigma_{rr} \\ \sigma_{\theta\theta} \\ \sigma_{r\theta} \end{array} \right\} = \frac{K_{II}}{\sqrt{r}} \left\{ \begin{array}{c} -\frac{5}{4}sin\frac{\theta}{2} + \frac{3}{4}sin\frac{3\theta}{2} \\ -\frac{3}{4}sin\frac{\theta}{2} - \frac{3}{4}sin\frac{3\theta}{2} \\ \frac{1}{4}cos\frac{\theta}{2} + \frac{3}{4}cos\frac{3\theta}{2} \end{array} \right\} \tag{6}$$

and the stress field from a L_I bounded asymptote is given by [Nils Cwiekala, Private conversation]

$$\left\{ \begin{array}{c} \sigma_{rr} \\ \sigma_{\theta\theta} \\ \sigma_{r\theta} \end{array} \right\} = L_I\sqrt{r} \left\{ \begin{array}{c} -\frac{3}{4}cos\frac{\theta}{2} - \frac{1}{4}cos\frac{5\theta}{2} \\ -\frac{5}{4}cos\frac{\theta}{2} + \frac{1}{4}cos\frac{5\theta}{2} \\ -\frac{1}{4}sin\frac{\theta}{2} + \frac{1}{4}sin\frac{5\theta}{2} \end{array} \right\} \tag{7}$$

where in plane strain

$$\sigma_{zz} = \nu\left(\sigma_{rr} + \sigma_{\theta\theta}\right) \tag{8}$$

so that Von Mises' criterion is

$$2\sigma_y^2 = \left(\sigma_{rr} - \sigma_{\theta\theta}\right)^2 + \left(\sigma_{\theta\theta} - \sigma_{zz}\right)^2 + \left(\sigma_{zz} - \sigma_{rr}\right)^2 + 6\sigma_{r\theta}^2. \tag{9}$$

Considering the effect of just the K_{II} loading we can write that along the line $\theta = 0$, which is both the possible line of frictional slip and the line along which the plastic front, $r_p\left(\theta\right)$, extends furthest,

$$\frac{2r_p\left(0\right)\sigma_y^2}{K_{II}^2} = 6 \tag{10}$$

independent of the transverse constraint, because a state of pure shear exists. Under oscillatory loading of magnitude ΔK_{II} shakedown will reduce the implied size of the shear stress by a factor of 4 (or we might think of this as replacing σ_y by $2\sigma_y$ to give the range of stress which might be accommodated), to give, in the steady state

$$r_p(0) = \frac{3}{4}\left(\frac{\Delta K_{II}}{\sigma_y}\right)^2, \tag{11}$$

which is indicative of the size of the plastic slip zone, but we also wish to examine its shape. If we have just mode II loading of either the contact edge or the crack tip it is straightforward to include information about the size of the implied plastic zone, which is self similar, and this is addressed in many undergraduate textbooks. Re-write equation (6) in the contracted form

$$\sigma_{ij}\left(r,\theta\right) = \frac{K_{II}}{\sqrt{r}} f_{ij}^{II}\left(\theta\right) \tag{12}$$

and so

$$2r_p(\theta)\left(\frac{\sigma_y}{K_{II}}\right)^2 = \left(f_{rr}^{II}(\theta) - f_{\theta\theta}^{II}(\theta)\right)^2 + \left(f_{\theta\theta}^{II}(\theta) - f_{zz}^{II}(\theta)\right)^2 + \left(f_{zz}^{II}(\theta) - f_{rr}^{II}(\theta)\right)^2 + 6f_{r\theta}^{II2}, \quad (13)$$

from which we may easily plot the shape of the normalised plastic zone. But the problem is more subtle if we have, also, a bounded pressure field present and so, in lieu of (12), the state of stress is given by

$$\sigma_{ij}(r,\theta) = \frac{K_{II}}{\sqrt{r}} f_{ij}^{II}(\theta) + L_I \sqrt{r} g_{ij}^{I}(\theta), \quad (14)$$

but we know that $K_{II}[FL^{-3/2}]$ and $L_I\left[FL^{-5/2}\right]$ so can bring out the internal length dimension, say d_0, by writing

$$d_0 = \left(\frac{K_{II}}{L_I}\right) \quad (15)$$

and so if we take equation (14) and divide through by $\sqrt{K_{II}L_I}\left[FL^{-2}\right]$ we see it may be re-written in the form

$$\frac{\sigma_{ij}(r,\theta)}{\sqrt{K_{II}L_I}} = \sqrt{\frac{d_0}{r}} f_{ij}^{II}(\theta) + \sqrt{\frac{r}{d_0}} g_{ij}^{I}(\theta). \quad (16)$$

This is an extremely convenient form for the solution because it separates out the effect of the magnitude of the load $\left(\sqrt{K_{II}L_I}\right)$ and the internal length scale, d_0. The expression for the plastic radius is now very much more complicated, but is capable of being written down in terms of a single parameter. Let

$$h_{ij}\left(\theta; \frac{r}{d_0}\right) = \sqrt{\frac{d_0}{r}} f_{ii}^{II}(\theta) + \sqrt{\frac{r}{d_0}} g_{ii}^{I}(\theta) - \sqrt{\frac{d_0}{r}} f_{jj}^{II}(\theta) - \sqrt{\frac{r}{d_0}} g_{jj}^{I}(\theta) \quad (17)$$

so that the plastic radius $r_p(\theta)/d_0$ is given by

$$2\frac{\sigma_y^2}{K_{II}L_I} = h_{r\theta}^2\left(\theta; \frac{r_p}{d_0}\right) + h_{\theta z}^2\left(\theta; \frac{r_p}{d_0}\right) + h_{zr}^2\left(\theta; \frac{r_p}{d_0}\right) + 6\left[\sqrt{\frac{d_0}{r_p}} f_{r\theta}^{II}(\theta) + \sqrt{\frac{r_p}{d_0}} g_{r\theta}^{I}(\theta)\right]^2. \quad (18)$$

3. Results - No slip comparison of implied plastic fields

The question arises 'What is a realistic choice of d_0?' and one way of answering this might be to attach the solution to a specific finite geometry, for example Hertz' problem. Substituting the calibrations for L_I, K_{II} into (15) we see that

$$\frac{d_0}{a} = \frac{Q}{4P} \quad (19)$$

Therefore, when there is no applied shear force $d_0 \to 0$ (so that the effect of the shear load vanishes, and the normal load dominates the problem). If we assume typical coefficients of friction for alloys we might expect the maximum value of Q/P to be around $1/2$ if the contact is in partial slip so that the maximum value of d_0/a is about $1/8$. Looking at the magnitude of the load we see that this is characterised by the left hand side of equation (18) and, making use of (3,5)

$$\frac{K_{II}L_I}{\sigma_y^2} = \frac{8}{\pi^2}\left(\frac{Q}{2a\sigma_y}\right)\left(\frac{P}{2a\sigma_y}\right) \tag{20}$$

In a real contact we might expect the maximum nominal contact pressure to be just about equal to the yield stress so that the right hand side of this equation, for maximum nominal shear force as above will be about $4/\pi^2$ or just under 0.5.

Contours of the position of the implied plastic front for various values of $\frac{K_{II}L_I}{\sigma_y^2}$ are plotted over normalised $\left(\frac{x}{d_0}, \frac{y}{d_0}\right)$ space in Figure 3 under conditions of plane strain with $\upsilon = 0.3$. The definition of x and y in this figure differ from those used in figure 2, the coordinate system is attached to the edge of the contact, rather than it's centre. It should be noted that there are two plastic zones present, a distorted version of the distinctive 'figure of eight' plastic zone associated with a K_{II} stress field growing outwards from $r = 0$ and a 'c' shaped plastic zone associated with an L_I stress field growing inwards from $r = \infty$, with the boundary $r = d_0$ providing a rough partition between these two zones.

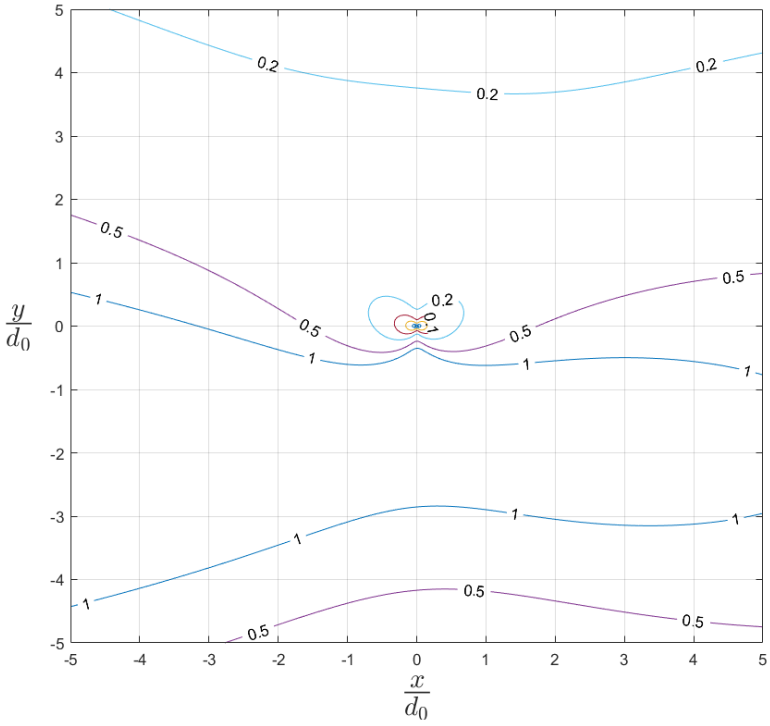


Figure 3: Contours of the implied plastic front for various values of normalised applied load $\frac{K_{II}L_I}{\sigma_y^2}$.

Figure 4 provides a plot of the implied plastic zone front shape in the region $r < d_0$, and the nearest 'pure mode II' ie. crack tip field for comparison. The latter is found in the following way: we 'open out' the polar plot and display, in Cartesian form, $r_p(\theta)$ for $-\pi < \theta < \pi$ for the contact edge. We then think of a second representation, viz. the crack tip K_{II} field, but where the magnitude of the best choice of the multiplier is initially left as a parameter whose magnitude (i.e. the multiplier $\frac{K_{II}L_I}{\sigma_y^2}$) is found by doing a least-squares fit, and where the correlation coefficient provides a rigorous measure of the proximity of the contact edge field to the crack tip field. For each pair of these contours the coefficient of determination, R^2, was calculated to ascertain the quality of the fit. These are given in table 1. The K_{II} stress field is normalised in exactly the same way as the combined $L_I + K_{II}$ stress field, and values of $\frac{K_{II}L_I}{\sigma_y^2}$ are provided for comparison.

R^2 is defined as

$$R^2 = 1 - \frac{SSR}{TSS} \tag{21}$$

where the sum of squares of the residuals is defined as

$$SSR = \sum \left[r\left(\theta_i\right) - f\left(\theta_i\right) \right]^2 \tag{22}$$

and the total sum of squares is defined as

$$TSS = \sum \left[r\left(\theta_i\right) - \bar{r} \right]^2 \tag{23}$$

in which $r\left(\theta\right)$ is the plastic radius from the $L_I + K_{II}$ stress field, $\bar{r}$ is the average plastic radius from the $L_I + K_{II}$ stress field and $f\left(\theta\right)$ is the plastic radius from the best fitted pure K_{II} stress field. An R^2 value of 1 implies a perfect fit between the $L_I + K_{II}$ plastic zone and the pure K_{II} plastic zone, an R^2 value of zero implies that the fitted K_{II} stress field has the same amount of variance as simply averaging the $L_I + K_{II}$ plastic zone (i.e. fitting a circle) and negative values of R^2 indicate that the fitted K_{II} plastic zone has higher variance than simply averaging the plastic radius.

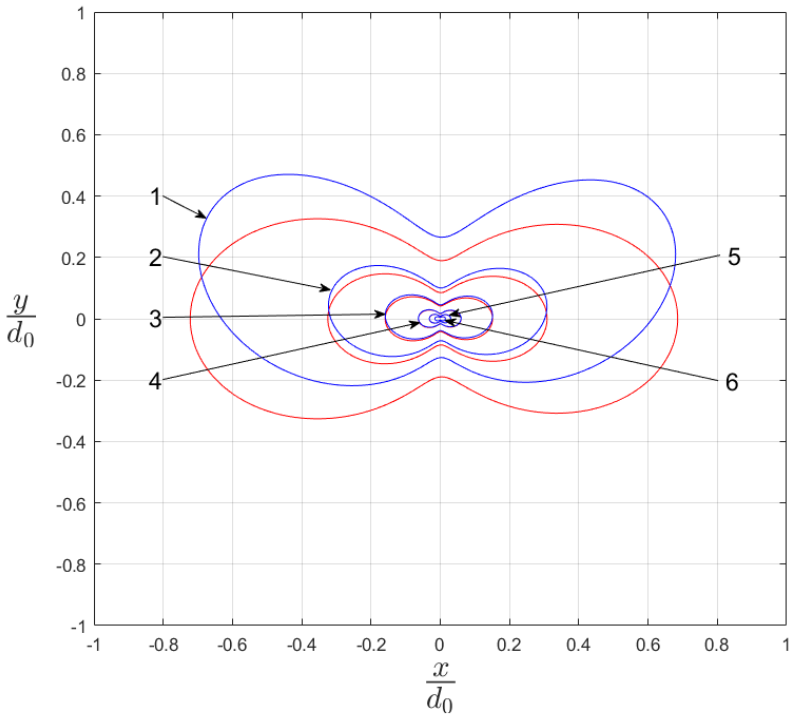


Figure 4: Comparison between combined $L_I + K_{II}$ implied plastic fronts (Blue) and pure K_{II} implied plastic fronts (Red) for various values of $\frac{K_{II}L_I}{\sigma_y^2}$.

Contour	$\frac{K_{II}L_I}{\sigma_y^2}$ for $K_{II} + L_I$	R^2	$\frac{K_{II}L_I}{\sigma_y^2}$ for K_{II}
1	0.2	0.379	0.22847
2	0.1	0.864	0.10274
3	0.05	0.967	0.05033
4	0.02	0.995	0.02001
5	0.01	0.999	0.00999
6	0.005	0.999	0.00498

Table 1: A Table giving the coefficient of determination for each of the contours in 4.

4. Small Scale Slip

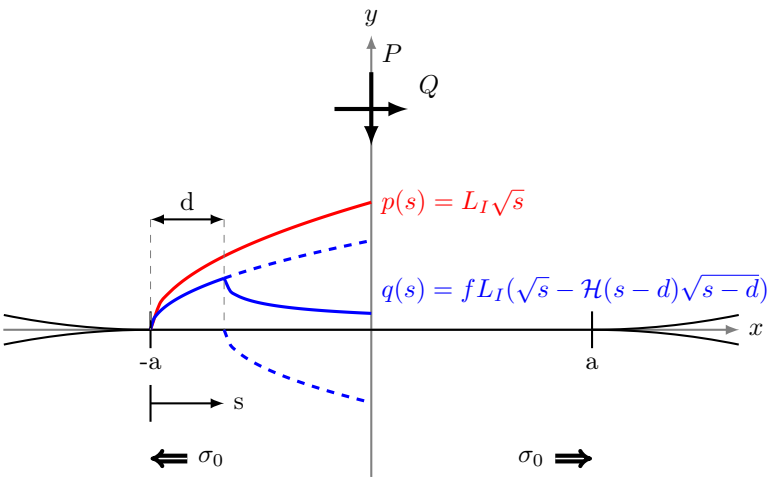


Figure 5: A diagram of the geometry for the partial slip case showing loads and local stress asymptotes

The steady state slip zone size, d, allowing, for frictional shakedown, is given by [Dini et al, 2005]

$$fd = \frac{\Delta K_{II}}{L_I} = d_0 \tag{24}$$

where f is the coefficient of friction, and the relative plastic and frictional slip extent is given by

$$\frac{r_p\,(0)}{d} = \frac{3f\Delta K_{II}L_I}{4\sigma_y^2}. \tag{25}$$

If $r_p\,(0)\,/d > 1$ the plastic zone envelops the slipping region of the interface, and when this is true the frictional slip may have only a mild effect on crack nucleation. Under these conditions a fretting contact edge will behave like a notch of angle 2π, i.e. a crack tip, as suggested by Giannakopoulos [Giannakopoulos et al, 2000]. We have just a constant normal pressure problem given by equation (4) together, in the limit, when $f \to \infty$, with a reversing singular field, where

$$\Delta q(s) = \frac{\Delta K_{II}}{\sqrt{s}} \tag{26}$$

This is as described above (in§1), except for the bounded pressure problem, which is constant in time and will, therefore, shake down. The solution provides an estimate of the plastic front position for a perfectly sticky interface, although there is a violation of the slip law over the region $0 < s < d$.

The other possibility is that slip envelops the plastic region. When $\sigma_Y \to \infty$ the plastic zone will vanish. The normal contact solution is still given by (4), and the shear traction distribution in lien of (2) will instead be given by [Dini et al, 2005]

$$q(s) = L_{II}\sqrt{s} - L_{II}\sqrt{s-d} = fL_I\sqrt{s} - fL_I\sqrt{s-d}. \tag{27}$$

as illustrated in figure 5, where $\mathcal{H}(s-d)$ is the heaviside step function. The stress field from a square root bounded shear asymptote is given by [Nils Cwiekala, Private conversation]

$$\left\{ \begin{array}{c} \sigma_{rr} \\ \sigma_{\theta\theta} \\ \sigma_{r\theta} \end{array} \right\} = L_{II}\sqrt{r} \left\{ \begin{array}{c} \frac{3}{4}sin\frac{\theta}{2} + \frac{5}{4}sin\frac{5\theta}{2} \\ \frac{5}{4}sin\frac{\theta}{2} - \frac{5}{4}sin\frac{5\theta}{2} \\ -\frac{1}{4}cos\frac{\theta}{2} + \frac{5}{4}cos\frac{5\theta}{2} \end{array} \right\} \tag{28}$$

5. Plasticity Zone Calculation with Finite Slip

The ideas put forward in the last section may be investigated in more detail by looking at the implied size of the plastic front, again based on an elasticity solution plus violations of the yield criterion, but now for the elastic state of stress given by a slipping contact. This is readily achieved by superposing two bounded, sliding shear traction distributions separated by the slip zone length (equation (28)). We will again work in the framework of the normalisation devised for the full-stuck solution: the size of the steady state slip zone, d, is given by equation (24) and the internal length dimension, d_o, is given by equation (15).

The stress field is now given by

$$\sigma_{ij}(r,\theta) = L_{II}\left[\sqrt{r}g_{ij}^{II}(\theta) - \sqrt{\rho}g_{kl}^{II}(\phi)\right] + L_I\sqrt{r}g_{ij}^{I}(\theta) \tag{29}$$

where $L_{II} = fL_I$, ie.

$$\sigma_{ij}(r,\theta) = L_I\left[\sqrt{r}\left(g_{ij}^{I}(\theta) + fg_{ij}^{II}(\theta)\right) - f\sqrt{\rho}g_{kl}^{II}(\phi)\right] \tag{30}$$

and

$$\rho^2 = d^2 + r^2 - 2rdcos\theta \quad sin\phi = sin\theta\left(\frac{r}{\rho}\right).$$

The stress components referenced by $g_{kl}^{II}(\phi)$ have been rotated by $\theta - \phi$ using the transformation law for the Cauchy stress tensor to ensure all stresses are in the same coordinate system.

Note that, although this appears superficially to be a square root bounded distribution the difference between two bounded terms separated by a (small) distance d, or d_o/f appears like a square root singular field when $r >> d$.

Unlike the no slip case we cannot reduce the problem to a single parameter space; instead the plastic zone depends on two dimensionless parameters/groups, $\frac{K_{II}L_I}{\sigma_y^2}$ and the coefficient of friction, f. Figure 6 shows contours of

$\frac{K_{II}L_I}{\sigma_y^2}$ for a coefficient of friction of 0.7. It can clearly be seen that in this case there is no evidence of the 'figure of eight' plastic zone normally associated with a K_{II} singular stress field.

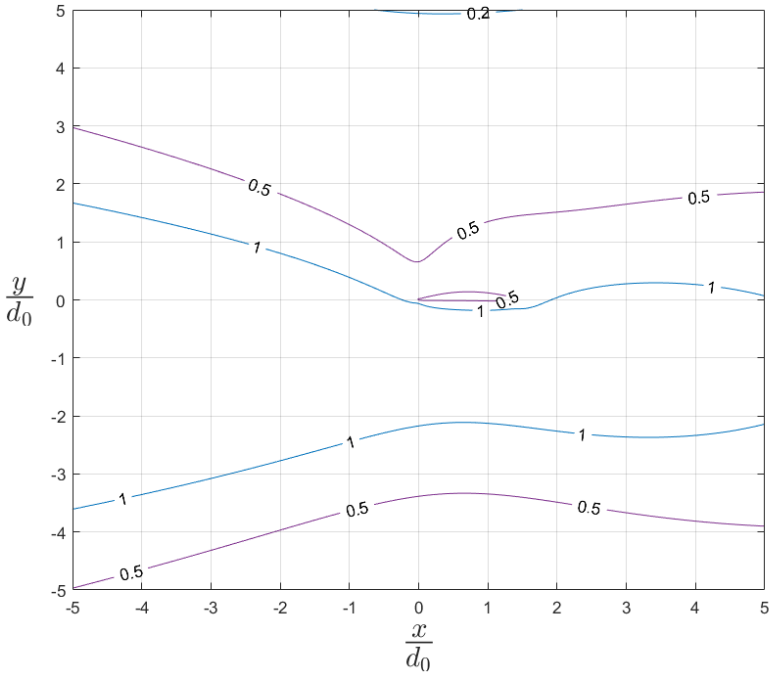


Figure 6: Implied plastic zones for values of $\frac{K_{II}L_I}{\sigma_y^2}$ for the partial slip problem with $f = 0.7$ $\left(\frac{d}{d_0} \approx 1.4\right)$.

6. Conclusion

In conventional fracture mechanics we require the extent of the plasticity zone to be small, sufficiently small for it to be surrounded wholly by a region in which the singular field controls the hinterland before higher order terms in a series expansion of the crack tip field start to become important. Equally, in the crack nucleation problem we generally require, at the contact edge, the plasticity zone to be sufficiently small for the hinterland to be controlled by the dominant singular term if that does, indeed control crack nucleation. In the case of a complete contact this means that we would require the plastic zone to be small enough to be controlled by the mode I eigensolution, but at an incomplete contact edge the problem is rather different. There is a constant bounded symmetric field (pressure) together with a singular anti-symmetric

oscillatory field. For the problem to behave like a crack tip the process zone must be smaller than the region where distortion to the nominal traction from K_{II} to L_I domination takes hold, and a good estimate of the boundary of the undistorted region is provided by d_0. Notice that the requirement is stronger than that from LEFM, as we require both the extent of the plasticity zone and the extent of frictional slip to be small.

So, provided that both requirements of small scale slip are satisfied we anticipate that the value of ΔK_{II} will have a dominant effect on the nucleation process. The mode I field is also square root singular at a crack tip but is only square root bounded at an incomplete contact edge. We have a simple means, in this formulation, of quantifying what we mean by small scale slip; it is when the hinterland is controlled by the singular shear traction field, i.e. when $r < d_0$. Interpreted in terms of frictional slip, this means that $d/d_0 < 1$, or, from equation (29), that $f > 1$ and this, is, of course, an impractical requirement. On the question of small scale plastic yield the maximum practical load may be more acceptable. If we use equation (11) and limit the maximum plastic radius to d_0 this would mean that the requirement would be

$$\frac{r_p}{d_0} = \frac{3}{4}\frac{\Delta K_{II} L_I}{\sigma_y^2} < 1,$$

or

$$\frac{\Delta K_{II} L_I}{\sigma_y^2} < \frac{4}{3} \tag{31}$$

If we specialise to Hertz geometry and take representative values (equation 20) we know that a heavily loaded contact might give rise to a left hand side of this equation of about unity. So, frictional slip is a more concerning problem in terms of the fidelity of the mode II loading field.

In Figure 7 we show the dimensionless slip zone size and dimensionless plastic zone size for a range of practical experiments conducted on a range of geometries and with a wide range of materials [Dini, 2005b], [Szlowinski, 1998], [Hojjati-Talemi et al, 2014], [Nowell, 1988]. The graph is partitioned into two regions, with the upper triangular region corresponding to tests where plasticity is dominant and the lower triangular region corresponding to tests where slip is dominant. Additionally, if the data point is sufficiently near the origin $\left(\frac{r_p}{d_0} < 1, \frac{d}{d_0} < 1\right)$ small scale plasticity and small scale slip apply and the problem is K_{II} field dominated. It can be seen that for all the data sets, except those from the low alloy steel tests , the plastic zone size is small enough to be considered as 'small scale plasticity' $\left(\frac{R_p}{d_0} < 1\right)$. In contrast none of the data sets have slip zones small enough for them to be considered as 'small scale frictional slip' $\left(\frac{d}{d_o} < 1\right)$which reflects that very few real material combinations have coefficients of friction greater than 1. Due to these large slip zones none of the tests were performed in the region where the stress fields are K_{II} dominated (indicated by the square in the lower left corner of the chart) and the influence of the normal load is therefore likely to be important.

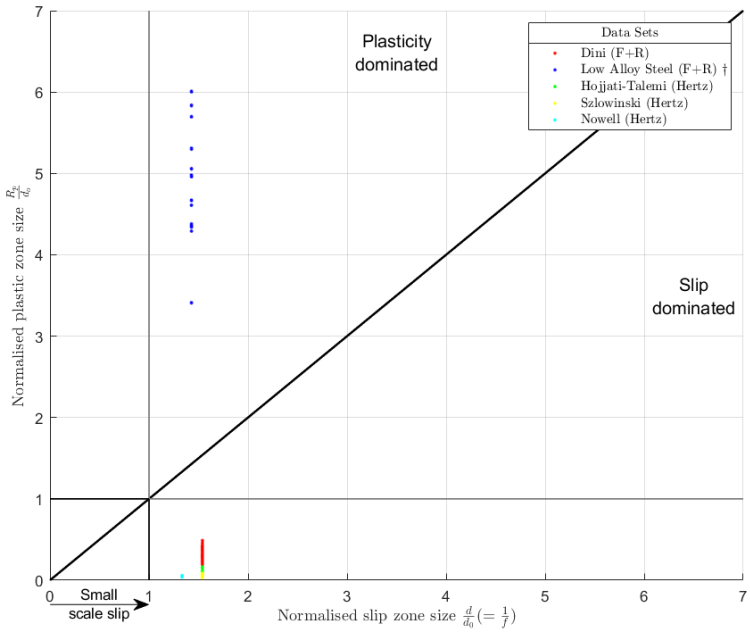


Figure 7: Various data sets plotted on axis of normalised plastic zone size and Normalised Slip zone size, and indicating the region over which the K_{II} Stress field dominates ($r < d_0$).

7. References

Zabala A, Infante-García D, Giner E, Goel S, Endrino J L, Llavori I (2020), On the use of the theory of critical distances with mesh control for fretting fatigue lifetime assessment, *Tribology International*, **142**, 105985

Chambon L, Journet B (2006), Modelling of fretting fatigue in a fracture-mechanics framework, Tribology International, **39**, (10), 1220-1226

Dini D, Sackfield A, Hills DA, (2005), Comprehensive bounded asymptotic solutions for incomplete contacts in partial slip, *Journal of Mechanics and Physics of Solids*, **53**, 437-454, ISSN: 0022-5096

Giannakopoulos A E, Lindley TC, Suresh S,(1998) Aspects of equivalence between contact mechanics and fracture mechanics: theoretical connections and a life prediction methodology for fretting Fatigue. Acta Mater., **46**, (9) 2955-2968.

Giannakopoulos A E, Venkatesh T C, Suresh S, Chenut C, (2000) Similarities of stress concentrations in contact at round punches and fatigue at notches: implications to fretting fatigue crack initiation, Fatigue & Fracture of Engineering Materials & Structures, **23**, 561-571

Hills D A, Fleury R M N, and Dini D, (2016), Partial slip incomplete contacts under constant normal load and subject to periodic loading International Journal of Mechanical Sciences, **108**–**109**,115-121.

Dini D and Dyson I, (2005b), Fretting Fatigue test results for Ti 6/4 (D4.1), Analysis of results and validation of assessment criteria (D5.2): issue 2, UTC Report No. 219, University of Oxford

Szolwinski M P, Farris T N, (1998), Observation, analysis and prediction of fretting fatigue in 2024-T351 aluminum alloy, Wear, **221**, 24–36

Hojjati-Talemi R, Wahab M A, De Pauw J, De Baets P, (2014), Prediction of fretting fatigue crack initiation and propagation lifetime for cylindrical contact configuration, Tribology International, **76**, 73-91

Nowell D, (1988), An analysis of Fretting Fatigue, DPhil Thesis, University of Oxford

8. Acknowledgements

James Truelove expresses with thanks the award of an iCASE award ref 17000027 from Rolls-Royce plc which has enabled him to carry out this work.

We would also like to thank TechnipFMC for allowing us to to use data collected as part of a project at the University of Oxford in the creation of figure 7 (†)

Statement of Authorship for joint/multi-authored papers for PGR thesis

To appear at the end of each thesis chapter submitted as an article/paper

The statement shall describe the candidate's and co-authors' independent research contributions in the thesis publications. For each publication there should exist a complete statement that is to be filled out and signed by the candidate and supervisor **(only required where there isn't already a statement of contribution within the paper itself).**

Title of Paper	A Comparison of the State of Stress at an Incomplete Fretting Contact Edge with a Crack Tip
Publication Status	☑Published □ Accepted for Publication □Submitted for Publication □Unpublished and unsubmitted work written in a manuscript style
Publication Details	Truelove, J. P. J., & Hills, D. A. (2021). A comparison of the state of stress at an incomplete fretting contact edge with a crack tip. Tribology International, 153, 106643.

Student Confirmation

Student Name:	James Truelove		
Contribution to the Paper	Writing of MATLAB code, analysis of results, production of figures, editing of manuscript.		
Signature	James P J. Truelove	Date	17/07/23

Supervisor Confirmation

By signing the Statement of Authorship, you are certifying that the candidate made a substantial contribution to the publication, and that the description described above is accurate.

Supervisor name and title: Prof D A Hills		
Supervisor comments James made substantial contributions to the arguments concerning a caparison of contact edge and crack tip behaviour. He does himself down by suggesting he only coded the problem up – he also contributed to the analaysis.		
Signature	Date	19th July 2023

This completed form should be included in the thesis, at the end of the relevant chapter.

4 Measurement of Moment Coupling in Fretting Fatigue Experiments

The paper presented in this chapter has been published as: *Truelove, J. P. J., Hills, D. A., & Blades, L. (2021). Measurement of moment coupling in fretting fatigue experiments. Proceedings of the Institution of Mechanical Engineers, Part C: Journal of Mechanical Engineering Science, 235(24), 7726-7733.*

One of the major pieces of fretting fatigue apparatus present in the Oxford Fretting fatigue laboratory is the 'Fort Rig'. This piece of testing apparatus was originally designed to perform experiments mimicking the contact conditions present in aircraft engines; the rig was therefore designed with a significant amount of clearance around the test contact and significant distance between the specimen and hydraulic actuators so that it would be possible to use an environmental chamber or furnace to simulate the effects of engine temperature and gas flows without damaging the actuators and their instrumentation.

An unfortunate consequence of this rig design is that the resulting apparatus lacks rigidity – the long load paths and significant distances from the contact to the support frames cause a significant amount of deflection when loads are applied. Multiple attempts have been made to stiffen the rig to reduce the effect of these deflections, initially by adding additional support bars, later by adding plate springs.

Another side effect of this rig design is that the loads in the rig are coupled. As there is a significant distance between the contact and the support structure the application of shear load to the contact simultaneously generates a moment. The existence of this coupling has been recognised for a long time, but no detailed attempts to measure or account for it have been made.

The sub sea connector experiments used pads with a flat much wider than those typically found in experiments, which were consequently much more sensitive to the coupled moment. When running these tests the effect of this moment coupling was extremely noticeable – the rocking of the pads being visible to the naked eye – raising concerns about the effect of the moment on the contact pressure solution and the potential for pad lift off.

In the following paper we describe an investigation that was carried out into the effect of moment coupling in this test rig. Digital image correlation is used to measure the deflection of the pads, the equivalent applied moment is measured and is shown to be significant. The effect of the moment is to increase the contact pressure at one edge of the contact and decrease it at the other, and so as a final stage an iterative solver is used to find a method of varying the applied normal load to remove the effect of the moment at one edge of the contact.

Measurement of Moment Coupling in Fretting Fatigue Experiments

Journal Title
XX(X):1–6
©The Author(s) 2021
Reprints and permission:
sagepub.co.uk/journalsPermissions.nav
DOI: 10.1177/ToBeAssigned
www.sagepub.com/
SAGE

J.P.J. Truelove[1], D.A. Hills[1] and L. Blades[1]

Abstract
Moment coupling in fretting fatigue experiments refers to the generation of moments when a shear force is applied, caused by the difficulty in designing fretting fatigue experiments where the shear is reacted out on the same plane as the contact. Digital Image Correlation is used to measure the effect of moment coupling, and a model is created to calculate the effect of the applied moment at any point during a loading cycle on near-edge contact properties. The effects of the changing contact pressure on the slip zone sizes are considered. Finally, the model derived is used to find a load cycle including the effect of normal contact force that creates a truly constant near-edge contact pressure distribution at one edge of the flat and rounded pad. Although the calibrations found in this paper are valid only for the specific rig and specimen geometry used in this paper, the method could be readily applied to other experiments.

Keywords
Contact Mechanics, Fretting, Fatigue, Solid Mechanics, Experimental techniques

Introduction

Fretting fatigue occurs in contact problems in the presence of partial slip, meaning that some region of the contact is permanently stuck and some region of the contact is undergoing cyclical reversing slip. The contacts conditions resulting from fretting fatigue processes result in a region where cracks can initiate, which can eventually result in component failure. Understanding the effect of fretting fatigue on component lifetime is therefore essential for assemblies in which crack propagation from contacts could result in dangerous failures of components, such as the contacts present at the root of fan blades in aero engines.[1]

Experimental investigations in fretting fatigue are primarily based on matching the contact stress fields in a real problem with those in a much simpler geometry which is easier to analyse , such as a dog bone specimen in contact with a pair of profiled pads.[2] To match the stress field in the dog bone to that in the real geometry there are four loads that must be controlled; the differential bulk tension σ and shear load Q which affect the shear stress distribution along the contact interface, while the normal load P and moment M which affect the contact pressure distribution.[3]

When contact problems are analyzed in half plane theory it is assumed that P and Q are applied through a point located at the centre of the pad and on the plane of the contact, so that their effects are uncoupled. In test machines it is difficult to react out the shear in the plane of the contact, so instead it is often supported at a fixed distance from the contact plane. In addition there is always a finite projection of the pad which behaves like a short cantilever in the presence of a tip shear force. This results in 'moment coupling', where the application of a shear load results in the simultaneous application of a moment. This presents a particular problem when 'flat and rounded' or 'square' pad geometries are used, as the application of a moment can result in significant changes in the normal contact pressure adjacent to the edge of contact, or, in extreme cases, the lifting off of one edge of the punch.[4]

Experimental Setup and Measurements

Experiments were conducted using the rig, Figure 1, located in the Servo-Hydraulic Laboratory at the University of Oxford. This test apparatus was originally designed to perform high temperature experiments to simulate the conditions present in gas turbine engines, which resulted in the support frame being extremely large to ensure there was sufficient thermal isolation between the specimen and the hydraulic components. This has resulted in significant problems with rigidity, and, in order to allow for the installation of a furnace, the shear force is reacted out through the plate springs (A) at a significant distance from the contact interface (B).

An overview of the rig showing the load paths present is given in Figure 2. The left and right actuators apply loads to each end of the dogbone specimen, while a third actuator at the bottom of the rig applies the pad normal load, P. The shear load applied to each pad is therefore given by $\frac{1}{2}(F_L - F_R)$ The shear force applied to each pad is supported through four plate springs attached to each pad holder, designed in such a way that they are compliant in the direction of the normal load. The significant distance between the plane of the contact between the pad and dogbone and the springs

[1]University of Oxford, UK

Corresponding author:
Department of Engineering Science, University of Oxford, Parks Road, Oxford, OX1 3PJ, UK
Email: james.truelove@eng.ox.ac.uk

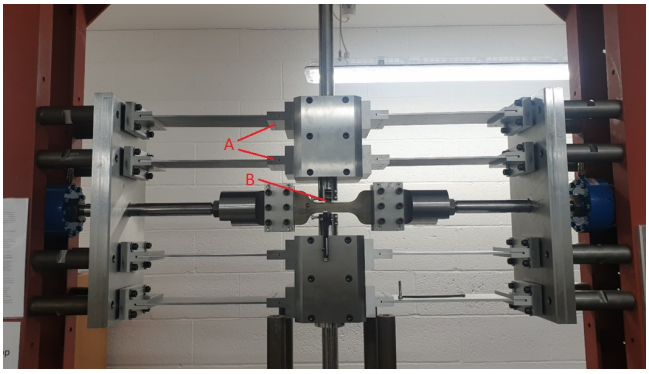


Figure 1. A photo of the fort rig, showing the significant distance between the contact and the springs where the shear load is supported.

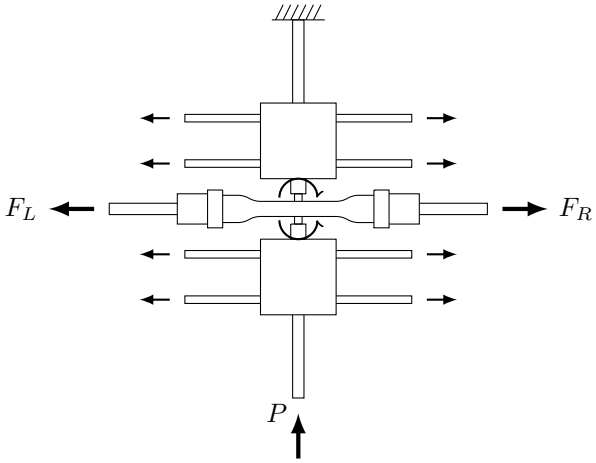


Figure 2. A schematic diagram of the fort rig, showing the load paths through the apparatus

supporting the applied shear load results in the generation of a coupled moment, M, at the contact interface.

In tests a pair of flat and rounded pads with 15mm central flat and 1.5mm corner radius were used. These were pressed into a steel dogbone 30mm high with a thickness of 6mm.[5] The ends of the dogbone were serrated to provide a fatigue resistant connection to the actuators, and pin joints were subsequently fitted between the dogbone and the horizontal actuators to prevent twisting of the dogbone due to any slight misalignments (not present in Figure 1). This pad and dogbone geometry was used throughout all subsequent measurements.

It is not possible to measure the coupled moments or contact pressure directly, so instead the surface displacements of the pad and dogbone are measured, and the moment calculated from the resulting deflections. Digital image correlation (DIC) was used to measure these displacements; in this method a speckle pattern is applied to the surface of the components, a series of pictures of the component is taken during the load cycle and software is used to derive the motion and deflection of the components. Digital image correlation has previously been applied to fretting fatigue experiments, for the measurement of coefficient of friction[6], slip[7] and strains[8], for example.

It was suspected that there would be a small amount of coupling between the application of the normal load and the moment, due to distortion of the frame. A series of digital image correlation measurements was therefore taken. The pads and dogbone were prepared with a speckle pattern using black and white matt spray paint. A Point Grey camera was used to capture greyscale images of the dogbone and pads at 2 frames per second at a resolution of 4240 x 2824 pixels. The digital image correlation software MatchID was used to check the quality of the speckle pattern and to process the collected images. The loads given in table 1 were used, to cover fully those arising in typical fretting fatigue tests. To ensure that only partial slip was present a maximum shear force of 15% of the normal load was applied to each pad. The actuator at the left hand of the rig was set to maintain a fixed load of 15kN, while the actuator at the right hand side of the rig was cycled to apply the shear load.

Table 1. Loads used for measurement of moment coupling

Normal load (kN)	Shear load amplitude (kN) (Total load)	Plane strain equivalent normal load (N/mm)	Plane strain equivalent shear load amplitude (N/mm) (Per pad)
5	1.5	833	125
10	3	1667	250
15	4.5	2500	375
20	6	3333	500
25	7.5	4167	625
30	9	5000	750
35	10.5	5833	875

After the images were processed the DIC software was used to track the vertical displacements of two regions of points located adjacent to each edge of the pad. For each of these regions the vertical displacement of the edge of the pad was measured and the difference between the two measurements was used, in conjunction with the known width of the pad, to calculate the angle of pad tilt. By matching the image with the maximum amount of pad tilt to the peak of the load cycle it is possible to generate a plot of pad tilt vs applied shear load, an example of which is shown below in Figure 3, for the case of 20kN applied normal load. It was found that for all 7 cases investigated the angle of pad tilt varied linearly with applied shear force.

In order to ascertain how the angle of pad tilt per unit shear varied with applied normal load a linear model was fitted to the measurements for several values of normal load, and the gradient of the line found, given in table 2. It was revealed that there was no systematic variation in the amount of pad tilt per unit shear load with changing normal load, the value being fixed at a mean value of 0.0039 degrees/kN.

Calculation of Equivalent Moment and Creating a Calibration

In order to convert the measured angle of pad tilt into an equivalent applied moment a closed form solution for a tilted flat and round contact subject to normal load and moment is used, derived in[9]. This was implemented in a MATLAB script, kindly provided by Dr H. Andresen[10]. The magnitude of the moment developed will depend on the normal load and the angle of pad tilt, so for each value of the applied

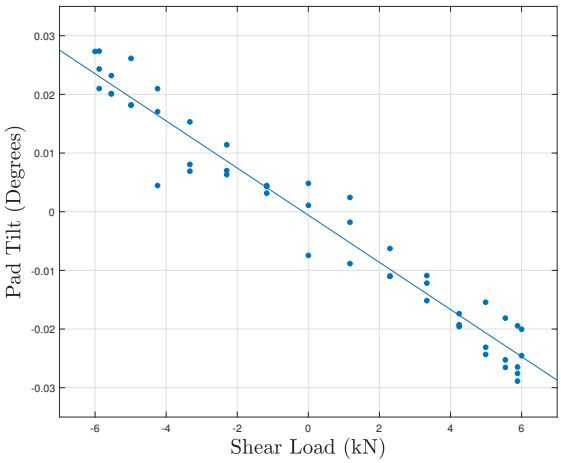


Figure 3. A plot of pad tilt as a function of applied shear load, in this case for an applied normal load of 20kN

Table 2. The measured coupling between pad tilt and shear load at each of the applied normal loads.

Normal Load (kN)	Pad tilt per kN shear (degrees/kN)
35	0.0037
30	0.0040
25	0.0039
20	0.0040
15	0.0040
10	0.0041
5	0.0035
Average	0.0039

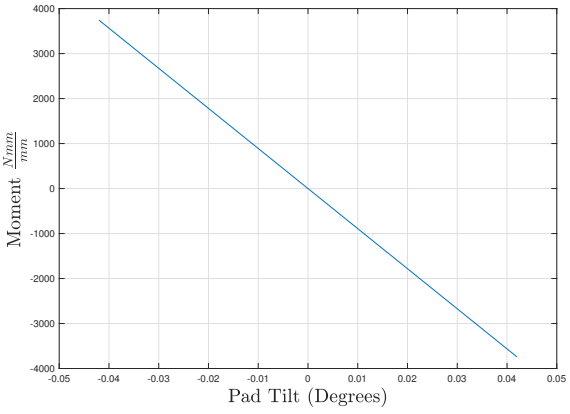


Figure 4. A plot of the relationship between pad tilt and moment for an applied normal load of 35kN

normal load the equivalent moment was calculated at steps of 0.001 degrees over the full range of pad tilt experienced at each value of normal load. It was found that, over the range considered, the magnitude of the moment varied linearly with pad tilt for all 7 loading cases considered. An example plot for the case of a normal load of 35kN is shown in Figure 4.

The final thing considered is the effect of the normal load on the magnitude of the moment coupling. For each value of normal load the moment per degree of pad tilt was

Table 3. The effect of varying the normal load on the magnitude of the moment coupling

Normal load (kN)	Plane strain equivalent moment per degree pad tilt ((Nmm/mm)/degree)
35	89100
30	88900
25	88600
20	88400
15	88100
10	87800
5	87400
Average	88300

noted, and the results are shown in table 3. Although there is some variation of the moment with applied normal load, with higher normal loads implying a greater degree of coupling, this effect was extremely small, with the difference between the 5kN case and the 35kN case less than 2%. It was therefore decided to ignore this effect and assume that the relationship between moment and pad tilt was constant, with the value simply given by the mean of the calculated values.

It is now possible to create a calibration that allows us to express the magnitude of the coupled moment developed as a function of the applied shear load. Starting with the data in table 2 we can express the relationship between the angle of pad tilt and the plane strain equivalent shear as

$$\theta = 4.68 \times 10^{-5} S \tag{1}$$

where θ is the angle of pad tilt in degrees and S is the plane strain equivalent shear load, in $\frac{N}{mm}$ (force per unit pad thickness). Note that in order to convert the actuator shear load to its per pad equivalent it must be divided by 2, as the actuator shear force is simultaneously applied to two pads. Likewise using the data in table 3 it is possible to write the coupled moment as a function of the angle of pad tilt

$$M = 88300\theta \tag{2}$$

where again θ is measured in degrees and M, the moment per unit pad thickness is given in units of $\frac{Nmm}{mm}$. Combining the two expressions we therefore arrive at equation (3), which characterizes the behaviour of the rig over the full range of loads used in conjunction with this pad and dogbone geometry.

$$M = 4.13S \tag{3}$$

In order to validate this expression the equivalent moment was calculated at the point of maximum shear force for each of the 7 load cases that were measured. This moment, in conjunction with the normal load are used as inputs to the tilted pad solution[9], and it was found that the implied angle of pad tilt was the same as the maximum angle of pad tilt measured with DIC.

Effect of the Coupled Moment

Having found an expression that allows us to calculate the magnitude of moment developed in a fretting fatigue

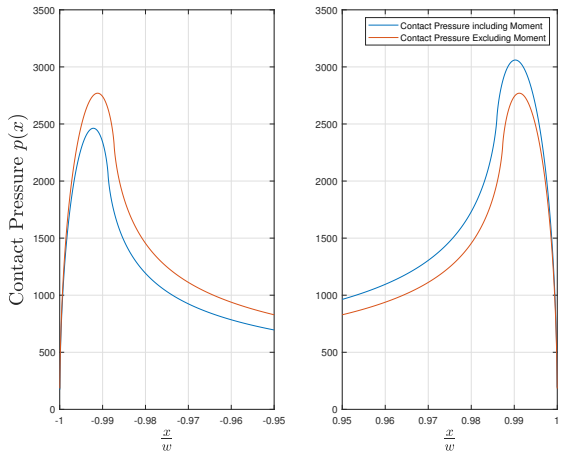


Figure 5. A comparison of the contact pressure, including and excluding the effect of the coupled moment at each edge of the fretting pad

experiment we now wish to consider briefly what effect it will have on the contact, first by finding its effect on the contact pressure distribution, and finally on the size of the slip zones. In the following calculations we will consider only the behaviour of the pad for the 35kN normal load case as a representative example.

The load on the dogbone will vary between two points as the shear is cycled. At the first point the left actuator (when viewed from the front, as in Figure 1) will be applying 15kN of tension while the right is applying 4.5kN, resulting in an overall shear force of 10.5kN acting to the left and a bulk tension of 25MPa. At the second load point the left actuator will be applying 15kN tension while the right actuator applies 25.5kN, resulting in an overall shear force of 10.5kN acting to the right and a bulk tension of 83.3MPa.

Effect on Contact Pressure

Figure 5 shows a direct comparison between the contact pressure for the flat and rounded pad both including and excluding the effect of the moment, at the point in the load cycle where the right actuator is applying a tension of 4.5kN. The plots here show only the outermost regions of the contact, $-0.95 \geq \frac{x}{w} \geq -1$ and $0.95 \leq \frac{x}{w} \leq 1$, where the width of the contact is $2w$. As expected it can clearly be seen that the application of the moment results in an increase in contact pressure at one edge of the contact, and a decrease at the other. The peak contact pressure is given in the first row of table 4. The tilting of the punch will also affect its geometry, and in doing so will change the location of the maximum pressure. This is given in the second row of the table. Furthermore as the pad tilts the half-width of the contact will increase at the high pressure end and reduce at the low pressure end, these effects are shown in the third row of table 4, with the contact extent being measured from the centre of the flat. It is worth nothing that the overall width of the contact remains essentially unchanged as the moment is applied.

Table 4. Some measures of the effect of the moment on the normal load distribution

Contact Property	No moment	Left Edge	Percentage Change	Right Edge	Percentage Change
Peak Contact Pressure MPa	2770	2460	-11.2%	3060	+10.5%
Location of Maximum pressure from centre mm	7.530	7.540	+0.13%	7.520	-0.13%
Contact Extent mm	7.600	7.590	-0.13%	7.610	+0.13%

Table 5. The effect of the coupled moment on the size of the slip zone at each edge of the contact.

	Left Edge μm	Percentage Change	Right Edge μm	Percentage Change
No Moment	22.315	-	14.589	-
Moment - 10.5 kN Shear to left	11.517	-48.4%	24.818	+70.1%
Moment - 10.5 kN Shear to right	32.544	+45.8%	3.791	-74.0%

Effect on Slip Zone Size

We will now briefly discuss what effect the application of the moment has on the size of the slip zones at each end of the contact, again for the 35kN normal load case. The steady state slip zone size for a contact subject to varying moment, normal load, shear load and bulk tension can be found analytically, as analyzed in[11]. The slip zone sizes found in this way are shown in table 5, given in microns, and assuming a coefficient of friction of 0.55. It can be seen that the change in slip zone size is rather significant in this setup, as the change in the half width of the contact is of the same order of magnitude of the slip zone size.

Removing the Effect of the Moment

Calculating a Load Cycle

We now wish to create a loading cycle such that the effect of the moment is cancelled out at one edge of the contact. In the previous section we saw that when the shear load was acting to the left the left hand edge of the pad lifted off, and the contact pressure reduced. To counteract this we could therefore simultaneously increase the pad normal load when we apply the shear, such that the local contact pressure remains constant. We can treat the case when a shear load is applied to the right in a similar manner. The left hand edge of the pad 'digs in', and the contact pressure increases; we must therefore reduce the pad load to maintain a constant contact pressure.

It should be noted that it is only possible to cancel the effect of the moment coupling at one edge of the contact, and varying the normal load in this manner will increase the pressure variation at the other edge of the contact. In the majority of fretting fatigue experiments this is unlikely to be

Table 6. The load required to remove the effect of the moment at the left hand edge for the 35kN normal load cycle, with shear loads as given in table 1.

	No Correction	Shear to Left	Shear to Right
Actuator Load kN	35	40.65	29.32
Plane strain equivalent N/mm	5833	6775	4887

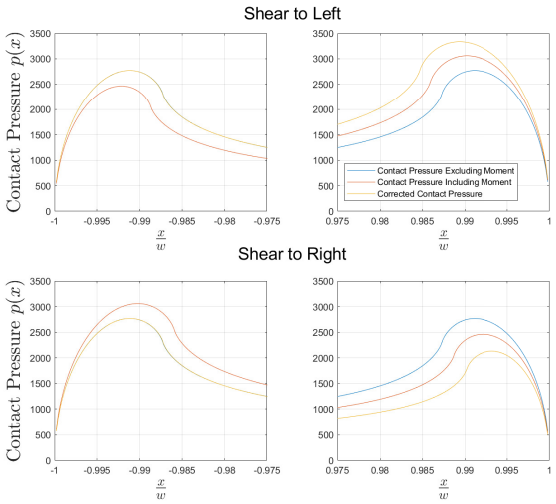


Figure 6. A three way comparison plot, showing the contact pressure from a contact with no moment present (blue), the contact pressure including the effect of the moment coupling (orange), and the contact pressure with the normal load correction (yellow). Note that in the left plots the blue and yellow lines are coincident.

important because we are concerned with matching the near edge contact pressure only in the neighbourhood of crack nucleation. Most specimens are loaded with a combination of shear and bulk tension, the effects of which are additive at one edge of the specimen and subtractive at the other. For most tests we know at which edge of the contact failure will occur before starting the experiment.

In the following example we will match the contact pressure at the left hand edge of the contact by adjusting the peak contact pressure to that found in the no moment case. A MATLAB script is used with an iterative solver to find the appropriate change in normal load. Using this solver we arrive at the load cycle given in table 6.

Figure 6 shows a three way comparison between the contact pressure for the idealised case where no moment is present, the contact pressure including the effect of the unwanted moment, and the contact pressure from the load cycle with the normal load correction. The top plots are for the case where the shear force is acting to the left, the bottom plots are for the shear acting to the right. As predicted it can be seen that by varying the normal load appropriately an extremely close match in the contact pressure at the left edge of the contact may be achieved, but at the expense of a larger deviation at the right hand edge.

Table 7 contains a variety of contact properties, calculated for both the idealised no moment case and the moment corrected load cycle. It can be seen that in comparison to tables 4 and 5 that the error is much smaller, in all cases

Table 7. A table comparing a number of properties of the left hand edge of the contact for the idealised case with no moment coupling (only shear and normal loads), and the corrected load cycle with the shear acting both to the left and the right

Contact Property	No Moment	Shear to Left	Percentage Change	Shear to Right	Percentage Change
Peak Pressure MPa	2769	2769	-	2769	-
Contact Extent (from C/L) mm	7.596	7.596	0.00%	7.597	+0.01%
Slip Zone Size μm	22.315	22.184	-0.59%	22.423	+0.48%

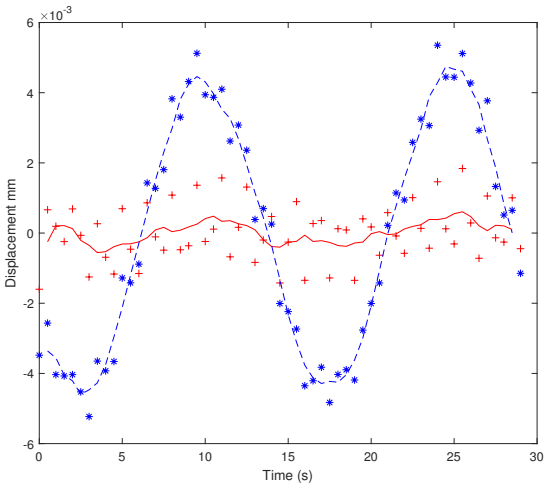


Figure 7. The vertical deflection of each end of the pad during two load cycles for the 20kN nominal normal load case.

being less than 1%, indicating a good match between the theoretical constant load cycle and the moment corrected cycle.

Experimental validation using DIC

The same DIC setup that was used to measure the magnitude of the moment coupling was used to check that varying the normal load created a constant contact pressure at one edge of the contact. The Test rig was set up with the same specimen and pad combination as used in the measurements, and were loaded with the derived varying normal load cycle. The vertical displacement of each corner of the pad was recorded over 2 load cycles.

Figure 7 shows a plot of the vertical displacement of each end of the pad for the 20kN nominal normal load cycle. It can be seen that the varying normal load cycle has successfully removed the effect of the moment coupling at one end of the pad, with the vertical deflection being reduced to approximately zero.

Conclusion

Moment coupling - the development of a rocking moment as a shear force on the contact is applied - is an unavoidable

feature of fretting fatigue tests. It can be reduced by careful design but cannot be fully eliminated. When modelling the behaviour at the edge of contacts in fretting fatigue it is important that the action of moment coupling effects are accounted for. A method of measuring the magnitude of the moment coupling is derived through the use of DIC and a closed form solution for flat and rounded contacts, and a way of accounting for the coupled moment is found. The effect of the coupled moment is found to be non-trivial, particularly its effect on the predicted slip zone sizes. A load cycle with varying normal load is used to offset the effect of the moment, then DIC is used to validate that the resulting load cycle results in a truly constant normal pressure at one edge of the contact. Through this procedure it is therefore possible to match the behaviour of an experiment to an analytically derived load cycle in rigs with variable normal load actuation.

Acknowledgements

James Truelove expresses with thanks the award of an iCASE award ref 17000027 from Rolls-Royce plc which has enabled him to carry out this work.

Declaration of conflicting interests

The Authors declare that there is no conflict of interest

References

1. Haijun Tang, Dashu Cao, Hongyu Yao, Mingli Xie, Ruichun Duan, (2009), Fretting fatigue failure of an aero engine turbine blade, *Engineering Failure Analysis*, **16 (6)**, pp 2004-2008
2. Hills D A, Nowell D, (2014), Mechanics of fretting fatigue—Oxford's contribution, *Tribology International*, **76**, pp 1-5
3. Andresen H, Hills D A, (2020), A review of partial slip solutions for contacts represented by half-planes including bulk tension and moments, T*ribology International*, **143**
4. Sackield A, Truman C E, Hills D A, (2000) The tilted punch under normal and shear load (with application to fretting tests), *International Journal of Mechanical Sciences*, **43**, pp 1881–1892
5. Blades L E, Hills D A, Wormsen A, Macdonald K A, (2020), Fretting fatigue design of subsea connectors: Matching results between pairs of tests, *Proceedings of the International Conference on Offshore Mechanics and Arctic Engineering - OMAE*, Volume 2A-2020, Article number V02AT02A039
6. Nesládek M, Španiel M, Jurenka J, Růžička J, Kuželka J, (2012), Fretting fatigue – Experimental and numerical approaches, *International Journal of Fatigue Volume*, **44**, pp 61-73
7. De Pauw J, De Waele W, Hojjati-Talemi R, De Baets P, (2014), On the use of digital image correlation for slip measurement during coupon scale fretting fatigue experiments, *International Journal of Solids and Structures*, **51 (18)**, pp 3058-3066
8. Texier D, Atmani F, Bocher P, Nadeau F, Chen J, Zedan Y, Vanderesse N, Demers V, (2018) Fatigue performances of FSW and GMAW aluminum alloys welded joints: Competition between microstructural and structural-contact-fretting crack initiation, *International Journal of Fatigue*, **116**, pp 220-233
9. Andresen H, Hills D A, Vázquez J, (2019), Closed-form solutions for tilted three-part piecewise-quadratic half-plane contacts, *International Journal of Mechanical Sciences*, **150**, pp 127 - 134
10. Andresen H, (2020) Frictional Half plane contacts in partial slip in the steady state, *DPhil Thesis, Oxford University*
11. Andresen H, Hills D A, Barber J R, Vázquez J, (2020), Steady state cyclic behaviour of a half-plane contact in partial slip subject to varying normal load, moment, shear load, and moderate differential bulk tension, *International Journal of Solids and Structures*, **182 - 183**, pp 156 - 161

Statement of Authorship for joint/multi-authored papers for PGR thesis

To appear at the end of each thesis chapter submitted as an article/paper

The statement shall describe the candidate's and co-authors' independent research contributions in the thesis publications. For each publication there should exist a complete statement that is to be filled out and signed by the candidate and supervisor **(only required where there isn't already a statement of contribution within the paper itself).**

Title of Paper	Measurement of Moment Coupling in Fretting Fatigue Experiments
Publication Status	☑Published □ Accepted for Publication □Submitted for Publication □Unpublished and unsubmitted work written in a manuscript style
Publication Details	Truelove, J. P. J., Hills, D. A., & Blades, L. (2021). Measurement of moment coupling in fretting fatigue experiments. Proceedings of the Institution of Mechanical Engineers, Part C: Journal of Mechanical Engineering Science, 235(24), 7726-7733.

Student Confirmation

Student Name:	James Truelove		
Contribution to the Paper	Preparation of specimens, performing experiments, collection of data and images, use of DIC software to analyze images, analysis of results, writing MATLAB scripts, production of figures, writing manuscript.		
Signature	James P J. Truelove	Date	17/07/23

Supervisor Confirmation

By signing the Statement of Authorship, you are certifying that the candidate made a substantial contribution to the publication, and that the description described above is accurate.

Supervisor name and title: Prof D A Hills		
Supervisor comments James' remarks are accurate. This piece of work was 95% his. Luke is a postdoc and guided but the work was his alone.		
Signature	Date	19th July 2023

This completed form should be included in the thesis, at the end of the relevant chapter.

5 Moment–Normal Load Equivalence

The paper presented in this chapter has been published as: *Truelove, J. P., Hills, D. A., & Blades, L. E. (2023). Flat and rounded contacts: Modelling the effect of a moment with application to fretting fatigue tests. The Journal of Strain Analysis for Engineering Design, 58(2), 91-97.*

In the previous chapter the moment coupling present in one of the pieces of test apparatus in the fretting fatigue laboratory was measured, and a method of removing the effect of the moment based on varying the normal load was derived. The method used was somewhat ad hock and based on the use of an iterative solver, it was therefore felt advantageous to attempt to solve the problem using an analytical method.

Such a method would have applications outside of simply removing the effect of a coupled moment, it would also be possible to use it to simulate the effect of a moment in a rig that does not have independent moment control. This would have great utility on the most recent fretting fatigue rig built in the Oxford laboratory (called the 'cornerstone' rig), which was designed to eliminate moment coupling by having the support structure in the same plane as the contact, and which does not support independent moment control.

In this paper asymptotic methods are applied to the solution for a flat faced punch under combined normal load and moment loading to find a representation of the contact pressure in the region surrounding the edge of contact. From these asymptotic representations of the contact pressure it is possible to find combinations of normal load and moment which create the same local stress field in the sharp edged punch model.

This method is used to calculate pairs of matched loads, which were applied to a half plane model of a rounded punch and the difference between the contact pressures measured. It was found that the model worked extremely well over a wide range of geometries and loads, with both a very large moment and a very narrow punch required for the load combinations to diverge.

The expressions found for matching load pairs are extremely simple, which makes them ideal for use in calculations of test loads, or for direct use in the test control system.

Journal Title
XX(X):1–6
©The Author(s) 2021
Reprints and permission:
sagepub.co.uk/journalsPermissions.nav
DOI: 10.1177/ToBeAssigned
www.sagepub.com/
SAGE

Flat and rounded contacts - modelling the effect of a moment with application to fretting fatigue tests

J. P. J. Truelove[1], D. A. Hills[1] and L. E. Blades[1]

Abstract

The problem of elastic indentation by a punch having the form of a flat front face but with edge rounding, and subject to both a normal load and moment, indenting an elastically similar half-plane is considered. Contact pressure in the neighbourhood of the edges shows a local peak, and the object of the paper is to show how different combinations of normal load and moment can give rise to the same near edge behaviour and peak pressure. The result found is very simple, and of direct practical application in fretting fatigue studies, both analytical and experimental.

Keywords

Fretting fatigue, Contact mechanics, Solid mechanics, Experimental techniques, Contact pressure

Introduction

The most common form of stationary contact we encounter in studies of fretting fatigue is one where the basic geometry of the contact-defining body has the form of a flat face with small radii at the ends. This is the basic shape of the dovetail root of a gas turbine fan blade and also the locking segments found in riser-wellhead connectors. Therefore, in order to obtain the best match of the behaviour of a contact under experimental conditions, that is also the form of the pad we use in laboratory fretting fatigue tests. There are four quantities which are important in defining the contact edge state of stress, including the effects of slip or localised plasticity: these are the normal load, P, and any moment present, M, together with the shear force supported by the contact, Q, and the presence of differential tensions acting parallel with the free surface. In the case of a Hertzian contact (which cannot support a moment) and other contact geometries which are very well represented by half-planes,certian combinations of material properties can result in the problem being uncoupled, such that the first two quantities define the normal problem and the contact pressure distribution while the second two excite shear and therefore encourage frictional slip.

Contacts having the 'flat and rounded' form, Figure 1, may not be particularly well modelled using half-plane theory if the contact extends a significant distance around the corner radius, so that the contact half-width, a, is significantly greater than the flat contact length, b, but the limit $b/a \to 0$ implies a Hertzian contact which *is* represented well by half-planes. There has, so far, been no exhaustive examination of the limitations of the half-plane idealisation for these problems, although Davies[1] undertook a preliminary investigation. In fretting fatigue studies we are concerned primarily with the contact edges, which is where slip occurs and where cracks invariably nucleate, and the purpose of this paper is to undertake an investigation of near-edge conditions in the presence of a moment, and, in particular, to see how the moment modifies the local pressure distribution. Our motivation is to try to find how changes in normal load and moment interact, because we know that the prototypical problems experience a moment, but the test apparatus developed is not capable of applying an independent, controllable moment. On the other hand, in the test apparatus, because the shear force applied to the pad front face develops a moment within the projecting part of the pad, even if we contrive to react out the shear force in the plane of the contact a moment is still present, causing a small rotation and hence modification of the near-edge pressure distribution. This moment has been shown[2] to be proportional to the shear force, and the constant of proportionality between the two seems to be essentially a property of the test apparatus, and to depend only very weakly on normal load. In[2] we showed how the normal load might be varied so as to compensate for this effect, but the procedure used was *ad hoc* and based on a rather complex half plane solution for a three part punch[3], and so here we aim to set out a simple, closed form alternative.

Domain shape of the contact edge

Before we develop the theory itself it will be helpful to look in some detail at the nature of the contact edge and its characteristic form, and in this sense this is a development of the argument made at the beginning of the last paragraph. The geometry under consideration is shown in Figure 2, which shows a close up of the edge of the contact in Figure 1. For simplicity we will assume that the bodies forming the contact have the same elastic properties, with Young's modulus E and Poisson's ratio ν.

[1]University of Oxford, UK

Corresponding author:
Department of Engineering Science, University of Oxford, Parks Road, Oxford, OX1 3PJ, UK
Email: james.truelove@eng.ox.ac.uk

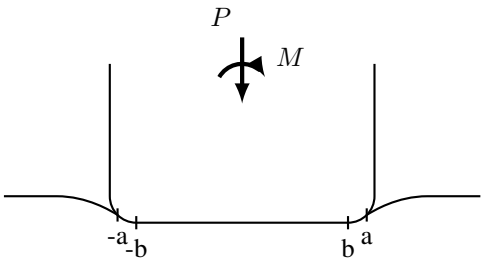


Figure 1. The geometry of a flat and rounded punch, as commonly used in fretting fatigue experiments

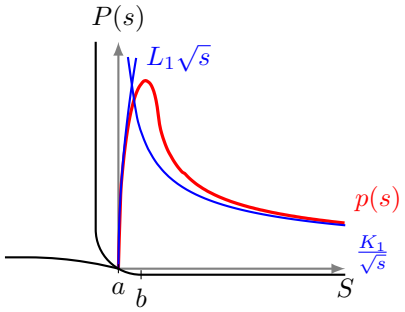


Figure 2. The geometry of the corner of the flat and rounded punch, showing the stress asymptotes

If, first, we zoom very close in to the extreme edge of the contact, each body clearly behaves like a half-plane, and therefore, if we take a coordinate s from the contact edge the contact pressure will vary in the form

$$p(s) = L_I\sqrt{s} \tag{1}$$

where L_I is a constant which may, in principle, be found for any specific contact geometry[4,5].

What we would like to do is to establish an asymptotic form which extends further out from the contact edge but, to do so we should, as a precursor, look at the characteristic from of the solution anticipated when $s \gg a - b$, although not so large that the solution 'feels' the presence of the opposite end of the contact. Refer, again, to Figure 2, but now look at what we might anticipate at remote points. The presence of the rounding will become increasingly irrelevant, and the characteristic solution will be governed by the effects of the half plane free surface together with the free straight surface - here shown as normal to the half-plane, but note that there are other possibilities. If, away from the contact edge the interface is stuck, the relevant domain shape becomes one of a monolithic wedge whose internal angle is the sum of the half-plane plus the contact-defining body, and so, for the problem illustrated, and also for the pads used in the test apparatus, this is a three quarter plane. The Williams solution[6] shows us that the contact pressure and, indeed, all components of stress within the pair of bodies must decay in a power order manner given by

$$\sigma_{ij}\left(r,\theta\right) = K_I r^{\lambda_I - 1} f_{ij}^I\left(\theta\right) \tag{2}$$

where $\lambda_I = 0.5445$, and the eigenvector $f_{ij}^I\left(\theta\right)$is fully specified. Guided by these results Fleury and Hills[4,5] developed a characteristic solution for a rounded quarter plane in partial slip contact with an elastically similar half-plane. One of the principal outcomes of that piece of work was the pressure distribution at the contact edge, and it was shown[7] that this solution could convincingly be used to introduce the effects of rounding to a sharp cornered contact. Although it was never extended to the effects of a moment, that could certainly also be done. But, although this solution is attractive because it is mathematically rigorous, the difficulty in employing it stems from the fact that the first, symmetric, solution (quoted above) and the second term in the series, which is antisymmetric, uncouple along the bisector line, and this means that it is very complicated indeed to make use of in the context of the contact problem because the normal loads and shear loads both excite both eigensolutions.

An earlier attempt to solve the same problem used the half-plane result for the contact pressure distribution induced by the finite flat and rounded punch[8,9] using uncoupled half-plane theory, taking the limit where, separately, $a, b \to \infty$, but where $a - b$ remains finite,[10]. When the limit stated is taken, we find that the contact pressure distribution takes the following form

$$\frac{2\pi R}{E^*}p(s) = 2\sqrt{ds} + (s-d)\,ln\left|\frac{\sqrt{d}-\sqrt{s}}{\sqrt{d}+\sqrt{s}}\right| \tag{3}$$

where $d = a - b$ and R is the radius of the corner rounding. When $s \gg d$ this reduces to the form

$$p(s) = \frac{K_I}{\sqrt{s}} \tag{4}$$

where the asymptotic equivalent of the contact law is

$$\frac{2\pi R}{E^*} = \frac{4\sqrt{d^3}}{3K_I} \tag{5}$$

and hence

$$p(s) = \frac{3K_I}{4\sqrt{d^3}}\left[2\sqrt{ds} + (s-d)\,ln\left|\frac{\sqrt{d}-\sqrt{s}}{\sqrt{d}+\sqrt{s}}\right|\right] \tag{6}$$

Very close to the contact edge, where $s \ll d$ the stress contact pressure will be square root bounded, with form given by equation 1 with

$$L_I \equiv \frac{3K_I}{d}. \tag{7}$$

This is a very attractive, clean, tidy solution *but* it incorporates the result that when the observation point is very remote from the contact edge the pressure decays in a square root manner, equation (4), whereas we expect, from our observations in the last paragraph that it *ought* to decay in the form $p(s) \sim s^{-0.45}$. It is this result which highlights the other possible way, as an alternative to elastically similar bodies, in which the requirement that Dundurs' second constant may be made to vanish. Specifically, if $E_1 \to \infty$ (the contact-defining body becomes rigid) whilst $\nu_2 \to 1/2$, ie the half plane becomes incompressible.

Other properties of the solution may be found. For example, the maximum value of the contact pressure, i.e. the peak in Figure 2, is given by

$$p_{max} = 1.074\left(\frac{K_I^2 E^*}{R}\right)^{1/3}. \tag{8}$$

Sharp edged punch approximation

If the edge radius of the contact-defining body is small compared with the contact half width the geometry of the punch may be approximated by a simple square-ended form, and when this pressed into contact with an elastic half plane by a normal force and clockwise moment the stress intensity factor at the left hand edge is given by [11].

$$K_I = \frac{1}{\pi\sqrt{b}}\left[P - \frac{2M}{b}\right] \tag{9}$$

where K_I is related to the near edge contact pressure by equation (4). It follows directly that, in any two problems, provided the value of this quantity is the same at a contact edge the local contact pressure and attendant stress field will be the same, i.e. if we have two contacts 1 & 2 local pressure will be maintained at the same value provided only that they are made from the same material and have the same edge radius, if

$$P_1 - \frac{2M_1}{b} = P_2 - \frac{2M_2}{b}. \tag{10}$$

Example Results and Comparisons

We will consider now how well the method derived applies to contacts found in practical problems, and the range of loads and geometries over which the solution could be thought of as valid. The semi-infinite solution cannot sense whether the load it is subjected to arises from a normal load or a moment, so in order to see how well the solution applies to a real punch geometry the contact pressure distribution for a finite flat and rounded punch is required. The solution derived by Andresen, Hills, and Vázquez [3] was used, the contact pressure being given by:

$$p(x) = -\frac{\sqrt{(a+x)(c-x)}}{A\pi R}* \left[\frac{(b+x)\log\left(\left|\frac{(a+c)(b+x)}{(c-a)(x-b)+2(ac+bx)+2\sqrt{(a-b)(b+c)(c-x)(a+x)}}\right|\right)}{\sqrt{(a+x)(c-x)}} + \frac{(b-x)\log\left(\left|\frac{(a+c)(b-x)}{(c-a)(b+x)+2(ac-bx)+2\sqrt{(a+b)(c-b)(c-x)(a+x)}}\right|\right)}{\sqrt{(a+x)(c-x)}} + \cos^{-1}\left(\frac{-a+2b+c}{a+c}\right) + \cos^{-1}\left(\frac{a+2b-c}{a+c}\right)\right] \tag{11}$$

Where a and c, the locations of the edge of the contact are found using an iterative solver and the side conditions for normal (equation 12) and rotational (equation 13) equilibrium,

$$\frac{4PA}{(a+c)^2} = -\left(-\frac{\sqrt{(a-b)(b+c)}(-a+2b+c)}{\mathrm{R}(a+c)^2} + \frac{\cos^{-1}\left(\frac{-a+2b+c}{a+c}\right)}{2\mathrm{R}} - \frac{\sqrt{(a+b)(c-b)}(a+2b-c)}{\mathrm{R}(a+c)^2} + \frac{\cos^{-1}\left(\frac{a+2b-c}{a+c}\right)}{2\mathrm{R}}\right) \tag{12}$$

$$\frac{4PAs}{(a+c)^2} = (a-c)* \left(\frac{\sqrt{(a-b)(b+c)}\left(\frac{a^2-2b^2+c^2}{a-c} + \frac{1}{2}(a-2b-c)\right)}{3\mathrm{R}(a+c)^2} - \frac{\sqrt{(a+b)(c-b)}\left(\frac{a^2-2b^2+c^2}{a-c} + \frac{1}{2}(a+2b-c)\right)}{3\mathrm{R}(a+c)^2} + \frac{\cos^{-1}\left(\frac{-a+2b+c}{a+c}\right)}{4\mathrm{R}} + \frac{\cos^{-1}\left(\frac{a+2b-c}{a+c}\right)}{4\mathrm{R}}\right) \tag{13}$$

where s is the eccentricity of the normal load (such that $Ps = M$) and A is given by $A = \frac{4\left(1-\nu^2\right)}{E}$ under conditions of plane strain.

The inputs to the problem can be arranged into three dimensionless groups, $\frac{M}{Pb}$, $\frac{R}{b}$ and $\frac{K_I}{E^*\sqrt{d}}$, one of which defines the geometry of the punch, and two of which define the applied loading. The output contact pressure distribution is normalized by $\frac{K_I}{\sqrt{b}}$, which simply represents the combined magnitude of the moment and normal load.

It is worth noting that equation 9 sets an upper limit on the largest possible value of $\frac{M}{Pb}$. At the right hand edge of the contact separation will occur when the value of K_I becomes negative, which occurs when $\frac{M}{Pb} = \frac{1}{2}$.

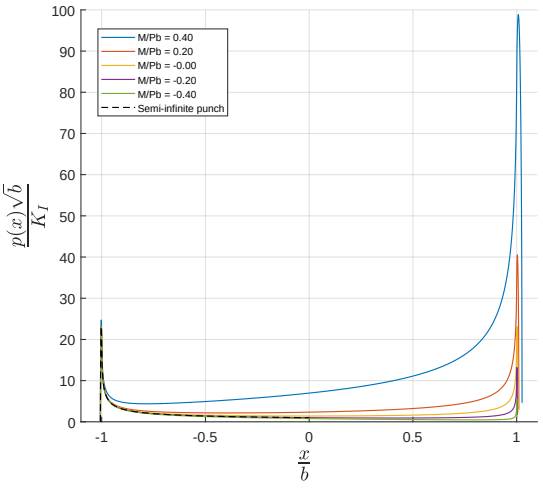


Figure 3. A plot of the contact pressures across the entire contact for various values of $\frac{M}{Pb}$, for $\frac{R}{b} = 0.1$, $\frac{K_I}{E*\sqrt{b}} = 0.001$

Figure 3 shows the contact pressure distribution for a number of moment-normal force loading mixtures, chosen through the use of equation 9 such that they have equivalent values of K_I at the left hand edge of the contact. In this plot the values chosen represent a punch having a geometry defined by $\frac{R}{b} = 0.1$, applied loading of $\frac{K_I}{E*\sqrt{b}} = 0.001$ and various values of loading mixture, $\frac{M}{Pb}$, from 0.4 to -0.4, values which roughly correlate with those that may be found in a typical fretting fatigue test. The figure illustrates clearly the effect of matching moment-normal load pairs: at the

left hand edge of the contact the local contact pressure distributions are almost identical; at the right hand edge they diverge drastically. Note that, although at this scale the contact pressure appears to be singular in character at the peaks in the distribution, these are, in fact, rounded.

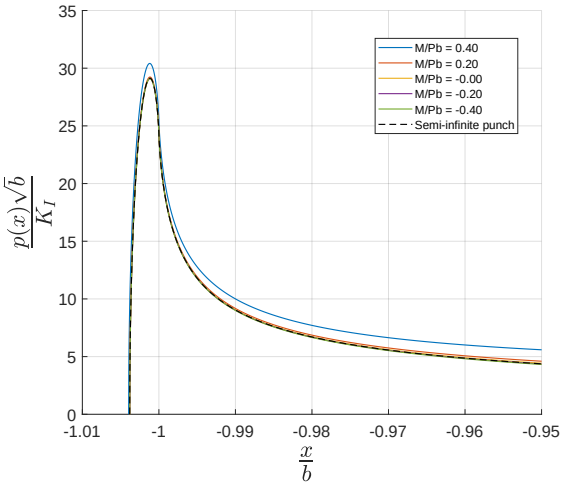


Figure 4. A plot of the contact pressures at the left hand edge of the contact, over a sweep of values of $\frac{M}{Pb}$, for $\frac{R}{b} = 0.1$, $\frac{K_I}{E*\sqrt{b}} = 0.001$

Figure 4 shows the detail of the leftmost edge of the contact pressure distribution, allowing closer inspection of the localised contact pressure in the region surrounding the corner rounding. As in figue 3 the various solid coloured lines are solutions from the finite width punch contact pressure distribution (equation 11), the dashed line represents the semi-infinite flat and rounded punch approximation (equation 6). It can be seen that for the majority of load cases the solutions lie extremely close together, with the plots only starting to diverge at large values of positive moment, due to the left hand edge of the contact sensing the effect of the increased contact pressure at the right hand side of the contact (with the sense of the moment being as drawn in figure 1, such that a positive value of moment causes an increase in contact pressure at the right hand edge of the contact).

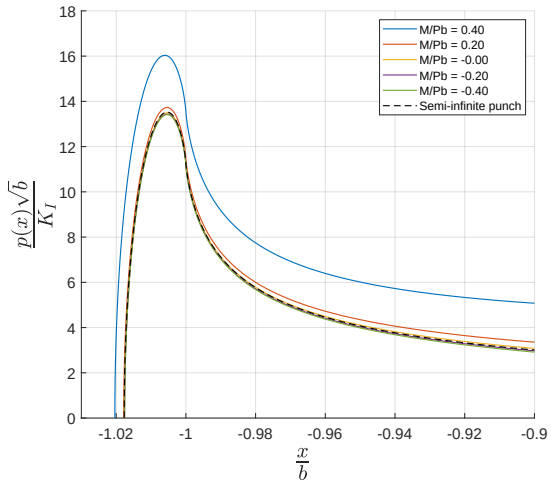


Figure 5. A further example of matching equivalent pairs of P-M loadings, in this plot for the case $\frac{R}{b} = 1$, $\frac{K_I}{E*\sqrt{b}} = 0.0005$,

Another example of the accuracy of the moment matching achievable is shown in figure 5, This time for the rather geometrically extreme case $\frac{b}{R} = 1$. We would intuitively not expect the method described to be valid in this regime as the assumption that the amount of corner rounding is small compared to the half width of the punch is evidently not valid, but as shown in figure 5 the method holds reasonably well, even under these conditions. The deviation with the application of large positive moments is greater than in the previous plot, as the reduced distance between the edges of the contact means that they influence each other to a greater degree.

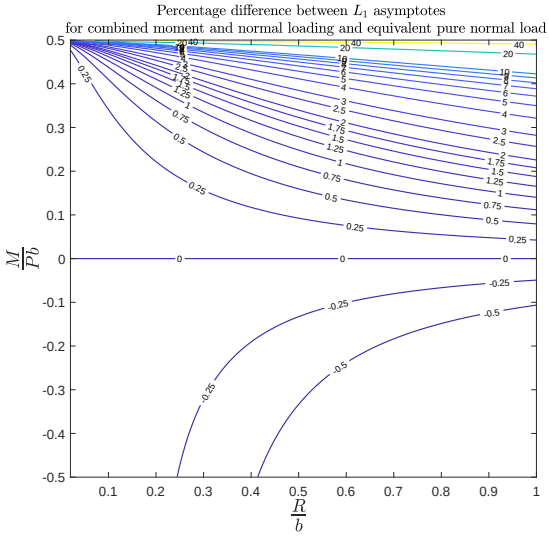


Figure 6. The percentage difference in the outer L_1 asymptotes comparing the moment and normal load problem to the equivalent normal load problem calculated using the method derived in this paper

It would seem a natural next step would be to attempt to quantify the difference between the theoretical semi-infinite pressure distribution and the pressure distribution

for a finite width punch over a range of loading conditions and geometries. Figure 6 shows the results of one method of attempting to measure this change. One way of characterizing the near edge stress field of an incomplete contact is through the use of a square root bounded asymptotic multiplier, L_I. In Figure 6 the value of P is held constant at a value of 1000 N/mm, with corner radius fixed at 1mm and steel like material properties, while the applied moment and contact flat width are varied. For each load/geometry combination the value of L_I is calculated for two load cases, the combination of moment and normal load indicated on the chart, and an equivalent pure normal load, found using equation 10. The percentage difference between these two values of L_I is calculated, naturally the better our model the closer we would expect the values of L_I to be and therefore the closer the equivalent stress fields. Since one of the primary assumptions we have made in this model is that the two ends of the contact are uncoupled and can be analysed independently we would expect good results when there is either significant geometric separation between the two ends of the contact ($b > R$) or when the loads are low enough to prevent the peaks in contact pressure from interfering The contour plot shows that the method found in this paper achieves a good level of agreement across a large range of loads and geometries, with even fairly severe load and geometry combinations producing single digit percentage differences.

Application to Fretting Fatigue Experiments

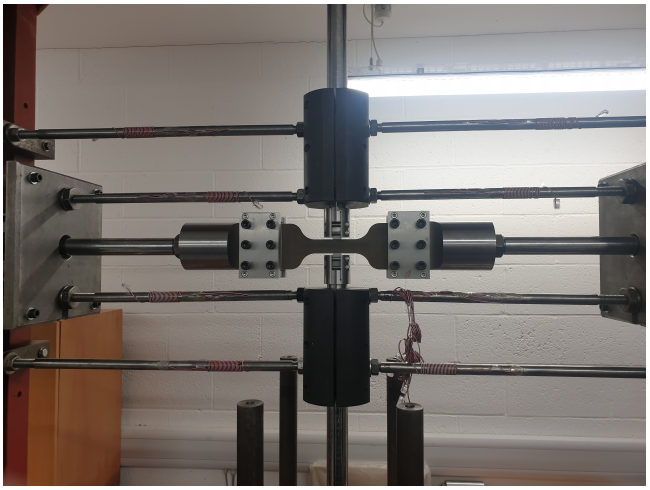


Figure 7. An image of the fort rig, a typical piece of test apparatus used in the study of fretting fatigue phenomenon.

An obvious application of this method is to the study of the effects of moments in fretting fatigue experiments. Figure 7 shows an example of a typical test rig used in Oxford for the study of fretting fatigue problems, and illustrates the typical layout of actuators. A pair of pads bear on a dogbone specimen, a hydraulic actuator at the base of the rig providing normal load. A further pair of actuators to the left and right of the specimen apply loads to it, so through the application of differential loads to each end of the specimen shear loading can be applied. The rig as built has no facilities to apply moments: only the normal load, shear load and bulk tension are controllable, but if a procedure such as the one derived in this paper is used it becomes unnecessary to be able to control the moment directly. Generally there are a couple of situations in which we may wish to account for the presence of a moment in an experiment:

- The study of contacts where the prototype component is loaded with large moments
- To account for the effects of moment coupling phenomenon arising from the design of the apparatus [2]

As an illustrative example let us briefly consider a problem of the second kind.

As described in [2], moment coupling is the generation of an undesired moment across a contact during a fretting fatigue experiment. These moments can arise from a number of sources, including deformation of the test apparatus, and the fact that it is impossible to construct a practical pad with true half plane geometry - the pad must include some form of projection which then deforms as a stubby cantilever under the application of shear load. For the fort rig illustrated in Figure 7 the load paths through the rig are a major source of coupled moments, in that the shear load is supported through leaf springs at a significant distance from the contact.

First, the coupling coefficient between the applied shear force on the pair of pads, Q, and the moment present must be found. One possibility we have successfully used is an optical lever across the width of laboratory, digital image correlation has also been used successfully. This provides k where

$$M = kQ \tag{14}$$

Therefore, through equation 9, if the prototype experiences a load set $(P_p, Q_p, M_p, \sigma_P)$ the loads which must be applied on the test apparatus, P_T, is given by

$$P_T = P_p - \frac{2(M_p - kQ_p)}{b_T}, \tag{15}$$

where b_T is the half-width of contact in the laboratory test.

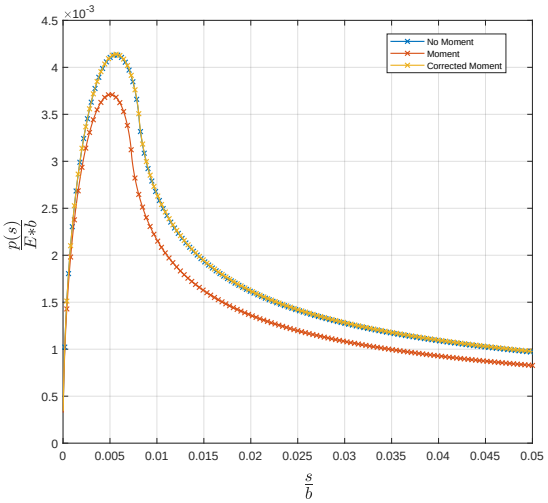


Figure 8. A 3 way comparison between the pressure distribution for a punch with no moment, a punch with a moment applied and a punch with normal load varied in a way such that the effect of the moment is canceled out.

As an example consider figure 8. This represents a case where we wish to run an experiment on a rig with a known amount of moment coupling, but where we would like to run the test under conditions equivalent to a constant normal force loading, i.e. the near edge contact pressure should remain constant throughout the loading cycles. The plot shows three lines; in blue we have the idealised pressure distribution without any moment, whereas in orange we have the pressure distribution that would actually occur at the point in the load cycle where maximum moment occurs, which corresponds to the point of maximum applied shear. Through the use of equation 15 with $M_P = 0$ it is possible to write down the equivalent value of P which will allow us to recover the same contact pressure distribution as the no moment case, shown in Figure 8 in Yellow. It can be seen that the blue and yellow pressure distributions are almost coincident, and so the effect of a moment has been removed on a test rig that does not have moment control. Using this procedure the contact pressure has only been matched at one edge of the contact, however, in most fretting fatigue experiments where a combination of shear and bulk load one end of the pad will be more highly loaded. As such we can predict which end of the pad will experience failure, and therefore we know end of the pad we should control the contact pressure at before the test is started.

Conclusion

In this paper we have described a method of modelling the effect of an applied moment to a flat and rounded punch by adding a local solution for corner rounding to a solution for a sharp ended punch. It was demonstrated that the sharp punch and rounding model approximated a finite flat and rounded punch solution over a range of contact geometries. The solution for a sharp edged punch was therefore used to find a way of connecting equivalent P, M pairs for flat and rounded contacts, and it is shown that this model applies over a wide range of punch geometries and load cases.

In the formulation used here the finite punch solution is an elastically similar elastic-elastic problem, whereas the square edged punch formulation uses a rigid punch on an incompressible half plane. Both these formulations result in Dundur's second parameter being equal to zero, so that the normal and tangential problems are uncoupled and the application of normal loading does not generate shear tractions across the contact interface.

The method outlined in this paper has practical application to fretting fatigue experiments, allowing for both the addition and removal of equivalent moments from experiments while using rigs that do not have facilities to control moment loading.

References

1. Davies M. Studies in contact mechanics with reference to fretting fatigue of gas turbine blade/disc attachments, 2012, D.Phil thesis, University of Oxford
2. Truelove J Hills DA and Blades LE. Measurement of Moment Coupling in Fretting Fatigue Experiments, *Journal of Proceedings of the Institution of Mechanical Engineers, Part C: Journal of Mechanical Engineering Science*, **235(24)**, 2021, pp. 7726-7733
3. Andresen H Hills DA and Vázquez J. Closed-form solutions for tilted three-part piecewise-quadratic half-plane contacts, *International Journal of Mechanical Sciences*, **150**, 2019, pp. 127-134
4. Fleury RMN Hills DA and Barber JR. A corrective solution for finding the effects of edge-rounding on complete contact between elastically similar bodies. Part I: Contact law and normal contact considerations, *International Journal of Solids and Structures*, **85–86**, 2016, pp. 89-96
5. Fleury RMN Hills DA and Barber JR. A corrective solution for finding the effects of edge-rounding on complete contact between elastically similar bodies. Part II: Near-edge asymptotes and the effect of shear, *International Journal of Solids and Structures*, **85–86**, 2016, pp. 97-104
6. Williams ML. Stress singularities resulting from various boundary conditions in angular corners of plates in extension, *ASME Journal of Applied Mechanics*, **19**, 1952, pp. 526-528
7. Hills DA Ramesh R Fleury RMN and Parel K. A unified approach for representing fretting and damage at the edges of incomplete and receding contacts, *Tribology International*, **108**, 2017, pp. 16-22
8. Ciavarella M Hills DA and Monno G. The influence of rounded edges on indentation by a flat punch. *Proceedings of the Institution of Mechanical Engineers, Part C: Journal of Mechanical Engineering Science*, **212(4)**, 1998, pp. 319–327
9. Steuerman I. Contact Problem of the Theory of Elasticity. *Gostekhteoretizdat, Moscow*, 1949
10. Sackfield A Mugadu A Barber JR and Hills DA. The application of asymptotic solutions to characterising the process zone in almost complete frictionless contacts, *Journal of the Mechanics and Physics of Solids*, **51**, 2003, pp 1333 – 1346
11. Sackfield A Truman CE and Hills DA. The tilted punch under normal and shear load (with application to fretting tests), *International Journal of Mechanical Sciences*, **43**, 2000, pp. 1881–1892

Acknowledgements

James Truelove acknowledges with thanks the award of an iCASE award ref 17000027 from Rolls-Royce plc which has enabled him to carry out this work.

David Hills and Luke Blades acknowledge Rolls-Royce plc and the EPSRC for their support under the Prosperity Partnership Grant: "Cornerstone: Mechanical Engineering Science to Enable Aero Propulsion Futures", Grant Ref: EP/R004951/1.

Statement of Authorship for joint/multi-authored papers for PGR thesis

To appear at the end of each thesis chapter submitted as an article/paper

The statement shall describe the candidate's and co-authors' independent research contributions in the thesis publications. For each publication there should exist a complete statement that is to be filled out and signed by the candidate and supervisor **(only required where there isn't already a statement of contribution within the paper itself).**

Title of Paper	Flat and rounded contacts – modelling the effect of a moment with application to fretting fatigue tests
Publication Status	☑Published □ Accepted for Publication □Submitted for Publication □Unpublished and unsubmitted work written in a manuscript style
Publication Details	Truelove, J. P., Hills, D. A., & Blades, L. E. (2023). Flat and rounded contacts: Modelling the effect of a moment with application to fretting fatigue tests. The Journal of Strain Analysis for Engineering Design, 58(2), 91-97.

Student Confirmation

Student Name:	James Truelove		
Contribution to the Paper	Writing of MATLAB scripts, production of figures, analysis of results, writing of manuscript.		
Signature	James P J. Truelove	Date	17/07/23

Supervisor Confirmation

By signing the Statement of Authorship, you are certifying that the candidate made a substantial contribution to the publication, and that the description described above is accurate.

Supervisor name and title: Prof D A Hills		
Supervisor comments: What James writes is true but he also got fully to grips with all the arguments and materially contributed to the application of the basic idea.		
Signature	Date	19th July 2023

This completed form should be included in the thesis, at the end of the relevant chapter.

6 Fretting Fatigue Experiments with Single Crystal Pads

In the turbine sections of a turbofan engine the turbine blades are often constructed from single crystal materials in order to improve their creep properties at the high temperatures present in the engine. These blades are typically fitted into a forged, polycrystalline hub with 'fir tree' or 'dovetail' connections.

During engine operation these contacts will experience fretting damage, arising from the vibrations of the fan blades and the varying centripetal force on the fan blades as the engine accelerates and decelerates. This can result in fretting fatigue induced cracking in the hub or the blades, a failure mode that has the potential to cause catastrophic damage to the engine.

The orientation of the crystal structure is controlled in only one direction, meaning that the orientation of the crystal structure in the contact varies significantly between different blades of the engine. Understanding the effect of crystal orientation on the life of the blade may therefore allow for the life of these contacts to be extended by simply controlling the orientation of the other axes of the crystal structure.

A few previous experiments in Oxford have involved the use of pads made from single crystal material in contact with polycrystaline specimens, although none of them were conducted in such a way that the effect of crystal orientation can easily be isolated. In the fist set of experiments the primary variable being investigated was the effect of contact geometry, and no attempt was made to control the orientation of the crystal structure. In later tests a number of properties were investigated during the tests including load ranges and the effect of elevated temperature, making isolation of just the effect of crystal orientation difficult.

In the following paper we therefore describe a series of experiments performed on the fort rig at the university of oxford with the intention of rigorously investigating whether the orientation of the crystal structure in single crystal pads has any effect on the fretting fatigue life of the resulting contact.

Fretting Fatigue Experiments with Single Crystal Pads

James Truelove, Luke Blades, David Hills, Robert Paynter

October 2022

Abstract

A series of experiments investigating the effect of crystal orientation on fretting fatigue life are described, and the results are presented. The trends found in previous work do not appear to hold in this investigation and the fretting life of the contact does not appear to vary with crystal angle, though several interesting trends were noted.

1 Introduction

The possible influence of Crystal orientation on the life of fretting contacts was first detected at Oxford in a series of experiments performed by Sarsfield, originally intended to investigate the effect of contact geometry on fatigue life [1]. In this experiment single crystal CMSX4 pads with various contact geometries were used in conjunction with Udimet 720Li specimens to investigate the difference in fatigue life between Hertzian and flat and rounded geometries. It was found, however, that no difference in fatigue life was detectable due to an enormous amount of scatter in the results. Performing repeat experiments using refinished pads showed that this reduced the scatter to expected levels, leading to suggestions that the orientation of the crystal structure was controlling the fatigue life in these experiments.

Those experiments were later re-analysed by Fleury [2], who used the conical indenter method developed by Huang et al [3] to measure the orientation of the crystal structure in the pads. His results, reproduced in Figure 1, appear to indicate a strong correlation between fretting fatigue life and the pad crystal orientation. The quality of these results was limited, however, by the experimental data available; the original experiments by Sarsfield used a variety of different geometries and loads, and no effort was made to control the orientation of the crystal structure. This resulted in only a very small number of results being directly comparable, a number of which were repeats, and necessitated the use of averaging the angle in the pads, as they were not the same in each pad.

The aim of this sequence of experiments was to investigate thoroughly whether the fatigue life of a contact depends upon the orientation of the crystal structure in the contacting pads and whether the trends observed by Fleury hold up under further investigation. To this end a series of 98 experiments have been performed using CMSX4 single crystal pads and inconel 718 specimens, where the specimen geometry and load cycle has been kept constant, but the crystal orientation within the pad varied.

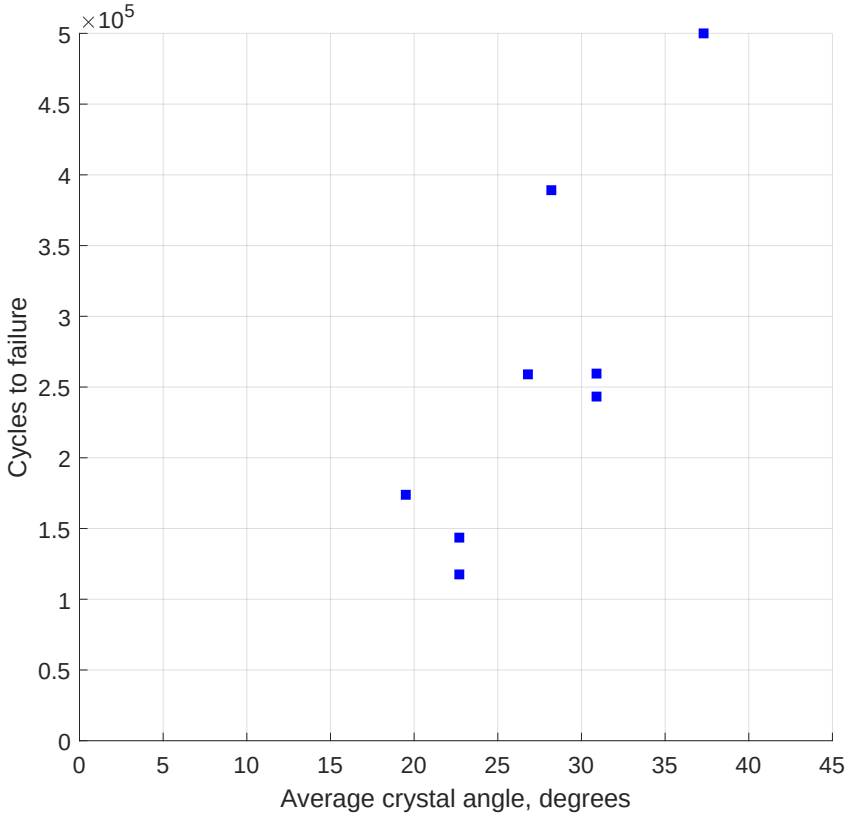
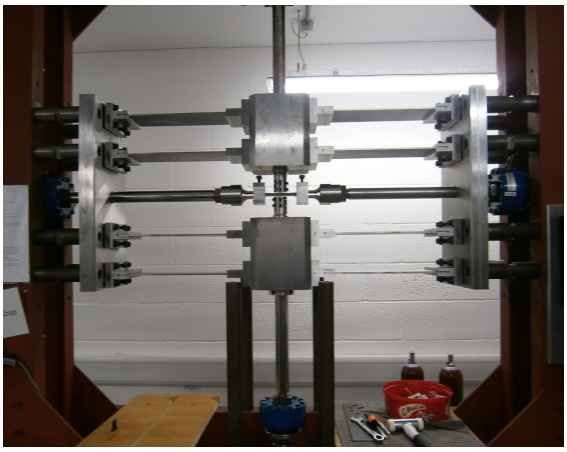


Figure 1: Variation in fretting fatigue life with crystal angle, Fleury [2].

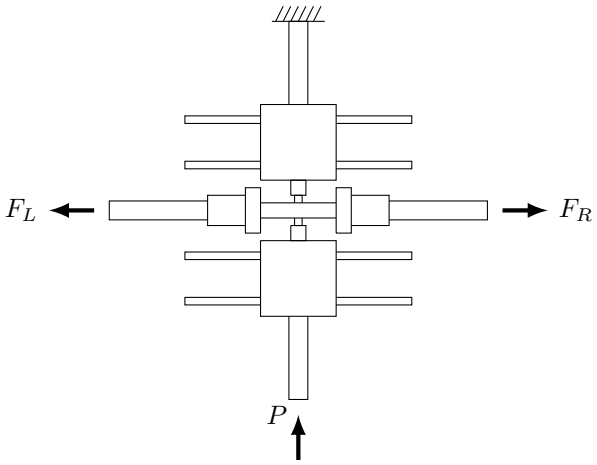
2 Experimental Setup

2.1 Experimental Apparatus

The experiments were performed on the fort rig, a three actuator fretting fatigue rig located at the University of Oxford. An image of the rig is shown in figure 2a, and a diagram of the rig showing the load paths is shown in figure 2a. Actuators to the left and right of the rig apply bulk tension and shear by applying loads F_L and F_R, while an actuator at the bottom of the rig controls the normal load P. Plate springs support the applied shear load at the pads while allowing the pad supporting rods and blocks to move vertically in response to the action of the bottom actuator. All three actuators are equipped with Kelsey K7500 servo controllers using cubus control software, which allow for independent control of load waveforms, amplitude and phase.



(a) An image of the fort rig, in the configuration used in these experiments.



(b) A schematic diagram of the fort rig, showing the application of the loads.

2.2 Specimen Material, Geometry and Loads

The specimens were manufactured from inconel 718, which was heat treated to the same specifications used by Rolls-Royce. Specimens has a nominal gauge section of 10mm by 10mm, though some were significantly smaller due to a mistake in manufacturing: due to this all specimens were measured with a micrometer prior to use and the applied loads adjusted accordingly. The specimens are attached to the rig via serrated grips to avoid fatigue at the connection points. Specimens were manufactured by first wire EDM machining the basic shape of the specimen and serrations, then surface grinding the fretting surfaces. Following the first few tests it was noticed that plain fatigue cracks were appearing from the surface roughness present on the sides of the specimen, and so in later specimens the sides were refinished.

The pads were made from single crystal CMSX4, supplied by Rolls-Royce in the form of 1/2" diameter cast bars. One axis of the crystal structure was roughly aligned with the axis of the bar while the orientation of the other two axis were uncontrolled. Flats were machined on the material to provide a clamping surface for the pad holders, and the contacting surface was ground to for a Hertzian contact with a 100mm radius cylindrical profile.

The apparatus used allows for independent control of the applied normal load, P, Shear load, Q and bulk tension σ. In the experiments performed here normal load is kept constant and the bulk tension and shear cycled with a sinusoidal waveform. Shear loads are fully reversing. The values given in the following tables are for total shear, this value is halved to find the shear load applied to each pad. The normal load initially used was 38kN, but this was reduced to 19kN after a small number of tests due to the edge of contact being extremely close to the edge of the pad. Values of shear load and bulk tension were found by running a number of trial experiments, adjusting the loads until the tests lasted for approximately 600,000 cycles - a test length that allows us to see variation in the initiation life but with little risk of the tests running out. The values arrived at were no shear load, and a bulk tension varying between 535 and 75MPa.

2.3 Crystal Orientation

The orientation of one of the axes of the crystal structure was measured by Rolls-Royce prior to delivery. Using X-Ray crystallography the orientation of the axis parallel to the length of the stock was measured, and the cone angle noted. To measure the orientation of the remaining two axes the conical indenter method developed by

huang et al [3] was used. A circular conical indenter is pressed into the material, but due to the variation in mechanical properties with rotation of a crystal structure a square indent is produced. An example of a typical indent is shown in figure 3, the two axes of the crystal structure are aligned with the edges of the square.

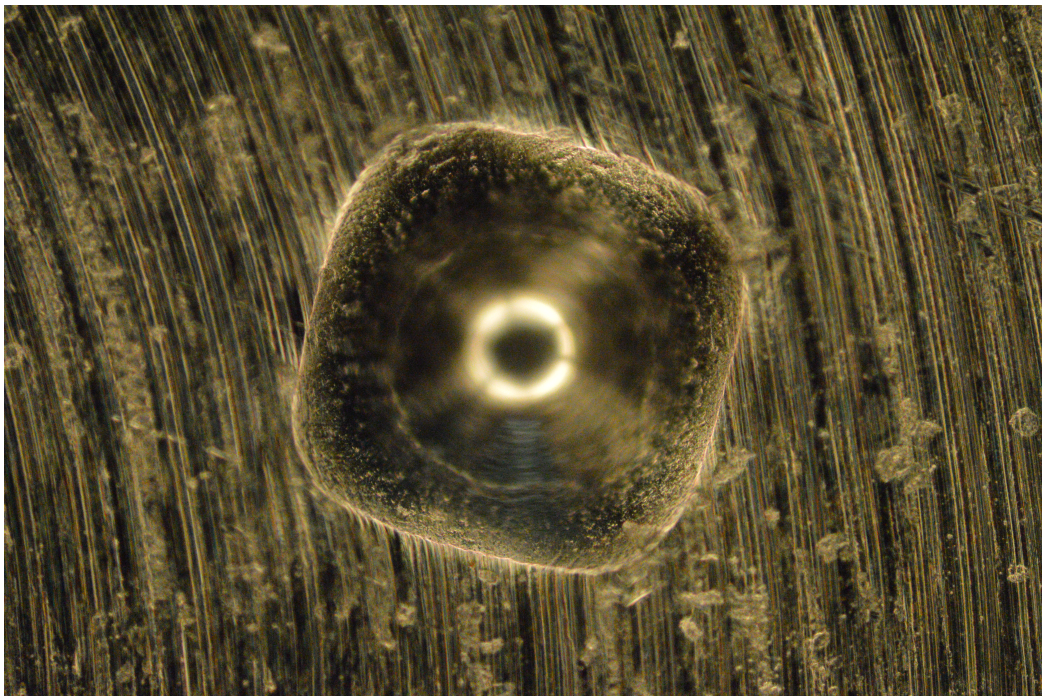


Figure 3: An example of the square indent left by indentation with a circular conical indenter. The crystal axes are aligned with the edges of the square

The initial plan was to manufacture pads with the crystal aligned in increments of 5 degrees. As the crystal structure is cubic it has 45 degree symmetry, this would allow us to investigate the whole range of possible crystal structures from 0 to 45 degrees with 10 tests. Three repeats at each orientation were planned, to allow any life effects due to variation in cone angle to be averaged out, for a total of 30 pairs of pads. To this end an index mark was made on each specimen, the orientation measured to that index mark, then the pads machined so that the crystal structure in the pads were in the orientation desired. Each pair of pads was made as one unit from a single piece of CMSX4 before being cut in two, producing two pads with identical orientation. Unfortunately due to a mistake in the manufacturing process the orientation of the crystal structure did not end up as planned, the actual orientation of the crystal was therefore measured after manufacturing.

Two series of experiments were performed. The first of these aimed to expand the results obtained by Sarsfield, and as such the orientation of the crystal was chosen to match. The [100] axis was aligned along the axis of the pad so that it was normal to the fretting contact (to within the accuracy of the cone angle). The [010] and [001] axes were in the same plane of the contact, and the angle between the axis and the direction of fretting, θ, was varied.

For the second series of tests the pad were rotated through 90 degrees, so that the pads were effectively on their side compared to the previous tests. The [100] axis was concentric with the cylindrical face of the contact, and the [010] and [001] axes were co-planar to the edge of the pad. Again the angle θ was measured relative to the direction of fretting.

3 Results

3.1 Repeatability Tests

Before beginning the experiments proper a series of 11 initial repeatability tests were performed using steel EN24T specimens and pads. The aim of these tests was to find a baseline level of repeatability for the experiments, to allow an experimental procedure to be defined, and to allow some baseline loads to be found. The results of these initial tests is presented in the following table.

Test No.	Pad Load (kN)	Shear load (Kn)	Max Bulk Tension (MPa)	Min Bulk Tension (MPa)	Cycles to Failure	Notes
1	14	5	530	40	374,816	
2	14	5	530	40	408,261	
3	14	5	530	40	367,286	
4	14	5	530	40	464,390	
5	14	5	530	40	314,390	
6	14	5	380	40	1,110,386	
7	14	5	380	40	2,000,000	run out
8	14	5	455	40	200,789	Same specimen as 7
9	14	5	455	40	796,387	
10	14	5	455	40	591,189	
11	14	5	455	40	586,766	

3.2 Test Series 1, Fretting on End of Pad

The results for the first series of tests, those where the [100] axis of the crystal was normal to the contact, are given below. Tests 1 to 3 were performed using polycrystaline inconel 718 pads to give a baseline fatigue life and a measure of repeatability, tests 65 through 67 performed the same function, but at adjusted loads. Tests 2 through 7 were performed at gradually reducing loads, to try to increase the life to approximatley 600,000 cycles. Tests 1 through 19 used specimens with sides having a raw wire EDM machined finish, later tests had milled sides after a couple of tests were noted to be failing in plain fatigue at the neck, rather than in fretting fatigue at the contact. The first set of grips produced turned out to be undersized, and failed in fatigue during test 15, it is suspected that the failure of test 14 in the incorrect location may have been caused due to partial failure of the grips. Three power cuts occurred during these tests, two of these resulted in the cycle count having to be estimated from the test run time while for the final one the cycle count was lost.

Test No.	Specimen ID	Crystal Cone angle (degrees)	Crystal angle, θ	Cross Sectional Area (mm^2)	Normal Load (kN)	Shear load (Kn)	Max Bulk Tension (MPa)	Min Bulk Tension (MPa)	Test Frequency (Hz)	Cycles to Failure	Notes
1	Polycrystaline	-	-	98.36	38	13.00	535	75	10	104,109	
2	Polycrystaline	-	-	98.39	38	13.00	535	75	10	109,961	
3	Polycrystaline	-	-	97.97	38	12.98	535	75	10	117,962	
4	01041 ZZ5	5	27.8	100.09	38	12.99	535	75	10	68,921	Stopped at 10k cycles
5	01040 ZZ3	3	10.9	99.73	38	12.98	535	75	10	83,422	Pads misaligned
6	01040 ZZ1	1	5.0	100.29	38	13.01	535	75	10	113,023	Slipped during setup
7	01038 ZZ7	7	34.3	100.26	38	13.00	535	75	10	55,119	
8	01040 ZZ10	10	44.2	100.30	19	10.03	535	75	10	83,074	
9	10140 ZZ10	10	5.0	100.11	19	5.00	535	75	10	69,507	
10	01038 ZZ6	6	31.3	100.86	19	0	535	75	10	163,944	
11	01038 ZZ6	6	43.4	101.15	19	0	535	75	10	461,074	
12	01041 ZZ5	5	12.8	100.22	19	0	535	75	10	491,363	
13	01043 ZZ4	4	17.5	100.24	19	0	535	75	10	289,465	
14	01043 ZZ4	4	9.6	99.79	19	0	535	75	10	523,922	Failed at serrations
15	01040 ZZ1	1	19.3	100.09	19	0	535	75	10	57,213	Grips broke during test
16	01038 ZZ7	7	9.9	100.03	19	0	535	75	10	310,869	
17	01042 ZZ10	10	8.7	100.76	19	0	535	75	10	433,708	Failed at neck
18	01042 ZZ10	10	29.2	99.59	19	0	535	75	10	444,456	
19	10141 ZZ4	4	1.1	100.05	19	0	535	75	10	565,829	Failed at neck
20	01041 ZZ4	4	16.4	99.30	19	0	535	75	10	701,255	
21	01040 ZZ7	7	19.4	98.85	19	0	535	75	10	421,716	
22	01041 ZZ3	3	21.6	99.01	19	0	535	75	10	437,716	
23	01041 ZZ3	3	8.2	98.89	19	0	535	75	10	1,138,664	
24	01041 ZZ3	3	19.8	99.05	19	0	535	75	10	662,751	
25	01041 ZZ3	3	1.2	99.49	19	0	535	75	10	723,473	
26	01038 ZZ11	11	15.6	98.89	19	0	535	75	10	439,547	
27	01038 ZZ11	11	44.6	99.51	19	0	535	75	10	586,394	
28	01041 ZZ2	2	18.6	99.19	19	0	535	75	10	502,570	
29	01040 ZZ2	2	9.3	99.06	19	0	535	75	10	698,474	
30	01039 ZZ5	5	6.2	99.27	19	0	535	75	10	660,106	

31	01041 ZZ13	13	42.7	99.05	19	0	535	75	10	431,987	
32	01041 ZZ13	13	19.9	102.30	19	0	535	75	10	295,705	
33	01039 ZZ5	5	10.5	98.81	19	0	535	75	10	390,316	Cycle count estimated
34	01043 ZZ4	4	17.5	99.70	19	0	535	75	10	714,212	
35	01041 ZZ5	5	12.8	99.10	19	0	535	75	10	406,355	
36	01038 ZZ7	7	9.9	99.26	19	0	535	75	10	549,135	
37	01040 ZZ3	3	21.6	97.27	19	0	535	75	10	468,717	
38	01041 ZZ2	2	18.6	96.26	19	0	535	75	10	545,760	
39	01040 ZZ7	7	8.2	96.64	19	0	535	75	10	473,460	Cycle count estimated
40	01040 ZZ3	3	10.9	97.24	19	0	535	75	10	422,363	
41	01041 ZZ3	3	1.2	97.79	19	0	535	75	10	448,404	
42	01041 ZZ2	2	9.3	96.53	19	0	535	75	10	456,741	
43	01041 ZZ4	4	16.4	96.59	19	0	535	75	10	518,677	
44	01041 ZZ13	13	19.9	98.09	19	0	535	75	10	381,291	
45	01041 ZZ13	13	42.7	96.72	19	0	535	75	10	537,461	
46	01041 ZZ3	3	19.8	97.46	19	0	535	75	10	514,613	Failed in plain fatigue
47	01041 ZZ5	5	27.8	96.98	19	0	535	75	10	797,810	
48	01038 ZZ11	11	15.6	96.82	19	0	535	75	10	358,850	
49	01038 ZZ7	7	9.9	96.65	19	0	535	75	10	532,705	
50	01041 ZZ4	4	16.4	97.34	19	0	535	75	10	483,015	
51	01040 ZZ7	7	8.2	96.44	19	0	535	75	10	522,415	
52	01041 ZZ3	3	1.2	97.00	19	0	535	75	10	528,777	
53	01041 ZZ5	5	11.8	97.37	19	0	535	75	10	652,914	
54	01040 ZZ3	3	21.6	96.64	19	0	535	75	10	618,392	
55	01040 ZZ3	3	10.9	97.08	19	0	535	75	10	568,085	
56	01041 ZZ2	2	9.3	98.06	19	0	535	75	10	411,595	
57	01043 ZZ4	4	17.5	96.04	19	0	535	75	10	599,995	
58	01041 ZZ4	4	1.1	96.75	19	0	535	75	10	620,412	
59	01038 ZZ7	7	34.3	95.66	19	0	535	75	10	455,361	
60	01042 ZZ10	10	9.6	96.81	19	0	535	75	10	787,906	
61	01042 ZZ10	10	29.2	96.84	19	0	535	75	10	836,358	
62	01042 ZZ10	10	8.7	97.51	19	0	535	75	10		Power cut during test
63	01038 ZZ6	6	43.4	97.51	19	0	535	75	10		Reused specimen, failed at old contact
64	01037 ZZ6	6	31.3	96.49	19	0	535	75	10	526,870	
65	Polycrystaline	-	-	96.82	19	0	535	75	10	654,145	
66	Polycrystaline	-	-	95.33	19	0	535	75	10	387,356	Moved during test
67	Polycrystaline	-	-	94.41	19	0	535	75	10	436,519	

The results of these tests, cycles to failure as a function of crystal angle, are plotted in figure 4. Due to the mistake made in manufacturing the data points are much more concentrated in the bottom half of the range, but data is still available over the entire range of 45 degrees.

The trend observed by Fleury does not appear to be present in the data, there is no observable variation in fatigue life as a function of crystal orientation. There is, however a significant amount of scatter present, with most experiments having lives in the range of approx 300,000 to 800,000 cycles.

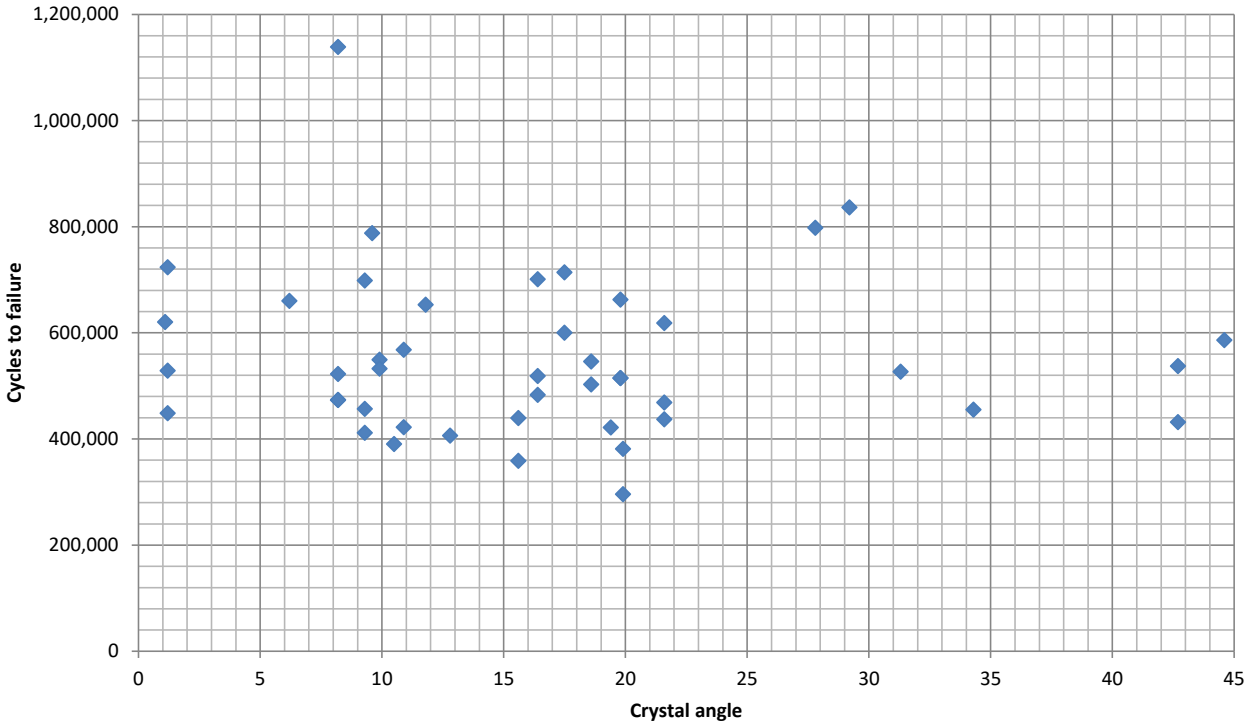


Figure 4: Variation in fretting fatigue life with crystal angle.

In figure 5 the same results are reproduced, but this time the points are coloured to show the single crystal specimens that the pads were made from. A number of interesting features are apparent, firstly it can be seen that repeat tests using the same pairs of pads appear to have fairly good repeatability. Secondly it appears that tests performed using different pads cut from the same specimen appear to have similar lives, even if the angle in those pads are radically different. All three experiments using pads made from specimen 01038 ZZ7 appear to have roughly the same life for example, even though 2 had the crystal oriented at 10 degrees, and one was oriented at 35 degrees. Experiments using pads made from sample 01041 ZZ13 have consistently low lives, while those made from 01043 ZZ4 have longer ones. This suggests that some feature of the single crystal specimens is controlling fatigue life, but that this feature does not correlate with the orientation of the crystal structure.

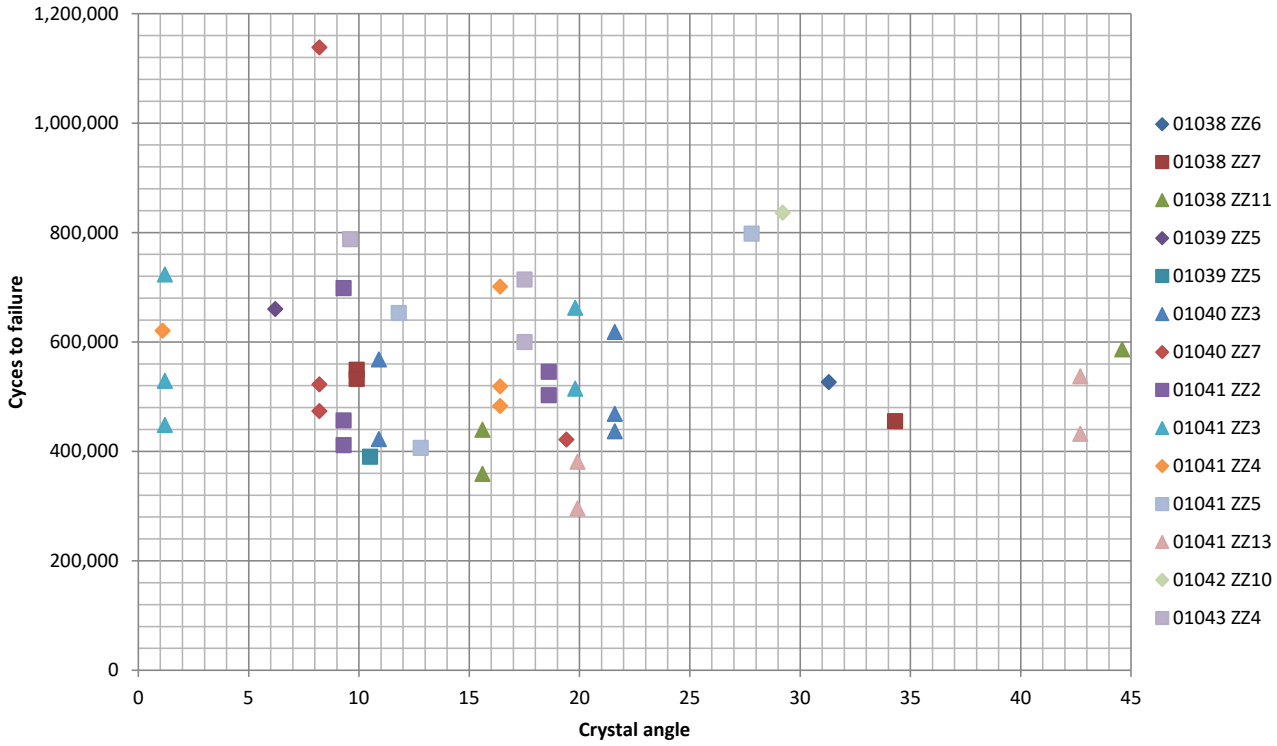


Figure 5: Variation in fretting fatigue life with crystal angle, with samples of material identified.

3.3 Test Series 2, Fretting on Side of Pad

For this second series of tests the pads were rotated through 90 degrees, so that the contacting surface was effectively on the side of the original pads. Tests 68 through 71 were performed at varying loads to find a load case that produced a reasonable fatigue life. Test 83 stopped at 110k cycles, and was restarted. During test 90 the hydraulic pump failed, and carelessness with repressurisation caused damage to the pad holding assembly which resulted in invalid results for the next two tests.

Test No.	Specimen ID	Crystal Cone angle (degrees)	Crystal angle, θ	Cross Sectional Area (mm^2)	Normal Load (kN)	Shear load (Kn)	Max Bulk Tension (MPa)	Min Bulk Tension (MPa)	Test Frequency (Hz)	Cycles to Failure	Notes
68	01041 ZZ5	5	12.8	99.83	15	0	320	45	10	2,000,000	Run out
69	01041 ZZ5	5	12.8	99.83	19	0	340	40	10	1,527,372	Same specimen as 68
70	01038 ZZ11	11	44.6	99.51	19	0	360	40	10	933,361	
71	01041 ZZ4	4	16.7	99.64	19	0	375	40	10	1,027,922	Pad misaligned
72	01038 ZZ6	6	43.4	99.77	19	0	400	40	10	699,622	
73	01041 ZZ5	5	17.8	100.87	19	0	400	40	10	744,621	
74	01038 ZZ11	11	15.6	100.08	19	0	400	40	10	683,295	
75	01040 ZZ7	7	9.4	99.81	19	0	400	40	10	861,170	
76	01038 ZZ7	7	9.9	100.39	19	0	400	40	10	649,170	
77	01042 ZZ10	10	8.7	99.99	19	0	400	40	10	716,068	
78	01040 ZZ3	3	10.9	100.17	19	0	400	40	10	888,030	
79	01039 ZZ5	5	10.5	100.52	19	0	400	40	10	621,890	
80	01041 ZZ13	13	19.9	100.14	19	0	400	40	10	719,901	
81	01041 ZZ3	3	19.9	99.70	19	0	400	40	10	758,236	
82	01041 ZZ13	13	42.7	100.32	19	0	400	40	10	729,901	
83	01042 ZZ10	10	29.2	100.66	19	0	400	40	5/10	703,309	Stopped at 110k
84	01040 ZZ10	10	44.2	99.84	19	0	400	40	5	729,238	
85	01040 ZZ3	3	21.6	100.33	19	0	400	40	10	633,450	
86	01038 ZZ6	6	31.3	100.09	19	0	400	40	10	878,065	
87	01040 ZZ1	1	19.3	99.89	19	0	400	40	10	630,132	
88	01040 ZZ7	7	8.2	100.06	19	0	400	40	10	577,144	
89	01041 ZZ2	2	18.6	100.84	19	0	400	40	10	641,412	
90	01038 ZZ7	7	34.3	100.38	19	0	400	40	10		Pump failed
91	01041 ZZ10	10	5.0	100.20	19	0	400	40	10	386,235	Pad misaligned
92	01043 ZZ4	4	17.5	99.78	19	0	400	40	10	359,786	Pad misaligned
93	01041 ZZ3	3	1.2	100.64	19	0	400	40	10	586,889	
94	01041 ZZ4	4	1.1	100.12	19	0	400	40	10	520,492	
95	01043 ZZ4	4	9.6	99.99	19	0	400	40	10	743,323	
96	01039 ZZ5	5	6.2	100.24	19	0	400	40	10	611,529	
97	01040 ZZ1	1	5.0	100.47	19	0	400	40	10	578,720	
98	01041 ZZ2	2	9.3	100.20	19	0	400	40	10	606,477	

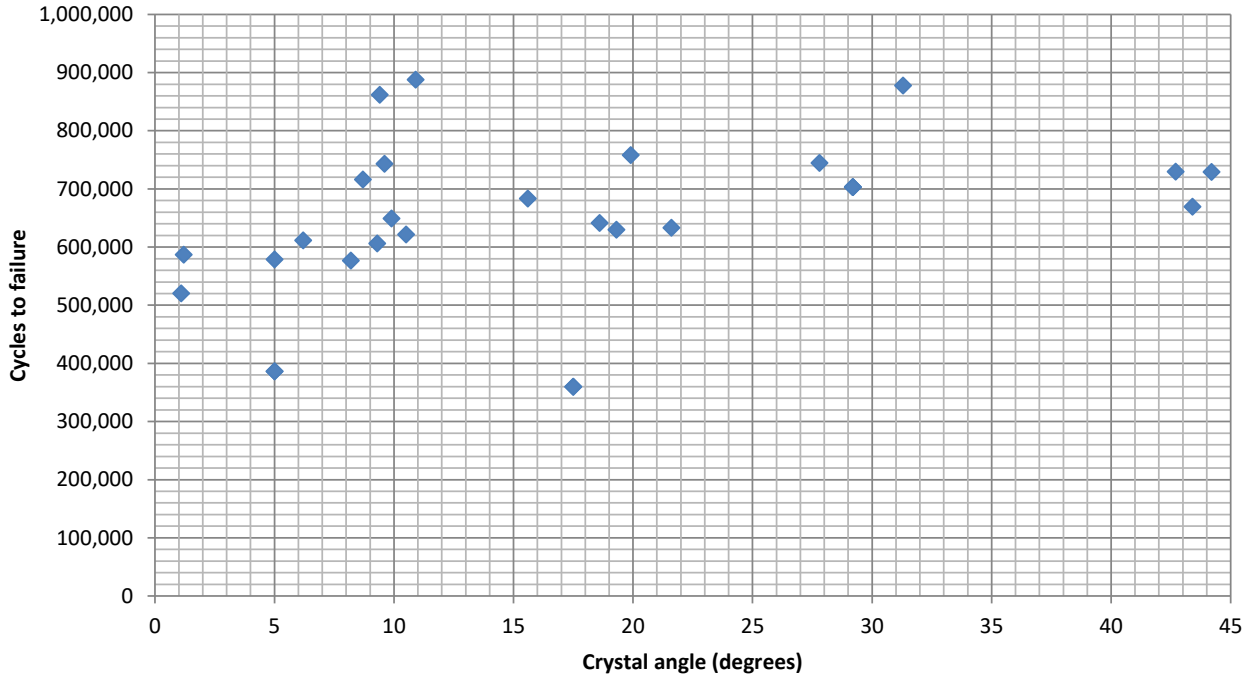


Figure 6: Variation in fretting fatigue life with crystal angle.

The results are plotted in figure 6. Just like the first series of experiments no trend is discernible in these results - fatigue life appears to be independent of crystal angle. There is, however, seemingly less scatter in the results than there was in the first series of results, with most experiments seeming to have lives between 550,000 and 800,000 cycles.

4 Conclusion

In this report we have described a series of tests designed to investigate the effect of crystal orientation of fatigue life in a fretting contact. Previous studies had suggested that the effect of orientation played a significant role in failure. In this investigation no trend linking fatigue life to the orientation of the crystal structure was found. It was found, however, that there is a significant amount of scatter in the results, and that variations in life exist when swapping between nominally identical samples of single crystal material. These results suggest that some other property of single crystal material is controlling the fretting life of these contacts, though what this property is is not obvious from these results.

References

[1] H. Sarsfield, "Fretting fatigue tests on udimet 720li with single crystal cmsx4 pads," Tech. Rep. 250, University of Oxford, 2008.

[2] R. Fleury, *Investigation of fretting fatigue in turbine fir tree blade to disc joints at high temperature.* PhD thesis, University of Oxford, 2015.

[3] X. Huang, T. Gibson, M. Zhang, and R. Neu, "Fretting on the cubic face of a single-crystal ni-base superalloy at room temperature," *Tribology International*, vol. 42, no. 6, pp. 875–885, 2009.

5 Acknowledgements

James Truelove acknowledges with thanks the award of an iCASE award ref 17000027 from Rolls-Royce plc which has enabled him to carry out this work.

David Hills and Luke Blades acknowledge Rolls-Royce plc and the EPSRC for their support under the Prosperity Partnership Grant "Cornerstone: Mechanical Engineering Science to Enable Aero Propulsion Futures", Grant Ref: EP/R004951/1.

Statement of Authorship for joint/multi-authored papers for PGR thesis

To appear at the end of each thesis chapter submitted as an article/paper

The statement shall describe the candidate's and co-authors' independent research contributions in the thesis publications. For each publication there should exist a complete statement that is to be filled out and signed by the candidate and supervisor **(only required where there isn't already a statement of contribution within the paper itself).**

Title of Paper	Fretting Fatigue Experiments with Single Crystal Pads
Publication Status	□Published □ Accepted for Publication □Submitted for Publication ☑Unpublished and unsubmitted work written in a manuscript style
Publication Details	

Student Confirmation

Student Name:	James Truelove		
Contribution to the Paper	Produced initial proposal for work, sourced materials from industrial sponsor, designed experiments, performed experiments, produced figures, interpreted results, wrote manuscript.		
Signature	James P J. Truelove	Date	17/07/23

Supervisor Confirmation

By signing the Statement of Authorship, you are certifying that the candidate made a substantial contribution to the publication, and that the description described above is accurate.

Supervisor name and title: Prof D A Hills		
Supervisor comments This work is 100% James' from beginning to end.		
Signature	Date	23 July 2023

This completed form should be included in the thesis, at the end of the relevant chapter.

7 The Effect of Load Path Under P-Q Loading

The paper presented in this chapter has been published as: *Truelove, J. P. J., Blades, L. E., & Hills, D. A. (2022). Half-plane contact problems in partial slip with varying normal and tangential loads. European Journal of Mechanics-A/Solids, 94, 104590.*

In many fretting contacts the loading of the contact is driven by a sinusoidally varying load, in a gas turbine engine this may be due to the centripetal loads on the blades during engine acceleration and deceleration, or it may be due to vibration of the blades during engine operation. In a sub sea connector the contact the contact experiences sinusoidal loading arising from the action of the waves on the attached pipe and platform.

As many fretting fatigue investigations attempt to match the experiment to a contact in an engineered assembly they often use load cycles where all the load components are sinusoidal in form and are applied in phase, so that the path through load space consists of a straight line between two points. While this is simple to implement in the test control system and a good way of studying failures in prototype components it severely limits the possibility of investigating the fundamental factors that cause fretting fatigue – in this style of test all the properties of the test are coupled together, to change one property (such as the slip zone size) the maximum and minimum values of the external loads have to be changed, which in turn affects all other properties of the contact.

In this paper we discuss the effect of varying the load path on the behaviour of the contact, i.e. the effect of changing the order in which the load components are applied. It is shown how by varying the order in which the loads are applied vastly different behaviour of the contact can result, it is possible, for example, to move between the same two end points in load space but for one load path to result in a contact which is fully stuck while another results in a contact which is slipping.

In this paper we restrict discussions to contacts loaded with a combination of a normal load, denoted P, and a shear load, denoted Q. The load paths are illustrated by application to a Hertzian contact.

Half-Plane Contact Problems in partial Slip with varying Normal and Tangential Loads

J P J Truelove, L E Blades and D A Hills

Department of Engineering Science, University of Oxford, Parks Road, Oxford, OX1 3PJ, UK

Abstract

Simple methods of finding the transient and steady state stick zones for frictional contacts subject to varying normal and shear forces are discussed. Particular emphasis is given to the Hertzian contact because the algebra is very simple for this geometry, but the methods and results may be carried over to any other contact geometry that can be solved within the framework of half plane theory, including the widely-occurring flat contact with radiused edges.

Keywords: Contact mechanics, Partial slip, Half plane

1. Introduction

The study of frictional, notionally static contacts subject to varying loads is important because they provide both frictional damping which controls the amplitude of vibrations in mechanical assemblies, and provide an environment which potentially leads to the nucleation of cracks. For many years studies of these problems were confined to cases where the normal load remained constant, from the seminal paper of Cattaneo [1] right through to 2011, when Barber, Davies and Hills [2] looked at the complicated case of a contact subject to harmonically varying normal and shear forces, of the same frequency, but with an arbitrary phase shift. It is certainly the case that this analysis is of practical value, as there are problems, such as eccentric weights on rotating shafts, which give rise to loads varying in this manner, but it is equally true that there are many problems where one external load induces changes in both normal and shear forces (which must therefore necessarily be in phase), and a second external load induces changes in the normal and shear forces, but in a different ratio. For example, in a wellhead riser clamp one external force could be the clamping force, hydraulically applied, and the other might be riser drift due to wave forces.

We have recently given attention to a number of contacts in which the contact supported a moment and normal force and the shear tractions present were excited by both a shear force and differential tension in the surfaces of the bodies [3, 4], in the steady state, but the formulations used avoided the need to look at the traction evolution. This is an illuminating way of looking at the problems, and is the subject of this paper. The study is restricted to uncoupled half-plane contacts, so that normal tractions induce no relative slip between surface particles, and shear tractions induce no relative normal displacement of surface

particles. Usually, the absence of coupling is achieved by requiring both bodies to be made from the same material. We restrict attention to problems where the contact is symmetric and of half width a, the normal load is P and the shear force present is Q. The load history will be displayed in $P-Q$ space and the coefficient of friction between the bodies is μ. It is tempting to infer that the lack of coupling in the solution means that the state of stress (and in particular, the traction distribution) present is independent of the loading path taken, but this is not so. It *is* true that the contact pressure distribution is independent of the loading trajectory, because the relative curvature of the bodies is unaffected by the shear tractions. On the other hand, if the normal load is increasing the contact patch is also gradually increasing in size, and the shearing tractions being developed will change in proportion to the change in normal load.

The starting point for these results is the observation that the Green's functions for normal and shear line forces (P, Q) on the surface of a half-plane produce the same corresponding surface displacements $(v(x), u(x))$. This result

$$\frac{v(x)}{P} = \frac{u(x)}{Q} \tag{1}$$

comes straight from Flamant's solution. It follows that, if we have similar *distributions* of direct and shear tractions they will give rise to similar normal and shear displacements, and from this stems the results enabling us to write down the results showing how incomplete contact problems may be represented as distributions of flat faced punches, associated with the names Mossakovskii [5] and Barber [6]. Turning the result the other way around, under conditions where the interface does not slip, changes in shear traction distribution will be proportional to changes in contact pressure.

2. Traction Evolution during increasing Normal Load

In order to be able to write down the results of this analysis in a compact but universal way, Barber defined the following notation: suppose that the contact law, defining the contact half width, a in terms of the normal load, P, is simply $a(P)$. The notation $p(x; P)$ then gives the contact pressure distribution over the interval $-a \le x \le a$, and is zero outside this range. As an example, consider a Hertzian contact, where

$$a^2 = \frac{4PR}{\pi E^*}, \tag{2}$$

and here R is the relative radius of curvature of the contacting bodies and E^* is the plane strain composite elastic modulus for the contacting bodies. The contact pressure distribution is given by

$$p(x; P) \equiv \frac{2P}{\pi a}\sqrt{1 - \left(\frac{x}{a}\right)^2} \quad |x| < a(P). \tag{3}$$

If we consider forming of the contact from an unloaded state, and we do so by increasing the normal and shear forces in proportion, so that

$$\frac{dP}{P} = \frac{dQ}{Q} \tag{4}$$

and, if we think of this as applying an oblique force, the tangent of the angle between the loading direction and the contact normal, λ, is simply Q/P. When $\lambda < \mu$ the contact does not slide, and so there is no rigid body motion. But, in fact, because $q(x)/p(x) = \lambda$ the contact is fully stuck at all points.

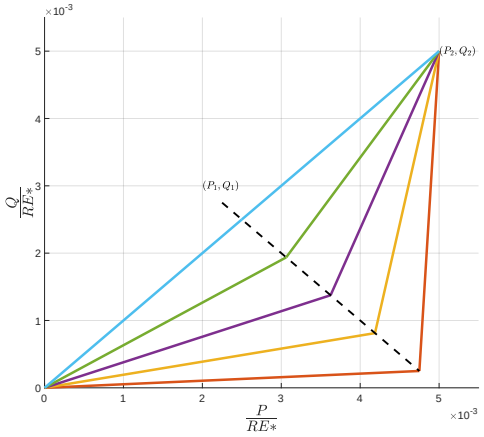
It is illuminating, next, to look at problems where the contact has been loaded to the point (P_1, Q_1), then loaded further, along a straight line in P-Q space to point (P_2, Q_2), example load paths are shown in Figure 1a. The change in shear traction distribution going from $1 \to 2$, assuming, for the time being, that it is fully stuck, is given by

$$\Delta q(x) = \frac{Q_2 - Q_1}{P_2 - P_1} \left[p\left(x; P_2\right) - p\left(x; P_1\right) \right] \tag{5}$$

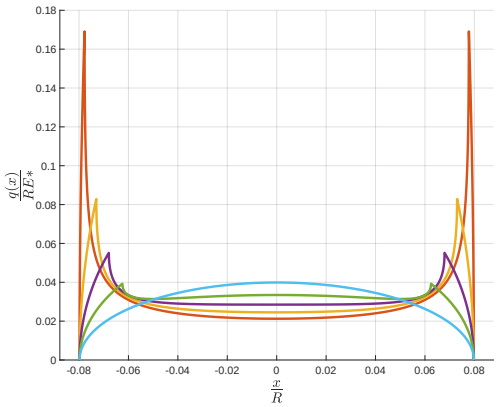
and so

$$q_2\left(x\right) = \frac{Q_1}{P_1} p\left(x; P_1\right) + \frac{Q_2 - Q_1}{P_2 - P_1} \left[p\left(x; P_2\right) - p\left(x; P_1\right) \right]. \tag{6}$$

In interpreting these equations bear in mind that the pressure $p\left(x; P_i\right)$ is present over the interval $|x| < a_i$, and $a_2 > a_1$. Examples of the resulting shear traction distributions, for a Hertzian contact, ending up at the same point (Q_2, P_2) but with various intermediate points (Q_1, P_1) are shown in figure 1b.



(a) Loading paths



(b) Shear traction distribution

Figure 1: Load paths and shear traction distributions for a fully stuck contact following a two piece straight line loading path

If $Q_2/P_2 < \mu$ the final contact will not be sliding, because it falls below the line $Q/P = \mu$. And, the change in traction ratio going from $1 \to 2$ is given by (from (5))

$$\frac{\Delta q(x)}{\Delta p(x)} = \frac{Q_2 - Q_1}{P_2 - P_1} \quad a_1 < |x| < a_2. \tag{7}$$

If this ratio exceeds the coefficient of friction there will be regions of slip, i.e. the contact will be in partial slip, noting that here we are considering changes in the shear and normal load.

This is illustrated in Figure 2, if the second point lies inside blue the triangle shown the contact will remain fully stuck, if the second point lies within the red triangle the contact will be fully sliding, and if the second point is outside this region the contact will be in partial slip.

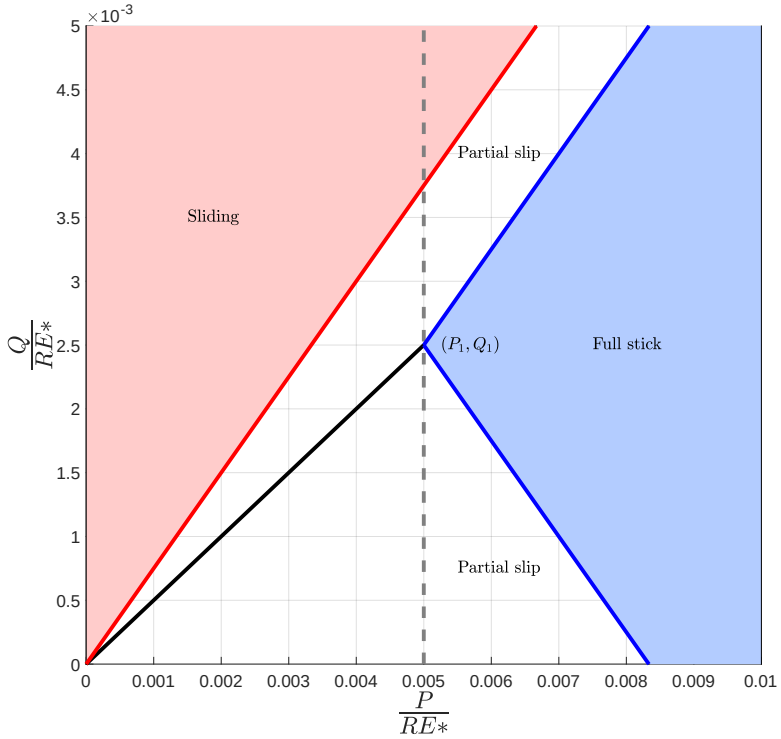


Figure 2: A figure illustrating the various types of behaviour the contact can experience following various loading paths from the same point, in this case for a coefficient of friction of 0.75. The contact is first loaded proportionally under conditions of full stick to (P_1, Q_1). If the contact is loaded under increasing normal load along a straight line to a point within the blue region the contact will remain fully stuck. If the contact is loaded into the red area the contact will slide. If the contact is loaded into the white regions then partial slip will occur. The gradients of the red and blue lines are the coefficient of friction.

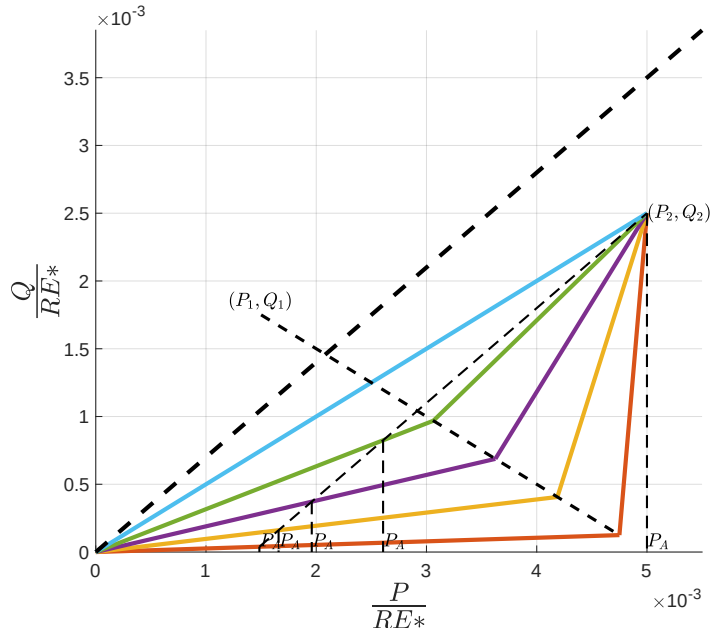
In cases where the gradient of the line exceeds the coefficient of friction the size of the slip zone will need to be found. This may be done by making use of the result discovered independently by Jäger [7, 8] and Ciavarella [9]) that the the requirement for stick to be preserved over a region $|x| < a_A$ when the actual contact size is $a_2 > a_A$ is given by

$$q(x) = \mu \left[p(x; P_2) - p(x; P_A) \right] \tag{8}$$

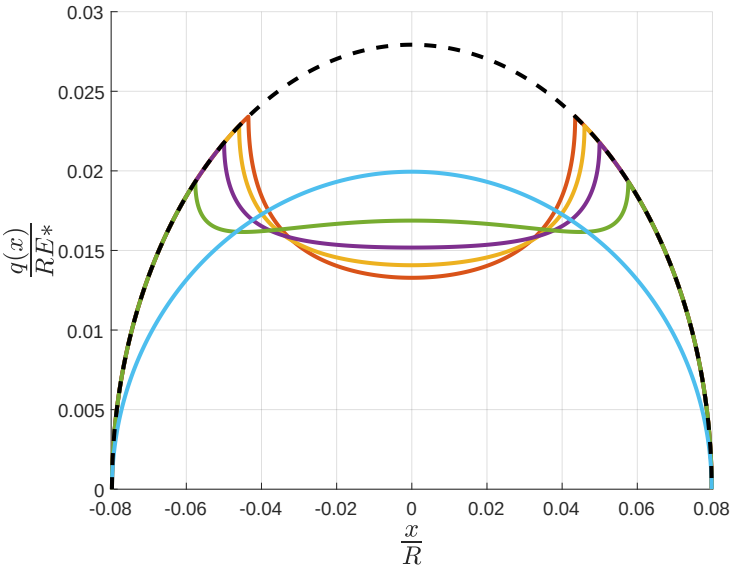
The shear traction is then given by

$$q_2(x) = \frac{Q_1}{P_1} p(x; P_A) + \mu \left[p(x; P_2) - p(x; P_A) \right] \tag{9}$$

and the value of P_A comes from the requirement of tangential equilibrium. It is the point of the initial loading trajectory defined by a line of gradient μ passing through point A, as shown in Figure 3a. Examples of the resulting shear traction distributions can be seen in Figure 3b, clearly demonstrating the varying size of stick zones resulting from different loading paths.



(a) Loading paths and construction to find P_A, showing how the value of P_A (and therefore the size of the slip zone) depends upon the loading path.



(b) Shear traction distributions for the load paths in figure 3a, and the limiting shear traction $\mu p(x; P_2)$ (black, dashed)

Figure 3: Load paths, geometric construction to find P_A and shear traction distribution for a two step loading with a frictional contact, showing the varying size of the slip zones under different loading paths (except light blue, which remains stuck everywhere).

2.1. Normal load applied first and held Constant

A special case of the above (and the one most frequently encountered in the literature), is when point 1 lies on the $Q = 0$ axis, and where $P_2 = P_1$. In this case the edge of the

contact does not move during the loading phase $1 \rightarrow 2$, and in the limit, equation (5) takes a different form. For the case where the coefficient of friction is sufficient to prevent all slip the change in shear traction is given by,

$$\Delta q(x) = \frac{Q_2 - Q_1}{\pi\sqrt{a^2 - x^2}} \tag{10}$$

where $a_2 = a_1 = a$, as the normal load does not change during loading. Note that the shear traction here is singular, and is infinite at the edges of the contact, while for loading cases where the normal load increases while the shear increases the shear traction is bounded and tends to zero at the edge of the contact, even under conditions of infinite coefficient of friction. It is worth briefly discussing how this singular behaviour can arise from a bounded result.

Under conditions of full stick the change in shear traction moving from point 1 to point 2 is given by equation 5. To find the shear traction distribution under sequential loading we can consider the case where we load initially to a point $(P, 0)$, then further to a point $(P + \Delta P, Q)$ and take the limit where $\Delta P \rightarrow 0$

The change in shear traction moving from $(P, 0)$ to $(P + \Delta P, Q)$ is given by

$$\Delta q(x) = \frac{Q}{P - (P + \Delta P)} \left[p(x; P) - p(x; P + \Delta P)\right] \tag{11}$$

Which we then take the limit $\Delta P \rightarrow 0$

$$\Delta q(x) = Q \lim_{\Delta P \rightarrow 0} \frac{p(x; P + \Delta P) - p(x; P)}{\Delta P} \tag{12}$$

Where it should be noted that the second term is the definition of the derivative

$$f'(a) = \lim_{h \rightarrow 0} \frac{f(a + h) - f(a)}{h} \tag{13}$$

So that the change in shear traction becomes

$$\Delta q(x) = Q \frac{\partial p(x; P)}{\partial P} \tag{14}$$

Taking the example of a Hertzian Contact, the contact law given by equations 3 and 2 can be written in the form

$$p(x, P) = \sqrt{\frac{PE^*\pi}{R} - \frac{x^2 E^{*2}\pi}{4R}} \tag{15}$$

Which has the derivative

$$\frac{\partial p(x; P)}{\partial P} = \frac{1}{\pi\sqrt{\frac{4PR}{E^*\pi} - x^2}} = \frac{1}{\pi\sqrt{a^2 - x^2}} \tag{16}$$

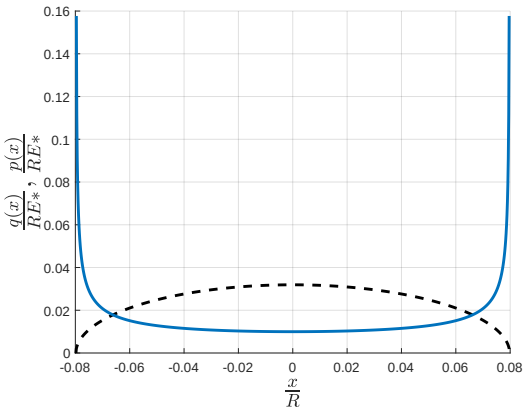
which leads us to equation 10. In more general terms it can be shown that the contact pressure immediately adjacent to the edge of any incomplete contact is square root bounded

in form, $p(s) = L_I\sqrt{(s)}$, where s is a coordinate set measured from the contact edge and L_I is an asymptotic multiplier. Changing the applied normal load changes the value of L_I and the location of the contact edge, but does not change the form of the pressure distribution. The derivative of the contact pressure is therefore square root singular in form, $\frac{dp}{ds} = \frac{K_I}{\sqrt{s}}$.

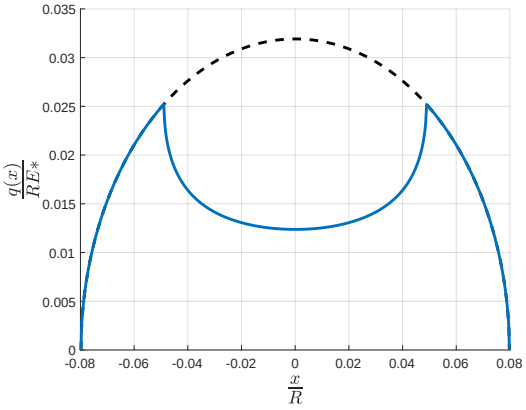
When slip is permitted the same principle for finding point A discussed in the section on two step loading continues to apply, and so by taking $P_2 = P_1$ and $Q_1 = 0$ we can state that in place of equation (9) we instead have

$$q_2(x) = \mu \left[p(x; P_2) - p(x; (P_2 - \frac{Q_2}{\mu})) \right] \tag{17}$$

which is the standard Jäger-Ciavarella solution.



(a) The shear traction and pressure distribution for a sequentially applied loading with no slip



(b) The shear traction and limiting shear traction, $\mu p(x; P_2)$, for a sequentially applied loading with frictional interface. This is the standard Jäger-Ciavarella solution.

Figure 4: Shear traction distributions for sequentially loaded contacts, under both full stick and partial slip conditions.

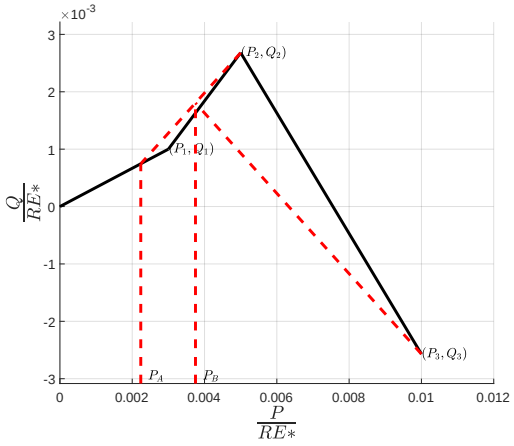
3. Unloading

Let us now consider the behaviour of the contact when it is unloaded, so that the direction of shear loading *increment* is reversed. The instant the direction of shear loading changes the entire contact will stick, as the increment of shear traction across the entire contact violates the orthogonality requirement for frictional slip, and any slip that occurred during the previous loading will be locked into the resulting stick zone. Assuming that the *overall* magnitude of the applied shear load is small enough to avoid full sliding the contact will remain fully stuck if the gradient of unloading is less than the coefficient of friction, and the change in shear traction will be described by equation 5. If, however, the gradient of unloading is greater than the coefficient of friction then zones of slip in the opposite direction will appear, starting from the edge of contact. The solution for a contact with zones of slip at each end with a stuck central portion is given by a Ciavarella-Jäger type distribution, so that the solution to the shear traction is, therefore, a superposition of the shear traction

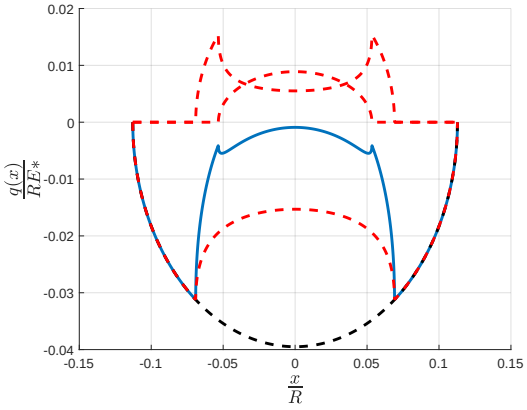
distribution representing the locked in slip from the previous loading stage, and a Ciavarella-Jäger distribution of magnitude $-\mu$ representing the newly slipping regions. Consider the load path in figure 5a. A contact that is loaded initially to point (P_1, Q_1) proportionally without slip, then loaded in an increasing manner further to point (P_2, Q_2) causing slip with stick zone associated with normal load P_A, then finally loaded under increasing normal load but decreasing shear to (P_3, Q_3) with associated slip zone size P_B. The shear traction distribution is given by

$$q_3(x) = \frac{Q_1}{P_1} p\left(x; P_A\right) + \mu\left[-p(x; P_3) + 2p(x; P_B) - p(x; P_A)\right]. \tag{18}$$

Where the $\frac{Q_1}{P_1} p(x; P_A)$ term represents the shear traction remaining from the proportional loading locked into the stick zone during the first stage of slip, $\mu\left[p(x; P_B) - p(x; P_A)\right]$ is the remaining shear traction distribution from the first stage of slip during loading, preserved over the stuck region during unloading, and $-\mu\left[p(x; P_3) - p(x; P_B)\right]$ is the shear traction distribution from the reverse slip during unloading, where the region between a_3 and a_B is now slipping in the reverse direction. these various shear tractions are shown in figure 5b.



(a) The loading and unloading paths used in this problem, illustrating the constructions used to find the normal loads corresponding to the size of the stick zone during loading, P_A, and the size of the stick zone during unloading, P_B.



(b) The resultant shear traction, shown in blue, along with the limiting shear traction for slip (black, dashed) and the three shear traction distributions that make up the distribution, as discussed in the text.

Figure 5: The loading paths and shear traction distributions for a contact that is initially loaded causing forward slip, then unloaded causing reverse slip, for the case where the region of reverse slip is smaller than the region of forward slip.

In this expression there is one unknown load, P_B, which can be found by considering horizontal equilibrium. Considering the total shear force due to each distribution in equation 18 we can write

$$Q_3 = \frac{Q_1}{P_1} P_A - \mu P_3 + 2\mu P_B - \mu P_A \tag{19}$$

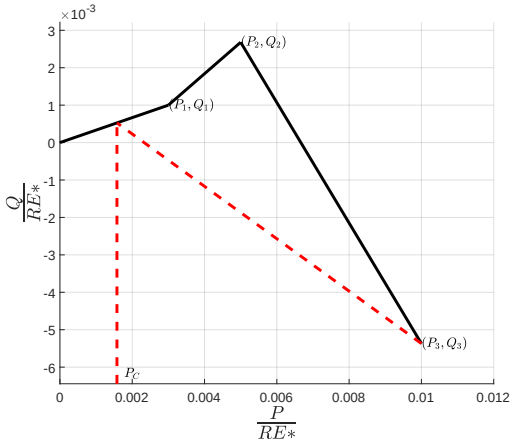
where we know the value of every term except P_B. Geometrically this expression is equivalent to finding the normal load at the intersection of a line of gradient $-\mu$ passing through (P_3, Q_3)

and a line of gradient μ passing through point (P_1, Q_1) (i.e. the line used to define the point P_A). This construction is shown in figure 5b.

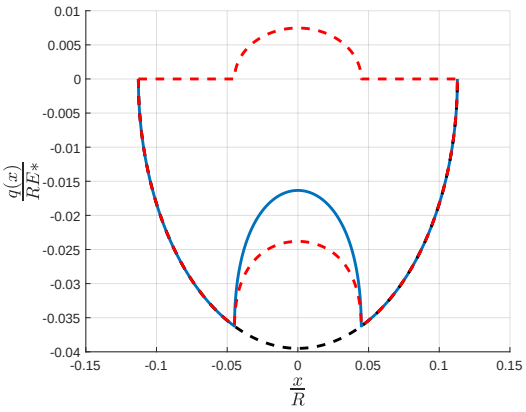
The previous solution applies as long as the region of reverse slip during unloading is smaller than the region of slip during loading. If the region of reverse slip becomes larger than the slip zone during the initial loading then the slip associated with the initial loading is completely erased, and the shear traction is instead given by

$$q_3(x) = \frac{Q_1}{P_1} p\left(x; P_C\right) + \mu\left[-p(x; P_3) + p(x; P_C)\right], \tag{20}$$

where the first term represents the shear traction from the initial loading path locked into the stick zone, and the second and third terms comprise a Ciavarella-Jäger type distribution corresponding to the region of reverse slip. The slip from the second stage of loading has, at this point, been entirely erased, and as such does not contribute to the shear traction distribution, note that the resulting shear traction is equivalent to a contact loaded straight to (P_3, Q_3) without the initial forward slip. The resultant shear traction is illustrated in Figure 6b.



(a) The loading path used for this contact and the contact, illustrating the construction used to find the value of normal load corresponding to the size of the stick zone during the unloading phase



(b) The resulting shear traction distribution for this loading path, shown in blue, along with the limiting shear traction in black and the two shear distributions that make up the overall shear traction, shown in red.

Figure 6: The loading path, construction, and resultant shear traction distribution for a contact where the size of the stick zone during unloading is smaller tha that present during loading.

Once again we can find the value of the unknown load P_C by considering horizontal equilibrium of the entire contact. Once again considering the total shear loads transmitted by each component of equation 20 we can write

$$Q_3 = \frac{Q_1}{P_1} P_C - \mu P_3 + \mu P_C. \tag{21}$$

Geometrically this is equivalent to finding the normal load at the intersection of a line of gradient $-\mu$ passing through point (P_3, Q_3) and the initial loading line to (P_1, Q_1), again this construction is illustrated in figure 6a.

4. Cyclic loading

A form of loading that frequently occurs in engineered systems is one where the loading takes some initial path through P, Q space to a large value, then a smaller cyclic loading is superposed. This type of loading may occur, for example, in aero engines where a large centripetal force is developed by a fan blade during spin up, followed by a smaller vibrational load. Let us consider a contact under the following load path - the contact is initially loaded in a proportional manner to a point (P_i, Q_i), and then repeatedly takes a straight line path between two other points in (P, Q) space, where (P_i, Q_i) lies on the path between them. A contact under this loading sequence has previously been studied by Fleury [10] by applying a simplified form of the results derived by Barber et al [2].

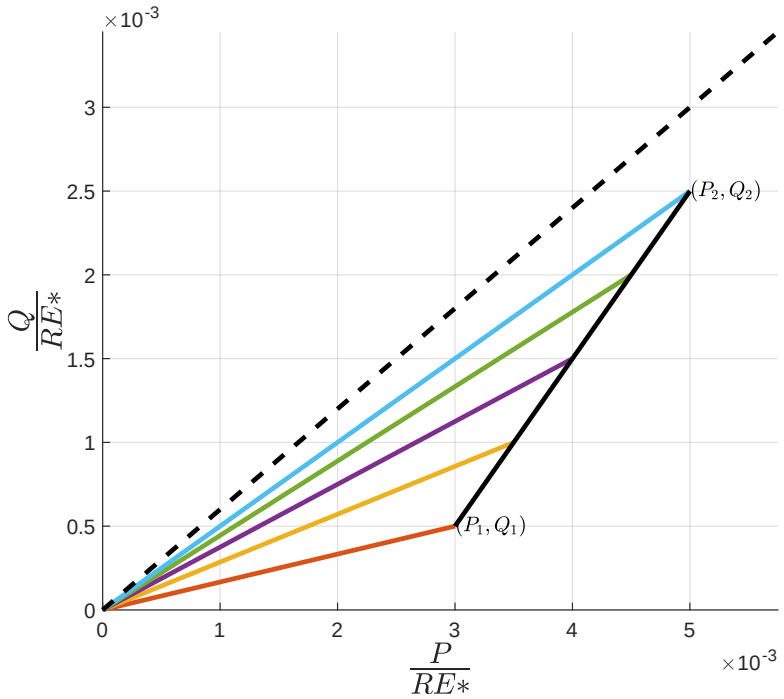


Figure 7: The load path taken through our cyclic loading example. The contact is initially loaded in a proportional manner to a point (P_i, Q_i) following the various coloured paths. The contact is then further loaded to point (P_2, Q_2), then cycled between (P_2, Q_2) and (P_1, Q_1). Note that the gradient of the cyclic loading is greater than the coefficient of friction (black, dashed).

The resultant shear traction following the initial proportional loading to (P_i, Q_i) then (P_2, Q_2) can be found in a manner identical to that discussed in section 2. The size of the stick zone during the initial load path is again given by the size of contact associated with normal load P_A, where P_A is found from the intersection of a line, passing through (P_2, Q_2) and with gradient μ with the initial load path. In the steady state the size of the permanent stick zone is given by the contact size associated with normal load P_K, where P_K is found from the intersection of a line with gradient μ passing through point (P_2, Q_2), and a line of gradient $-\mu$ passing through point (P_1, Q_1). This is shown in figure 8, which shows the

constructions to find load P_A in dashed black lines, and the constructions to find point P_K in dashed red lines. There are therefore two possible regimes to consider, following some loading paths the steady state stick zone will be larger than the transient stick zone, so some slip will be permanently locked into the contact, while other loading paths will result in a steady state stick zone that is smaller than the transient one, so the slip during the initial phase of loading will be erased.

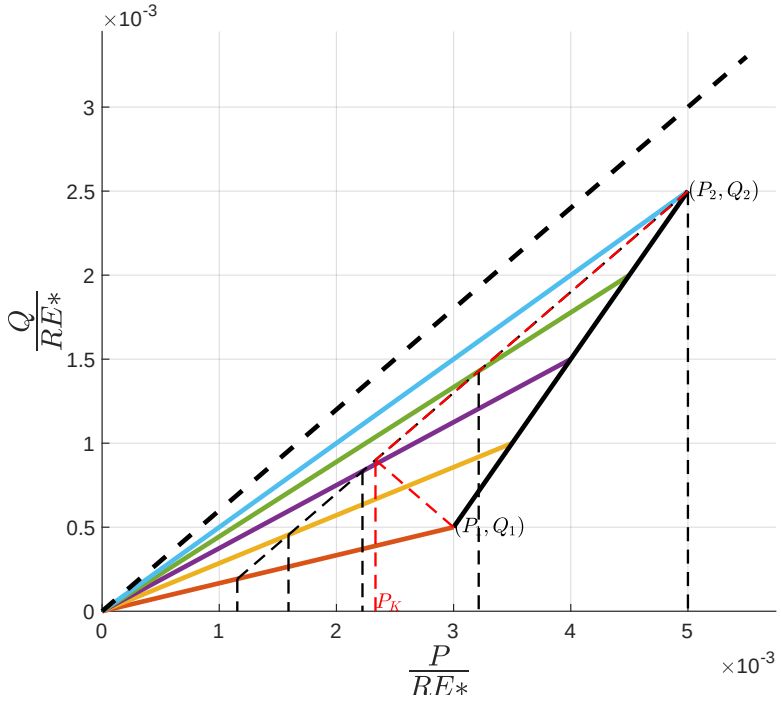


Figure 8: The load paths taken in the cyclic loading example, overlaid with the constructions for finding the loads that correspond to the size of the stick zone during the initial loading (P_A, black) and the size of the steady state stick zone (P_K, red)

As discussed the initial stage of the problem, loading up to point (P_2, Q_2) is exactly equivalent to the two step loading problem already studied. at the end of loading the shear traction distribution is therefore given by

$$q_2(x) = \frac{Q_i}{P_i} p(x; P_A) + \mu \left[p(x; P_2) - p(x; P_A) \right] \tag{22}$$

where P_A is found from horizontal equilibrium,

$$P_A = \frac{Q_2 - \mu P_2}{\frac{Q_i}{P_i} - \mu} \tag{23}$$

which is, once again, geometrically equivalent to the intersection of a line of gradient μ intersecting the initial loading line. Plots of the shear traction distributions at this point in the cycle for the load paths shown in figure 7 are shown in figure 9a.

We now unload the contact to point (P_1, Q_1) along a straight path from (P_2, Q_2). As discussed there are two possibilities to consider: if the steady state stick zone is larger than the transient stick zone ($P_K > P_A$) then the initial loading path will leave slip locked into the permanent stick zone. The solution to the shear traction is found by superimposing another Ciavarella-Jäger distribution on top of the existing shear traction distribution, giving

$$q_1(x) = \frac{Q_i}{P_i} p(x; P_A) + \mu \left[-p(x; P_1) + 2p(x; P_B) - p(x; P_A) \right], \tag{24}$$

where again P_B can be found through horizontal equilibrium,

$$P_B = \frac{Q_1 - Q_A + \mu P_1 + \mu P_A}{2\mu}. \tag{25}$$

For the case where the steady state stick zone is smaller than the transient stick zone the slip that occurs during unloading will erase any slip that occurred during the initial loading to point 2. In this case the problem is identical to a contact that is loaded to (P_i, Q_i) then straight to (P_1, Q_1), with the shear traction distribution given by

$$q_1(x) = \frac{Q_i}{P_i} p(x; P_C) - \mu \left[p(x; P_1) - p(x; P_C) \right]. \tag{26}$$

Note the change of sign of the second two terms, where P_C can again be found from horizontal equilibrium,

$$P_C = \frac{Q_1 + \mu P_1}{\frac{Q_i}{P_i} + \mu}. \tag{27}$$

This is the geometrically equivalent case to the intersection of a line of gradient $-\mu$ passing through (P_1, Q_1) and the initial loading path.

We now re-load the contact to (P_2, Q_2). At this point in the load cycle there are, again, two possibilities to consider - the contact may have locked in slip from the initial loading to (P_2, Q_2) still present in the stick zone, or it may have been erased in the unloading cycle. When the loading is reversed the contact will initially stick everywhere, and a slip zone will grow from the outer edge of the contact. The solution is once again formed by superimposing a Ciavarella-Jäger distribution on top of the exiting shear distribution.

For the case where the slip zone from the initial loading cycle is still present in the stick zone, the resulting shear traction will be given by

$$q_2(x) = \frac{Q_i}{P_i} p(x; P_A) + \mu \left[p(x; P_2) + 2p(x; P_B) - p(x; P_A) - 2p(x; P_D) \right], \tag{28}$$

whereas for the case where the slip from the initial loading was erased by the reversing load the shear traction is given by

$$q_2(x) = \frac{Q_i}{P_i} p(x; P_C) + \mu \left[p(x; P_2) - p(x; P_C) - 2p(x; P_D) \right], \tag{29}$$

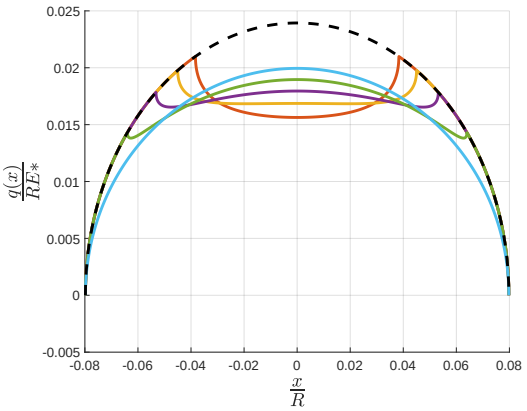
where once again we can find the value of P_D through horizontal equilibrium

$$P_D = \frac{-(Q_2 - Q_C - \mu P_2 - \mu P_C)}{2\mu} = P_B. \tag{30}$$

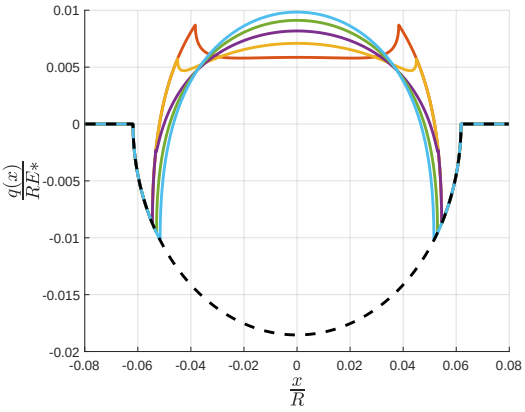
Note that the slip zone here does not extend into the stick zone that was present during the unloading stage, and so the slip locked into the stick zone remains unchanged.

Finally we unload the contact once again to (P_1, Q_1). Once again the contact will stick everywhere initially, with slip zones growing in from the outer edges, so once again the solution is given by the superposition of a Ciavarella-Jäger distribution on top of the existing shear traction. Since there was no additional slip in the stick zone during the loading to (P_2, Q_2) horizontal equilibrium tells us that the slip zone will be the same size as that present during the initial unloading to (P_1, Q_1). The solution to the stresses are therefore given by equations 26 and 24, for the cases where the slip zone during the first loading stage is locked into the steady state slip zone and erased respectively.

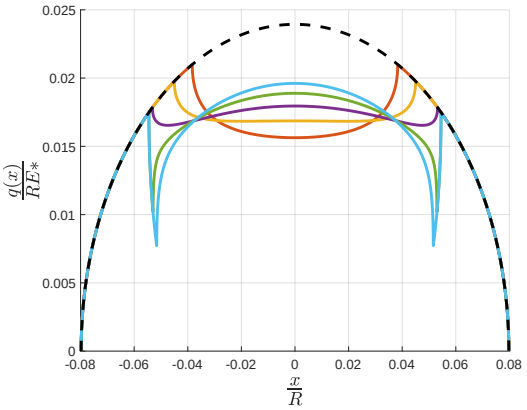
The solution has now reached its steady state, and any subsequent loading cycles will simply cause the state of stress to oscillate between the final two sets of equations. It is worth noting that the slip locked into the permanent stick zone means that there are regions of the permanent stick zone that reach the limiting coefficient of friction but which experience no further slip.



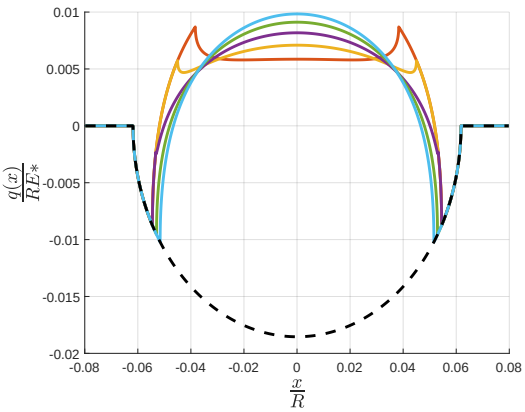
(a) The shear traction distributions following the initial loading to point (P_i, Q_i) then (P_2, Q_2). This is found in an equivalent manner to the shear traction distribution found in section 2 for a two step loading cycle



(b) The shear traction distributions following unloading to (P_1, Q_1). Note that in some of these loading paths the slip zone size during unloading is larger than the slip zone size during the initial loading to point (P_2, Q_2), while for some paths the opposite is true



(c) The shear traction distribution following re-loading to point (P_2, Q_2). The contact is now in the steady state portion of the loading cycle. Note that some of these shear traction distributions have regions within the permanent stick zone that reach the limiting coefficient of friction but which do not experience further slip displacement with further loading cycles



(d) The shear traction distribution following unloading to point (P_1, Q_1). Again for certain load paths the stuck region of the contact has regions which reach the limiting coefficient of friction but which do not experience further slip

Figure 9: Shear traction distributions for a Hertzian contact loaded through the path given in figure 7 at various points in the load cycle.

5. Conclusion

In this paper known solutions for the behaviour of a contact under various combinations of pressure and shear loading are given. The effect of various load paths are considered, and methods of finding the shear traction distribution through superposition are considered. The results given in this paper are applicable to any form of contact which can be represented by half planes, and the methods used to derive them can readily be extended to other loading histories.

References

[1] C. Cattaneo, "Sul contatto de due corpi elastici: Distribuzione locale deglisforzi," *Rendiconti dell'Accademia nazionale dei Lincei*, vol. 27, pp. 342–349, 1938.

[2] J. Barber, M. Davies, and D. Hills, "Frictional elastic contact with periodic loading," *International Journal of Solids and Structures*, vol. 48, no. 13, pp. 2041–2047, 2011.

[3] H. Andresen, D. A. Hills, J. R. Barber, and J. Vazquez, "Frictional half-plane contact problems subject to alternating normal and shear loads and tension in the steady state," *International Journal of Solids and Structures*, vol. 168, pp. 166–171, 2019.

[4] H. Andresen, D. Hills, J. Barber, and J. Vázquez, "Steady state cyclic behaviour of a half-plane contact in partial slip subject to varying normal load, moment, shear load, and moderate differential bulk tension," *International Journal of Solids and Structures*, vol. 182, pp. 156–161, 2020.

[5] V. Mossakovskii, "Application of the reciprocity theorem to the determination of the resultant forces and moments in three-dimensional contact problems," *PMM*, vol. 17, pp. 477–482, 1953.

[6] J. Barber, "Determining the contact area in elastic-indentation problems," *Journal of Strain Analysis*, vol. 9, no. 4, pp. 230–232, 1974.

[7] J. Jäger, "Half-planes without coupling under contact loading," *Archive of applied mechanics*, vol. 67, no. 4, pp. 247–259, 1997.

[8] J. Jäger, "A New Principle in Contact Mechanics," *Journal of Tribology*, vol. 120, no. 4, pp. 677–684, 1998.

[9] M. Ciavarella, "The generalized Cattaneo partial slip plane contact problem. I Theory," *International Journal of Solids and Structures*, vol. 35, no. 18, pp. 2349–2362, 1998.

[10] R. Fleury, D. Hills, R. Ramesh, and J. Barber, "Incomplete contacts in partial slip subject to varying normal and shear loading, and their representation by asymptotes," *Journal of the Mechanics and Physics of Solids*, vol. 99, pp. 178–191, 2017.

6. Acknowledgements

James Truelove acknowledges with thanks the award of an iCASE award ref 17000027 from Rolls-Royce plc which has enabled him to carry out this work.

David Hills and Luke Blades acknowledge Rolls-Royce plc and the EPSRC for their support under the Prosperity Partnership Grant "Cornerstone: Mechanical Engineering Science to Enable Aero Propulsion Futures", Grant Ref: EP/R004951/1.

Statement of Authorship for joint/multi-authored papers for PGR thesis

To appear at the end of each thesis chapter submitted as an article/paper

The statement shall describe the candidate's and co-authors' independent research contributions in the thesis publications. For each publication there should exist a complete statement that is to be filled out and signed by the candidate and supervisor **(only required where there isn't already a statement of contribution within the paper itself).**

Title of Paper	Half-Plane Contact Problems in partial Slip with varying Normal and Tangential Loads
Publication Status	☑Published □ Accepted for Publication □Submitted for Publication □Unpublished and unsubmitted work written in a manuscript style
Publication Details	Truelove, J. P. J., Blades, L. E., & Hills, D. A. (2022). Half-plane contact problems in partial slip with varying normal and tangential loads. European Journal of Mechanics-A/Solids, 94, 104590.

Student Confirmation

Student Name:	James Truelove		
Contribution to the Paper	Analysis, writing of MATLAB scripts, production of figures, writing of manuscript.		
Signature	James P J. Truelove	Date	17/07/23

Supervisor Confirmation

By signing the Statement of Authorship, you are certifying that the candidate made a substantial contribution to the publication, and that the description described above is accurate.

Supervisor name and title: Prof D A Hills		
Supervisor comments What James writes is true but in addition he contributed to developing the arguments concerning the underlying principles behind how this process works.		
Signature	Date	19th July 2023

This completed form should be included in the thesis, at the end of the relevant chapter.

8 The Effect of Load Path Under P-Sigma Loading

The paper presented in this chapter has been published as: *Truelove, J. P. J., Blades, L. E., Hills, D. A., & Paynter, R. J. H. (2023). Frictional half plane contacts subject to varying normal load and bulk tension under various load paths with application to fretting fatigue experiments. Tribology International, 185, 108563.*

In the previous chapter the effect of varying the load path on a contact under a combination of normal and shear forces was discussed. It was shown how by varying the order in which the loads are applied to the contact a wide range of behaviour can arise, an observation that offers new potentials for investigation into the fundamental causes of fretting fatigue.

Although the use of shear forces have some advantages when it comes to the analysis of the contact problem they have significant issues when applied to experiments, which make performing these experiments impractical. The use of shear forces may cause the development of unwanted moments due to moment coupling, as discussed in section 4. If the applied shear force is too great the contact may transition from partial slip to full sliding, which risks damage to the rig. Once a crack has initiated in a fretting contact it must propagate and grow to a length where it is detectable in order for the experiment to end, this requires that the stresses parallel to the surface of the half plane experience significant variation, which is not present in a shear force loaded contact.

In order to address these shortcomings an alternate form of test was proposed, utilising bulk tension instead of shear force – a contact loaded with bulk tension alone cannot slide, will not create a coupled moment and the bulk tension variation will act to propagate the crack.

In the following paper we restrict our analysis to a Hertzian contact as it is possible to find solutions analytically. A number of load paths are considered, and the slip behaviour and shear traction distribution for each is found.

A number of load paths with properties of great use to fretting fatigue experiments are derived. The sequential, proportional and hockey stick paths allow experiments to be run where the same maximum and minimum loads are applied, but significant differences in the slip behaviour exist, while the triangular load paths have the property that they slip in only one direction, allowing investigation of the effect of slip directionality and reversal.

Frictional Half Plane Contacts Subject to Varying Normal Load and Bulk Tension Under Various Load Paths with Application to Fretting Fatigue Experiments

J P J Truelove, L E Blades, D A Hills, and R J H Paynter

Department of Engineering Science, University of Oxford, Parks Road, Oxford, OX1 3PJ, UK

Abstract

In many fretting fatigue experiments the loads applied to the contact are sinusoidal and in phase, creating a straight line path through load space. Although this form of loading is a good representation of many of the load histories present in engineering assemblies, the usefulness of this form of load cycle when investigating the causes of fretting fatigue damage is limited. In this paper we first review solutions for uncoupled half plane contacts under bulk tension and normal loading, then develop some novel load paths with properties that are desirable in fretting fatigue experiments. Throughout this paper the results are illustrated via application to a Hertzian contact, although the principles apply to any contact capable of representation using half-plane theory.

Keywords: Contact mechanics, Fretting, Fatigue

1. Introduction

The understanding of frictional contacts subject to varying normal loads and bulk tension is of great importance in predicting the failure of components under fretting fatigue. Examples arise in all manner of engineering assemblies, such as those found at the roots of fan blades in a gas turbine engine, or those used in wellhead connectors.

In many of these applications the contact will experience a complex, multi stage load cycle. In a fan blade the contact experiences a combination of centrifugal and vibrational loading, in a well head connector a contact will experience forces arising from both the clamping action of the connector and, indirectly, the action of waves.

Many experimental investigations into fretting fatigue involve exposing a contact to cyclic, usually sinusoidal, variations in loads around a fixed midpoint. While such experiments are straightforward to design and relatively simple to analyse, this greatly limits the range of behaviour that it is possible to investigate, most experiments being confined to looking at straight line load 'cycles' between two points in load space.

In this paper we will first present various known solutions for contacts following a range of paths in a normal load-bulk tension load space. The contacting bodies are elastically similar, and one is subject to a bulk tension, σ. These solutions are used to construct load

histories with certain desirable properties: for example, we can create load paths which start and end at the same points in load space but where one gives rise to slip and one is under conditions of full stick, or we can create load paths where slip occurs in only one direction, or we can create load path loops that have equal but opposite shear traction and slip behaviour when the order of loading is reversed.

Throughout this paper we will adopt the notation devised by Barber et al [1] where possible, the contact half width is written in the form $a_i(P_i)$, where P_i is the applied normal load, and the corresponding contact pressure distribution is given by $P_i(x, P_i)x \in a_i$.

2. Full Stick

First, we consider the problem of a contact which remains fully stuck throughout the loading path, so that no slip occurs. The two factors that determine whether a contact will remain stuck are the load path taken and the coefficient of friction.

2.1. Constant Normal Load

When a bulk tension is applied to a contact under constant normal loading, so that the location of the edge of contact does not move, the resulting change in shear traction, $\Delta q(x; P)$, is singular and is given by [2]

$$\Delta q(x; P) = \frac{x\Delta\sigma}{4\sqrt{a(P)^2 - x^2}}. \tag{1}$$

It is worth noting that this result is independent of the form of the contact or the contact pressure distribution, it depends only on the contact width. Since the shear traction is singular at the edge of contact this implies that an infinite coefficient of friction is required to prevent slip.

2.2. Varying Normal Load

We now consider what happens when there is a simultaneous change in normal load, dP, and tension $d\sigma$. For an infinitesimal increment in contact force, the increment of contact pressure is given by [2]

$$dp(x; P) = \frac{dP}{\pi\sqrt{a(P)^2 - x^2}} \tag{2}$$

whereas for an infinitesimal increment in bulk tension, the increment of shear traction is [2]

$$dq(x; P) = \frac{xd\sigma}{4\sqrt{a(P)^2 - x^2}} \tag{3}$$

Because the shear traction has a multiplier, x, in its numerator the maximum ratio of shear traction to pressure will occur at the edges of contact, $x = \pm a$. To prevent slip the ratio

of shear traction to contact pressure must be less than the coefficient of friction [2], so that the change in loads must satisfy the inequality

$$\frac{d\sigma}{dP} < \frac{4\mu}{\pi a(P)}\,, \tag{4}$$

where μ is the coefficent of friction. Often it is more convenient to express this limit in terms of the change in bulk tension with respect to the contact half width, so that, equivalently,

$$\frac{d\sigma}{da} < \frac{4\mu}{\pi a(P)}\frac{dP}{da}. \tag{5}$$

2.3. Behaviour when Following an Increasing Normal Load Path

Above we gave the solution for the application of bulk tension under a fixed normal load, and showed how this form of loading would always result in slip, except in the unrealistic case of an infinite coefficient of friction. Let us now extend the analysis to look at loading cycles where both the normal load and bulk tension vary together, with finite friction. If the gradient of this load path satisfies inequality (4) the contact will remain fully stuck. This form of loading, with multiple load components varying together, occurs frequently in real contacts, for example in a gas turbine during acceleration the centripetal force on a blade generates a change in both the contact pressure and shear traction at the dovetail root due to the angled contact surface. Let us consider the behaviour of a contact loaded from a point (P_1, σ_1) to (P_2, σ_2) along a straight line in $P - \sigma$ space, so that

$$\frac{d\sigma}{dP} = \frac{\sigma_2 - \sigma_1}{P_2 - P_1}. \tag{6}$$

By integrating equation (2) we can write the change in contact pressure as

$$\Delta p(x)^{1\to 2} = \int_{P1}^{P2} \frac{dP}{\pi\sqrt{a^2 - x^2}} = p(x, P_2) - p(x, P_1), \tag{7}$$

and by integrating equation (3) we can write the change in shear traction as

$$\Delta q(x)^{1\to 2} = \int_{\sigma_1}^{\sigma_2} \frac{x}{4\sqrt{a^2 - x^2}} d\sigma. \tag{8}$$

Changing from an integral over σ to an integral over P through $d\sigma = \frac{d\sigma}{dP}dP$ and simplifying produces

$$\Delta q(x)^{1\to 2} = \int_{P_1}^{P_2} \frac{x}{4\sqrt{a^2 - x^2}} \frac{d\sigma}{dP} dP = \frac{\pi x}{4} \frac{\sigma_2 - \sigma_1}{P_2 - P_1} \int_{P_1}^{P_2} \frac{dP}{\pi\sqrt{a^2 - x^2}} \tag{9}$$

where the solution of the integral is just the change in contact pressure. The change in shear traction moving from point 1 to point 2 is therefore given by

$$\Delta q(x)^{1\to 2} = \frac{\pi x}{4}\frac{\sigma_2 - \sigma_1}{P_2 - P_1}\left[p\left(x; P_2\right) - p\left(x; P_1\right)\right], \tag{10}$$

which corresponds to the change in contact pressure multiplied by x, the gradient of loading and a constant factor of $\pi/4$. An example of the resultant shear traction for a fully stuck contact under varying load paths in $P-\sigma$ space is shown in Figure 1, for both Hertzian and flat and rounded geometries, illustrating the load path dependence of the solution, and how the stress field becomes more nearly singular as the gradient of the second step of loading increases.

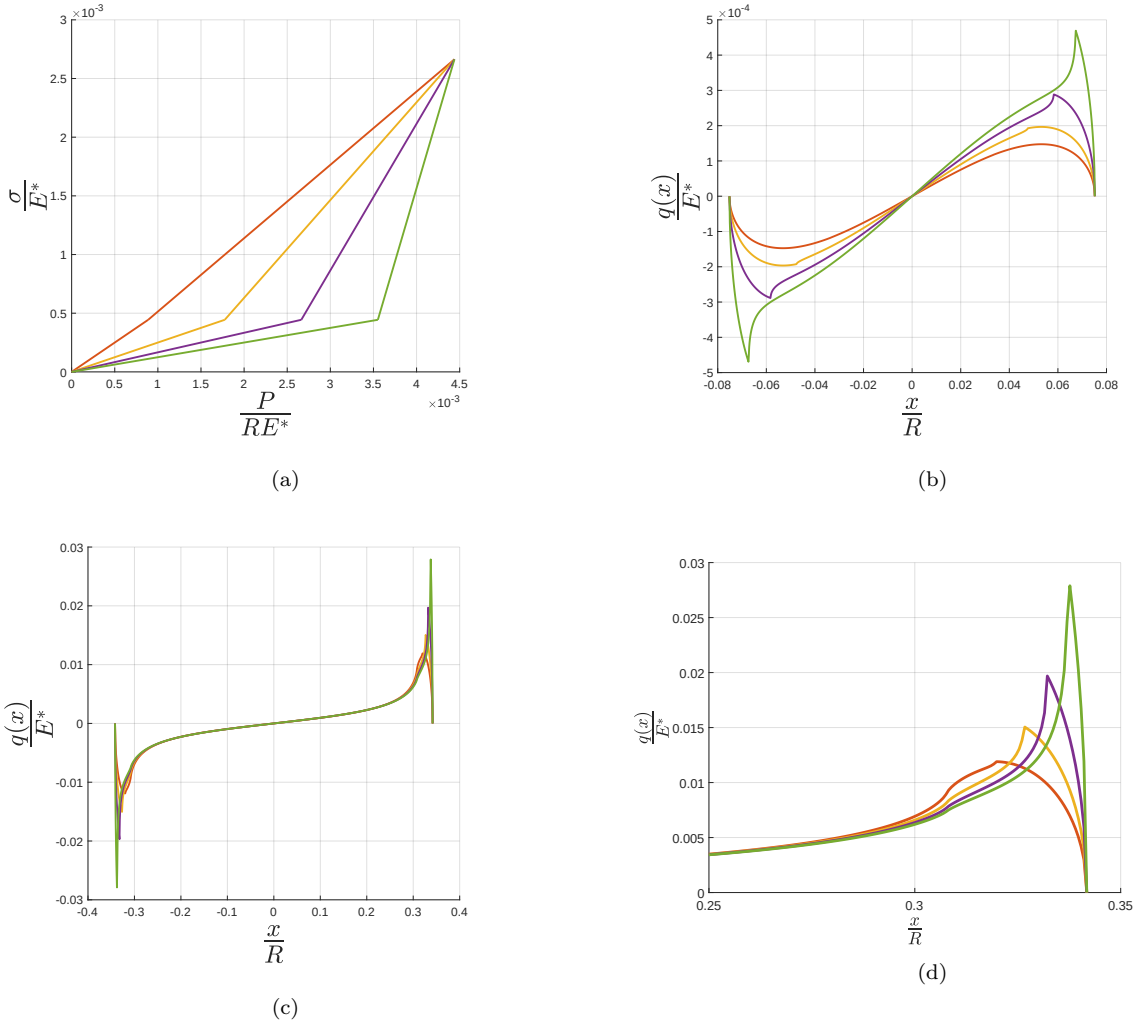


Figure 1: The shear traction distributions for fully stuck Hertzian and flat and rounded contacts under varying load paths. The hertzian contact has radius R, the flat and rounded contact has half width a and corner radius R, with a/R equal to $4/13$. (a) The loading paths taken through $P - \sigma$ space, (b) The resultant shear traction distribution for a fully stuck Hertzian contact taken through the loading paths shown in figure 1a, (c) The shear traction distributions for a fully stuck flat and rounded contact at the end point of the loading paths shown in figure 1a, (d) A zoomed in view of figure 1c, showing the shear traction at the edge of the contact.

3. Partial Slip

Having looked at the behaviour of a contact under conditions of full stick, let us now look at the solution when slip occurs. A contact where the tangentially loading arises just from bulk tension cannot experience *sliding* as the slip at each end of the contact is in opposite directions and an infinite bulk tension would be required for the slip zone to reach the centre of the contact.

3.1. Finding the size of the slip zone

The study of a Hertzian contact under a fixed normal load and increasing bulk tension was solved numerically by Nowell and Hills [3] and in closed form by Ciavarella and Macina [4]. These solutions were found by noting two properties of the contact - in the stick zone there is no relative displacement of the two surfaces, while in the slip zone the shear traction is the contact pressure multiplied by the coefficient of friction. Combining these two conditions defines an integral equation, the side condition of which provides the stick zone size, and the solution of which produces the shear traction. As an example, for a 2D Hertzian contact with radius R and contact half width a the size of the stick zone, a_K is given by [4]:

$$\frac{\sigma\pi R}{8a\mu E^*} = K\left(\sqrt{1-\frac{a_K^2}{a^2}}\right) - E\left(\sqrt{1-\frac{a_K^2}{a^2}}\right) \tag{11}$$

or, in terms of the applied normal load

$$\frac{\sigma}{16\mu}\sqrt{\frac{\pi^3 R}{PE^*}} = K\left(\sqrt{1-\frac{P_K}{P}}\right) - E\left(\sqrt{1-\frac{P_K}{P}}\right) \tag{12}$$

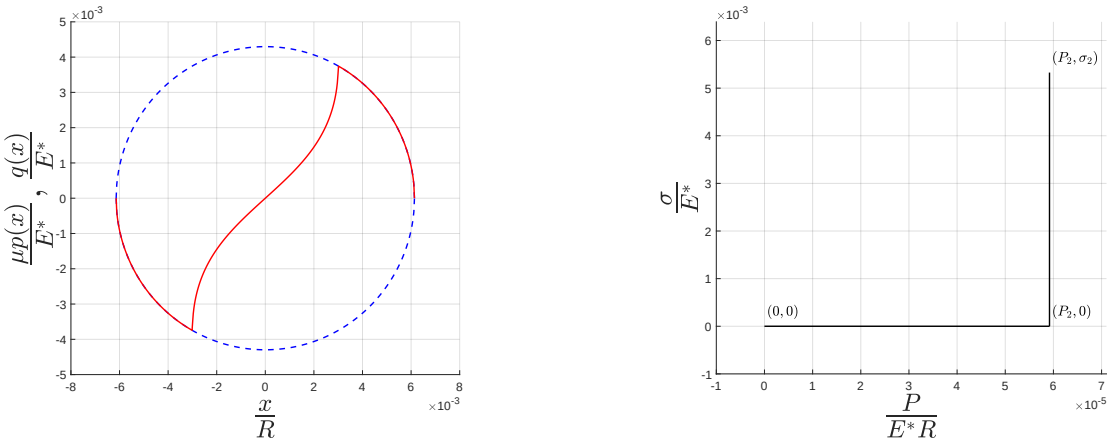
and the shear traction distribution is given by:

$$q(x) = sgn(x)\mu p(x;P) \quad a_K < |x| < a$$

$$q(x) = \frac{2\mu E^*}{\pi}\frac{x}{R}\sqrt{\frac{a_K^2-x^2}{a^2}}\left[\Pi\left(\sqrt{\frac{a^2-a_K^2}{a^2-x^2}},\sqrt{1-\frac{a_K^2}{a^2}}\right) - K\left(\sqrt{1-\frac{a_K^2}{a^2}}\right)\right] \quad |x| < a_K$$

where $K(k)$, $E(k)$ and $\Pi(n,k)$ are, respectively, complete elliptic integrals of the first, second and third kinds.

A plot of a typical shear traction distribution is given in Figure 2, showing the zones of slip at each end of the contact.



(a) (b)

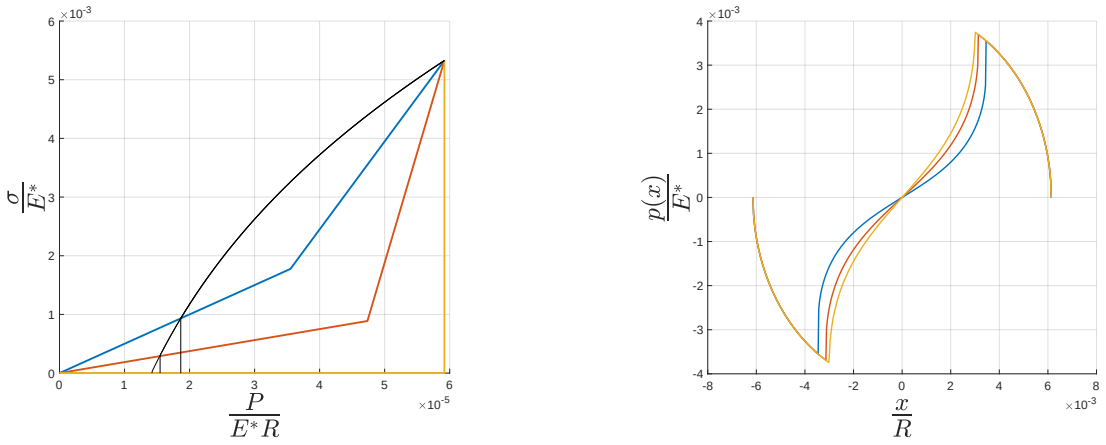
Figure 2: The shear traction distribution (a) for a Hertzian contact experiencing partial slip following a sequential loading, as illustrated in (b). The blue dashed lines show the contact pressure envelope, multiplied by the coefficient of friction, while the red line shows the shear traction distribution. Several notable features are visible, including the anti-symmetric form of the shear traction distribution, the slip zones of equal size but opposite direction, and the zero crossing in the shear traction at the centre of the contact.

4. Varying Normal Load with a Two step loading Regime

It is useful to consider what happens in a more general sense when a contact follows a load path constructed so that during the first part of the load path the contact is stuck, and during a subsequent load step slip occurs. By using a load path of this form a shear traction distribution can be locked into the contact before slip occurs. A simple example load path of this kind consists of two steps, as shown in figure 3; the contact is first taken from an unloaded state to a point (P_1, σ_1) under conditions of full stick, then further loaded to a point (P_2, σ_2), following a path such that slip occurs in the second stage of loading and where $P_2 > P_1$.

A loading step where the contact remains stuck locks a distribution of surface strains into the contact, which result in a shear traction distribution. If the contact then follows a load path so that it slips the solution during the slipping stage will have the properties that in the slip zones the shear traction is the contact pressure multiplied by the coefficent of friction, μ, while in the stick zone there is no relative tangential displacement between the two surfaces - the surface strains from the initial loading step are therefore preserved only in the region that does not slip. As shown in Ramesh et al [5], the solution can therefore be found by superimposing a partial slip shear traction distribution onto a full stick solution, consisting of the original stuck shear traction preserved only in the stick zone. This is because loading a contact along a path from P_1 to P_2 so that the contact slips during the later part of loading, creating a slip zone of size $a_k(P_k)$, is equivalent to loading the contact from P_1 to P_k along a fully stuck load path, then loading the problem sequentially from P_k to P_2, first applying the normal load to grow the contact to its full extent, then applying the bulk tension to

create a slip zone extending from $a(P_2)$ to $a(P_k)$. The size of the stick zone when there is a pre-existing shear traction can be found by looking for the intersection of equation 11 with a previously stuck point on the cycle, or another line defined by equation 11 from prior slip, this is illustrated for the two step loading shown in figure 3a. The resulting shear traction for these load paths is shown in figure 3b, where it can be seen clearly how changing the load path results in different shear traction distributions and slip zone sizes for the same final point in load space.



(a) (b)

Figure 3: The constructions used to find the size of the stick zone and resultant shear traction distributions for a hertzian contact following a two step load path. (a) The load paths and construction used to find the size of the stick zone in non-dimensional P, σ space, (b) The resultant shear traction distribution for a contact loaded following the path in figure 3a

Since the condition for full stick is a function of the contact half width, $a(P)$, the maximum gradient of loading in (P, σ) space will change as the normal load increases. For incomplete contacts, such as a Hertzian, the contact width will grow larger as the normal load increases, so that the maximum gradient of loading will decrease.

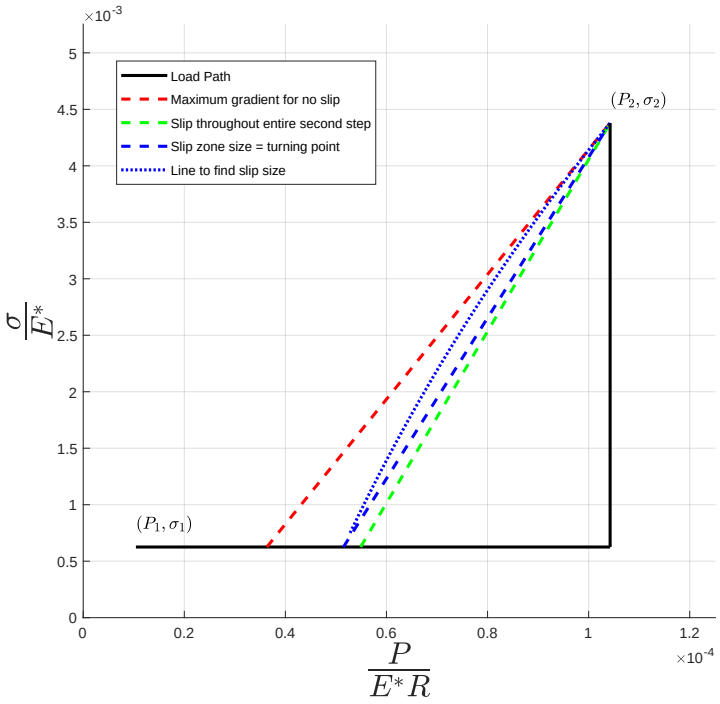


Figure 4: A plot showing the various regimes of behaviour that can occur when a contact is loaded along a two step path in (P, σ) space

Figure 4 shows examples of two step load paths, and the constructions giving the boundaries for various types of behaviour as applied to a Hertzian contact. In this load cycle the contact starts at a point (P_1, σ_1) and is loaded at a constant bulk tension to an intermediate point (P^*, σ_1). The contact is then loaded along a straight line to the maximum load point (P_2, σ_2). Limiting cases of this load path are given by $P^* = P_1$, which represents a purely proportional loading between these two points, and $P^* = P_2$, which represents a sequential loading (shown in black). For intermediate values of P^* a range of different behaviours can occur.

Let us start at the minimum value of P^*, $P^* = P_1$ and consider what happens as the value of P^* increases. In this case the two load points have been chosen such that the proportional loading path is fully stuck throughout the loading process, and inequality (4) is not violated at any point during the proportional loading. Further, any load path where the value of P^* is smaller than the value of P where the red line intersects the constant bulk tension loading will be fully stuck throughout the entire loading cycle, as the red line has a gradient so that inequality (4) is not violated.

As the position of P^* moves to the right of the red line slip will occur, but for points to the right of the green line this will only in certain parts of the loading cycle, not throughout the entire second step of loading. Inequality (4) is a function of the contact half width, with lower gradients of loading required to initiate slip for larger contacts, so following a straight

line load path in load space will result in slip occurring first at the maximum value of P.

For values of P^* which lie between the red and green lines of figure 4 slip will only occur at large values of P, i.e. as the second step of loading approaches (P_2, σ_2). The construction for finding the size of the stick zone at (P_2, σ_2) is given by equation (11), shown here in blue dots, and the load path where the value of $P^* = P_k$ is shown as a blue chain line. Using this the zone between the red and green lines can be subdivided further: load paths which lie between the red and blue lines will have final stick zone sizes defined by the intersection of the stick zone construction with the second stage of loading, so that the size of the stick zone depends upon P^*, whereas load paths lying between the blue and green lines will have stick zone sizes defined by the intersection of the stick zone construction with the line of constant σ loading, the size of the stick zone is the same for all load paths and is independent of P^*, though the slip displacements will differ.

Finally let us continue to increase the value of P^* so that the loading paths now lie to the right of the green line in figure 4. Once the value of P^* reaches this level the gradient of loading in the second step of the cycle is now sufficient to ensure that inequality 4 is violated at all points throughout the second stage of loading, and so slip initiates as soon as the second stage of loading begins. The final size of the stick zone is again given by the intersection of the construction line with the line of constant σ loading and as such is independent of the loading path, though the slip displacements will vary.

5. Cyclic Loading

In many real contacts the loading will be driven by some kind of varying or fluctuating process, so that the loading may vary cyclically in time. This kind of loading may occur, for example, in the hub of a turbofan engine where centripetal forces are developed during engine acceleration and deceleration, or, in our wellhead connector example, from the action of the waves. In these kinds of problems understanding the steady-state behaviour of the contact is of great importance, as damage may occur over tens of thousands or hundreds of thousands of loading cycles. As in the partial slip case the solutions found depend upon a knowledge of the contact law, so we will restrict ourselves to a Hertzian geometry for simplicity.

A load cycle that occurs frequently is one where the bulk tension and normal load both oscillate in phase. The results given here are a simplified form of the results found by Ramesh et al [5], who considered the more general case of a loading cycle with an arbitrary phase shift.

For a contact loaded with a shear force the size of the stick zones can be found through direct application of horizontal equilibrium to the various components of the Catteneo-Mindlin solution [1], this is equivalent graphically to looking for intersections of lines of gradient $\pm\mu$ with the loading paths though P, Q space.

For a contact under bulk tension loading the no slip condition is a function of a, so it is often more convenient to use the contact half width as a measure of normal load and instead move through a, σ space. For a Hertzian contact, for example, the maximum gradient of loading for no slip is then a constant, given by

$$\frac{d\sigma}{da} = \frac{2\mu E^*}{R} \tag{13}$$

The lines whose intersections define the size of the stick zone during loading and unloading are curves with form depends upon the geometry, for a Hertzian contact they are defined by [5]:

$$\bar{\sigma} = \bar{\sigma}_1 + \frac{4\mu\bar{a_1}}{\pi}\left[K\left(\sqrt{1-\left(\frac{\bar{a}}{\bar{a_1}}\right)^2}\right) - E\left(\sqrt{1-\left(\frac{\bar{a}}{\bar{a_1}}\right)^2}\right)\right] \tag{14}$$

during unloading and

$$\bar{\sigma} = \bar{\sigma}_2 - \frac{4\mu\bar{a_2}}{\pi}\left[K\left(\sqrt{1-\left(\frac{\bar{a}}{\bar{a_2}}\right)^2}\right) - E\left(\sqrt{1-\left(\frac{\bar{a}}{\bar{a_2}}\right)^2}\right)\right] \tag{15}$$

during loading, so that the size of the steady state stick zone during cyclic loading, $\bar{a_K}$ is given by

$$\begin{aligned}\left(\frac{\pi}{4}\right)\left(\frac{\bar{\sigma}_2-\bar{\sigma}_1}{\mu}\right) = \bar{a}_1&\left[K\left(\sqrt{1-\left(\frac{\bar{a}_K}{\bar{a_1}}\right)^2}\right) - E\left(\sqrt{1-\left(\frac{\bar{a}_K}{\bar{a_1}}\right)^2}\right)\right] \\ &+\bar{a_2}\left[K\left(\sqrt{1-\left(\frac{\bar{a}_K}{\bar{a_2}}\right)^2}\right) - E\left(\sqrt{1-\left(\frac{\bar{a}_K}{\bar{a_2}}\right)^2}\right)\right].\end{aligned} \tag{16}$$

Where $\bar{a}$ and $\bar{\sigma}$ are non-dimensional groups, defined by

$$\bar{\sigma} = \frac{\sigma}{E^*} \quad \bar{a} = \frac{a}{R}. \tag{17}$$

Let us now consider how we determine the state of stress at each point in the loading cycle, for the load path in black in figure 5. In this cycle a contact is first loaded proportionally from an unloaded point to a point (P_1, σ_1) without slip. The contact is then loaded further to a point (P_2, σ_2), where the gradient of loading is sufficient to ensure that slip occurs at *all* points along the second stage of loading. The contact is then cyclically loaded between (P_1, σ_1) and (P_2, σ_2) resulting in a zone of reversing slip.

In the upper graph of each sub figure the black lines show the load path, with the arrows showing the direction of loading in the current step and the red dot showing the current values of P and σ (denoted P^* and σ^* in the following discussion). The green solid lines show the construction for the transient problem, the red and blue solid lines show the construction during the steady state. The vertical dashed lines show the points of intersection, and correspondingly the normal load used to calculate the size of the slip zone.

The lower graph of each sub figure shows the shear traction distribution at each point in the cycle. The shear traction is shown in red, the contact pressure multiplied by the

coefficient of friction in blue. The vertical lines show the location of the slip/stick transition point, with each line's location corresponding to the size of the contact at the loads in the upper figure.

In the first step of loading the contact is loaded from an unloaded state to (P_1, σ_1), with the contact remaining fully stuck. The solution for this stage of loading is the same as that discussed in section 2, and the shear traction at normal load P^* is given by

$$q(x; P^*) = q_{FS}(x; P^*) \tag{18}$$

where

$$q_{FS}(x; P^*) = \frac{\sigma_1}{P_1}\frac{\pi x}{4}p(x; P^*). \tag{19}$$

In the second step of the cycle the contact is loaded from (P_1, σ_1) to (P_2, σ_2), with the gradient of loading being sufficient to ensure that slip occurs at all points during this phase. The stick zone construction and shear traction distribution are the same as those discussed in section 4, and are shown in figure 5a. The shear traction distribution at a load P^* is therefore given by

$$q(x; P^*) = q_{FS}(x; P_k) + q_{PS}(x; P^*; P_k) \tag{20}$$

where P_k is the load corresponding with the size of the stick zone, found from the intersection of a line defined by equation 15 with the first stage of the loading path, and $q_{PS}(x; P^*; P_k)$ is a partial slip shear traction distribution with overall size corresponding to load P^* and stick zone size corresponding to P_k. The size of the stick zone at the end of this loading step is henceforth denoted $a(P_{kL})$.

The third step of the cycle consists of the contact being unloaded from (P_2, σ_2) to (P_1, σ_1). As the gradient of unloading is greater than the frictional limit at all points during the unloading cycle reverse slip will occur. The shear traction therefore now has three components, a full stick term preserved only over the region that has never slipped, a reverse slip term which extends from the edge of contact to the unloading stick zone size, and a forward slip component between the other two distributions, representing the proportion of the slip from the second stage of loading that has not been erased. The size of the slip zone at a normal load P^* is found from the intersection of a construction curve with negative gradient with the construction from the end of step 2, equation 16 and the resulting shear traction is

$$q(x; P^*) = q_{FS}(x; P_{kL}) + q_{PS}(x; P_k; P_{kL}) - q_{PS}(x; P^*; P_k) \tag{21}$$

At the end of this step the reverse slip zone will be defined by load P_{kU}, which is larger than P_{kL}. The constructions for the stick zone are shown in figure 5b, and consist of a line defined by 14 emanating from the current load point and a line defined by 15 emanating from (P_2, σ_2), with their intersection defining P_k.

The contact has now shaken down, and its behaviour is in a steady state. In the following step of the load cycle the contact is reloaded from (P_1, σ_1) to (P_2, σ_2), forward slip occurs again during this step as the gradient of loading is greater than the full stick condition. The size of the slip zone is found from the intersection of a construction curve with positive gradient emanating from the current load point (equation 15) with the construction curve

from the end of step 2 (equation 14 from point (P_1, σ_1)), as shown in figure 5c. The shear traction is therefore given by

$$q(x; P^*) = q_{FS}(x; P_{kL}) + q_{PS}(x; P_{kU}; P_{kL}) - q_{PS}(x; P_k; P_{kU}) + q_{PS}(x; P^*; P_k) \tag{22}$$

At the end of this step of the loading cycle P_k will be equal to P_{kU}. This can be seen graphically in figure 5c: at the end of this load step the red and upper green construction lines will be coincident. The third term of the shear traction distribution will therefore be erased.

The final step to consider is the unloading of the contact in the steady state. Again reverse slip will occur, the construction being the same as in step 2, the intersection of a construction curve with negative gradient (equation 15) with the construction line from the second step of loading, this is illustrated in figure 5d. The resulting shear traction is therefore given by

$$q(x; P^*) = q_{FS}(x; P_{kL}) + q_{PS}(x; P_{kU}; P_{kL}) + q_{PS}(x; P_k; P_{kU}) - q_{PS}(x; P^*; P_k) \tag{23}$$

At the end of this step of the load cycle P_k will be equal to P_{kU}, in figure 5d this can be seen graphically, the blue line will be coincident with the lower green line. The third term of the shear traction expression is therefore erased and the shear traction is the same as it was at the end of the third step of loading, showing that we have indeed reached the steady state.

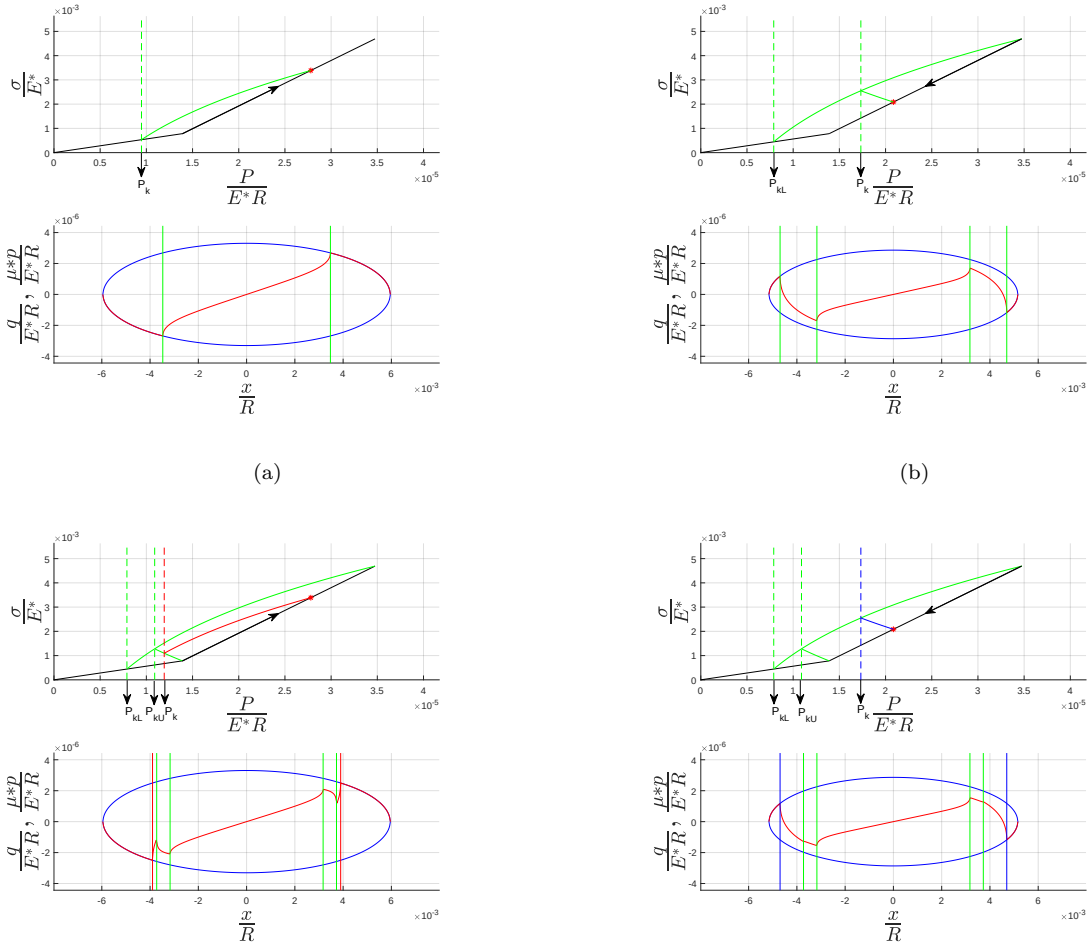


Figure 5: Shear traction distributions and stick zone constructions for a Hertzian contact under a cyclic loading cycle. (a) The stick zone construction and shear traction distribution during the transient loading step of a cyclic loading cycle, (b) The stick zone construction and shear traction distribution during the transient unloading step of a cyclic loading cycle, (c) The stick zone construction and shear traction distribution during the steady state loading step of a cyclic loading cycle, (d) The stick zone construction and shear traction distribution during the steady state unloading step of a cyclic loading cycle.

By combining the principles discussed in section 4 with those discussed above it is possible to create much more complex load paths involving multiple straight line stages of loading and unloading.

Figure 4 shows a number of examples of load paths of this form, by unloading along the same path used for loading, closed load paths suitable for use in fretting fatigue tests can be created. If a contact is stuck during the loading section of the load cycle it will remain stuck when unloaded along the same path. For loading paths where slip occurs during loading, reverse slip will occur during unloading, with the method of finding the size of the reverse slip zone being as described in this section.

Load cycles with the form of two straight line segments have a number of desirable properties when used in fretting fatigue tests. By following different two step load paths between the same pair of points in load space we can create experiments where a contact is exposed to the same remote stress field, but where the existence of slip, the shear traction distributions and the slip displacements vary.

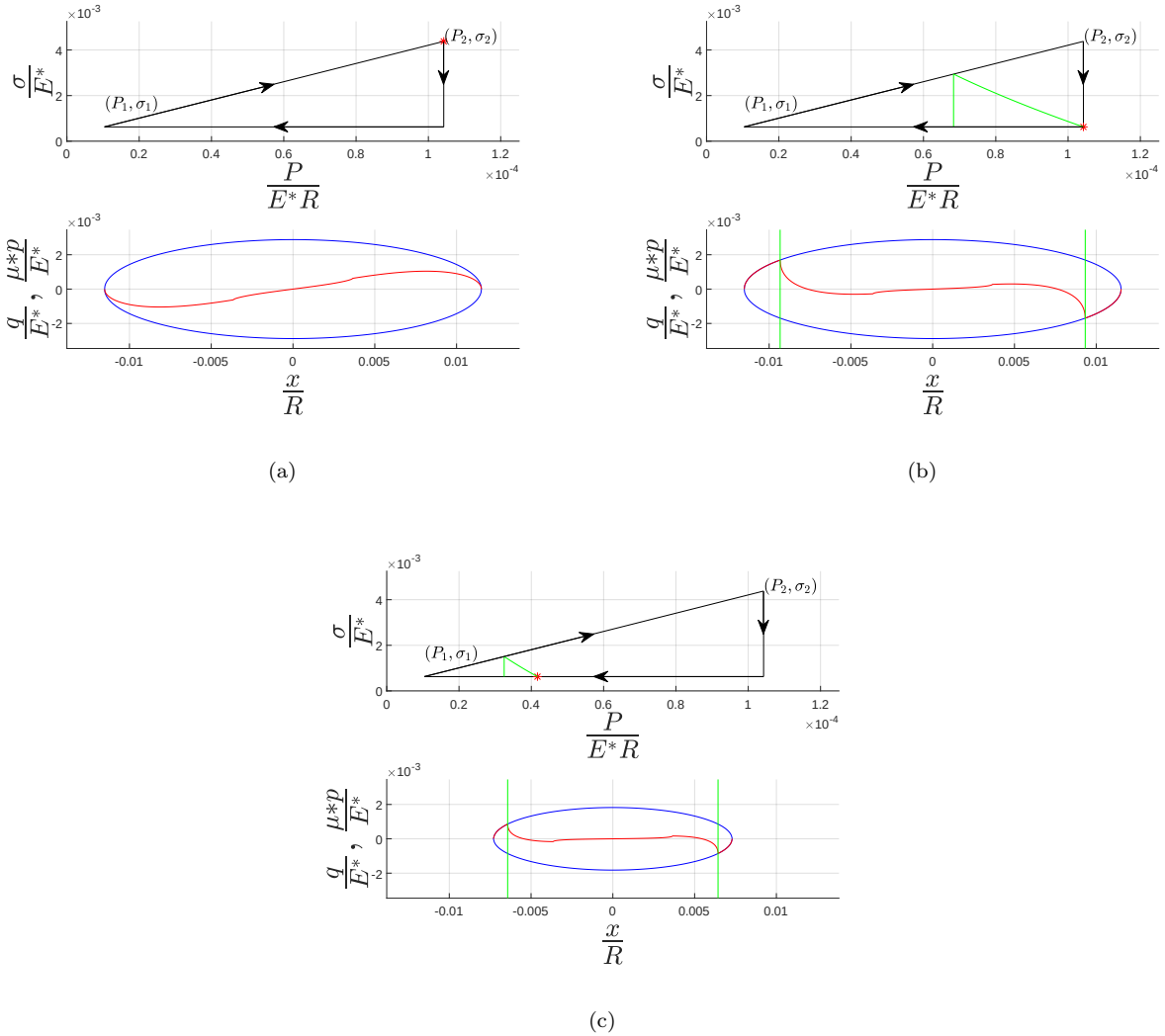
6. Triangular Loading Loops

One form of loading that has recently become of interest in our experimental work is those where the loading path and unloading path are different, so that the path travelled forms a loop. Ramesh et al [5] considered a problem consisting of an elliptical loop in (a, σ) space, here we will discuss some solutions formed from straight line loading segments. These load paths have the useful property that slip only occurs in one direction, so via their use it is possible to investigate the effect of slip direction on fretting fatigue life.

6.1. Right-angled Triangular Loops

One way of forming a load path in the form of a loop is to combine a proportional and sequential load cycle. A contact travels between two points in load space, (P_1, σ_1) and (P_2, σ_2), alternately following proportional or sequential paths. This results in a load path having the form of a right angled triangle, as shown below in figure 6. The behaviour of the contact and the resulting size of the slip zones vary depending upon which direction of loading is followed. The values of the load points are chosen so that the straight line proportional loading from (P_1, σ_1) to (P_2, σ_2) is under conditions of full stick.

6.1.1. *Clockwise Loading*



(a) (b)

(c)

Figure 6: The shear traction and stick zone constructions for a Hertzian contact following a right angled triangular loop in the clockwise direction. (a) The shear traction distribution at the end of the first stage of loading for the clockwise direction loop. The contact has been loaded proportionally from (P_1, σ_1) to (P_2, σ_2) locking in a distribution of shear traction, (b) The shear traction distribution for a Hertzian contact under a clockwise loading cycle at the end of the second step of loading. The applied bulk tension has been reduced from σ_2 to σ_1 at a constant normal load, creating a zone of slip, (c) The shear traction distribution at a point along the third step of the clockwise loading cycle. The normal load is being reduced from P_2 to P_1 at a fixed bulk tension, σ_1. During this stage of unloading a slip zone follows the edge of contact as it shrinks, with all particles in the zone $a_2 > x > a_1$ experiencing slip.

Let us first consider a contact traversing the load path in a clockwise direction, when viewed as in figure 6, so that the load cycle consists of proportional loading followed by sequential unloading. In the following discussion we start from the point of minimum load

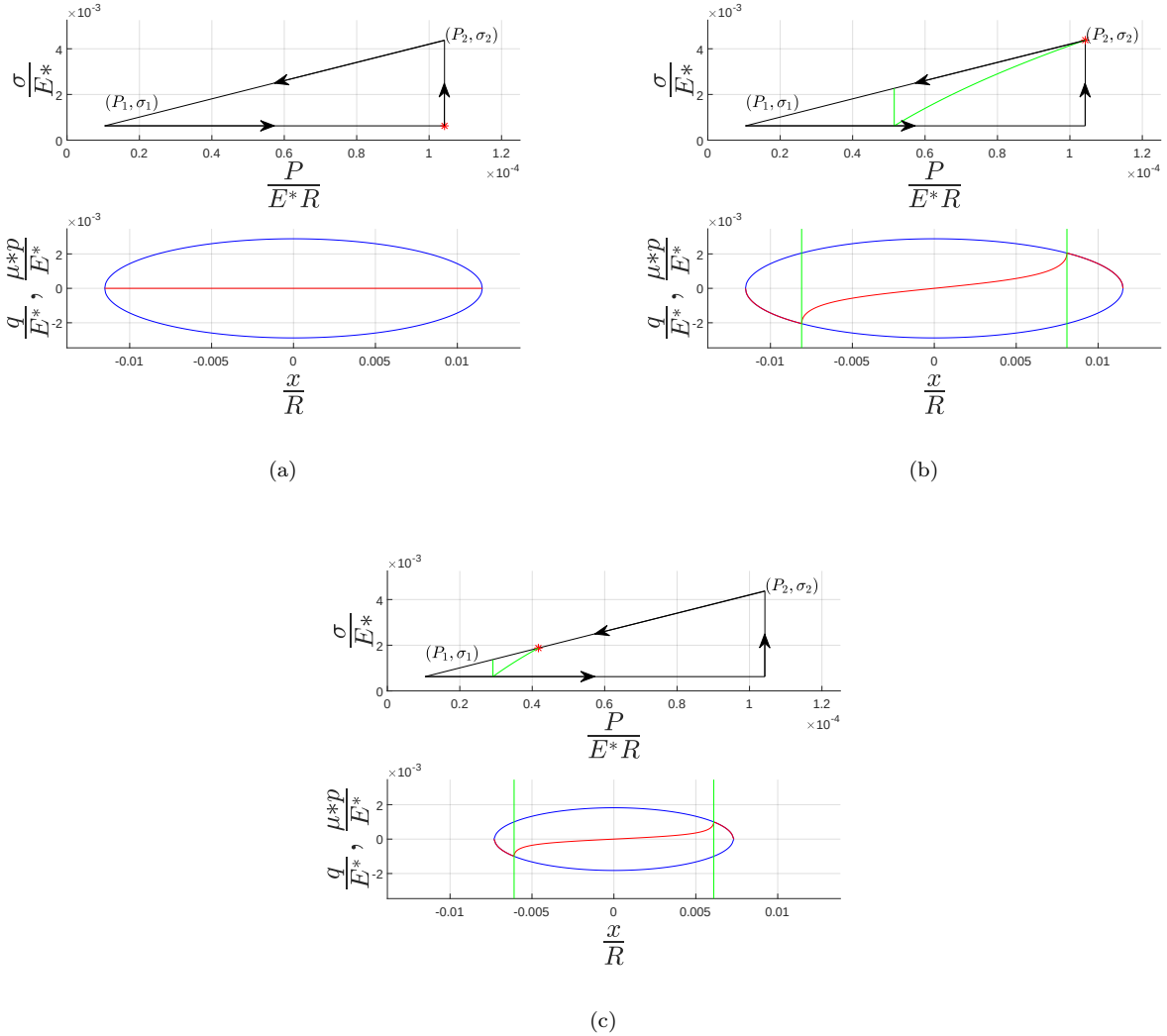
(P_1, σ_1) and proceed around the cycle in a clockwise direction.

During the first step of loading the contact remains fully stuck and a distribution of shear traction is laid down as discussed in section 2, the resulting shear traction is shown in figure 6a. While no slip occurs this does not mean that there is no displacement between the bodies, due to the applied bulk tension points that were opposite each other at point (P_1, σ_1) will be displaced tangentially relative to the other body at (P_2, σ_2) as the bodies deform while out of contact.

During the second stage of this load cycle the contact is unloaded from σ_2 to σ_1 at constant normal load. This results in the creation of a slip zone, with the size of the remaining stick zone given by the intersection of a line defined by equation 14 and the original proportional loading path. The shear traction distribution and stick zone construction is illustrated in figure 6b. It is worth noting here that the shear traction resulting from the unloading stage of the cycle are of the opposite sign to those that were locked in during the proportional loading step.

The final step of the load cycle consists of unloading the applied normal load at constant bulk tension σ_1. As the gradient of unloading during this step is less than the slip limit defined in section 2.2 (in this case it is 0) slip will continue in the same direction as the second step of loading. The construction is the same as that used in the second step of the cycle, it can be seen that as the size of the contact reduces a slip zone of continuously reducing size will follow the edge of contact until the size of the contact again reaches a_1.

6.1.2. *Anticlockwise Loading*



(a) (b)

(c)

Figure 7: The shear traction and stick zone constructions for a Hertzian contact following a right angled triangular loop in the anticlockwise direction (a) The shear traction distribution at the end of the first stage of loading. The contact has been loaded from P_1 to P_2 at constant bulk tension, so the contact interface is traction free, (b) The shear traction distribution at the end of the second stage of loading. A bulk tension has been applied at a fixed normal load, creating a slip zone, (c) The shear traction distribution at a point along the third stage of loading. The normal load and bulk tension are remove together in a proportional manner. as the contact is unloaded the slip zone size follows the edge of the contact, so that all points in the region $a_2 > x > a_1$ experience slip.

Let us now consider the behaviour of the contact when we reverse the direction of the loading cycle, so that the cycle consists of a sequential loading followed by a proportional unloading. The first stage of this cycle consists of applying normal load alone, so that the contact reaches its maximum extent but with a traction free interface, figure 7a. In this case

points which were opposite each other in the unloaded contact will remain opposite each other in the contact at its full extent - there is no tangential displacement.

In the second stage of this load cycle the contact is loaded at a constant value of P from σ_1 to σ_2, which results in the formation of a slip zone. The construction defining the size of the slip zone is the intersection of equation 15 with a line of constant σ, $\sigma = \sigma_1$. This is equivalent to the solution for the constant normal load case. The shear traction and stick zone size construction is shown in figure 7b.

In the final step of this load cycle the contact is unloaded along a proportional load path. As the gradient of unloading is less than the frictional slip limit at all points along this unloading slip will continue in the same direction as step 2. Figure 7c shows the stick zone construction and resulting shear traction for a point along this step of the loading cycle.

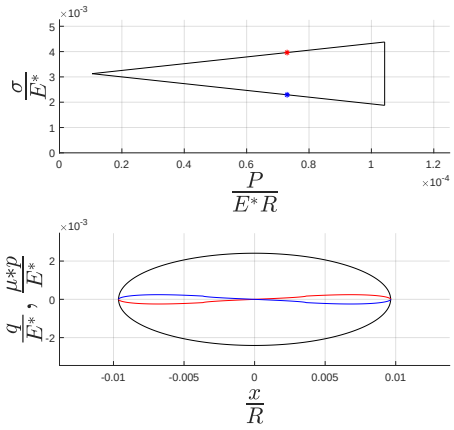
6.1.3. Comparison and Commentary

In comparing the clockwise and anticlockwise load paths a number of stark differences are evident. The first of these worth noting is that the clockwise loading cycle creates shear tractions in the contact interface that reverse direction during the loading cycle, while in the anticlockwise loop the shear traction is always in the same direction. All material must return to its original position by the end of the cycle, but in the latter case rather than occurring as reversing slip this occurs as tangential displacements while the two components are separated.

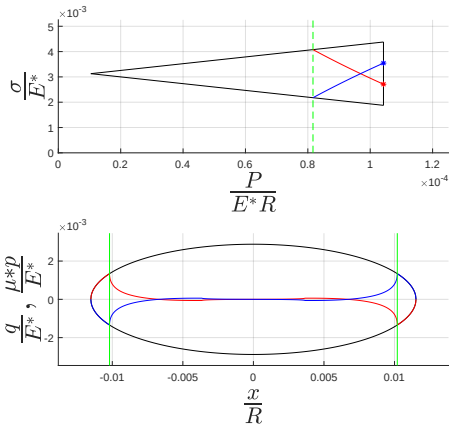
Another point worth noting is the drastic difference in the size of the stick zone. At the end of the constant normal load application or removal of bulk tension the stick zone is much smaller in the anticlockwise cycle than in the clockwise one; this can clearly be seen from the much reduced value of P_K in figure 7b when compared to 6b. This difference occurs because in the anticlockwise load cycle the slip is extending into a region where there is a pre-existing shear traction distribution which opposes the growth of the slip zones, while in the clockwise case the slip is extending into a traction free interface.

6.2. Isosceles Triangular Loops

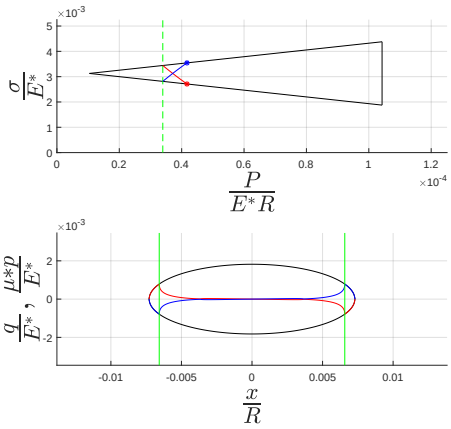
One potentially useful modification of the right angled triangular load path discussed previously involves constructing a load path that has the same behaviour in the clockwise and anticlockwise directions. One such load path that can be constructed entirely from straight line loading segments has the form of an isosceles triangle, as shown in figure 8. By following a load path of this form the shear tractions present are have the same distribution but opposite sign when the direction of loading is reversed.



(a)



(b)



(c)

Figure 8: The shear traction distributions and slip zone constructions for a contact under an isosceles triangle load path, showing the symmetry of the solution in the clockwise and anticlockwise directions. (a) The shear traction distribution at a point along the first step of loading, a proportional loading, with clockwise and anticlockwise solutions superimposed, (b) The shear traction distribution and slip zone constructions during the second step of an isosceles load path, during which the bulk tension is applied or removed at contant normal load, (c) The shear traction distribution and slip zone constructions during the final step of an isosceles load path, a proportional unloading.

The first step of this load cycle is a proportional loading under full stick. The shear traction solution during this step is the same as the solution given in section 2. The shear traction distribution at a point along this step of the loading cycle is shown in figure 8a, showing the symmetry of the shear traction distribution.

In the second step of this loading cycle the contact undergoes a change in the bulk tension load at a constant normal load, resulting in the formation of a slip zone. The size of the stick

zone is given from the intersection of a curve defined by equation 14 or 15 with the initial proportional loading, depending upon the direction of travel. This is illustrated in figure 8b, which shows the symmetrical constructions for both clockwise (red) and anticlockwise (blue) load paths. Again, it can be seen that, for equivalent points on the clockwise and anticlockwise loading cycles, the stick construction is identical, so therefore the slip zones are also the same size.

Finally the contact is unloaded along a proportional straight line path back to the starting load point. Once again the gradient of unloading is less than the condition for no full stick, so slip will continue in the same direction as the second step, with the size of the stick zone is found from the intersection of the curve construction, as shown in figure 8c. As in the right angled load path a small slip zone follows the edge of contact as it is unloaded, such that the entire change in contact experiences slip at some point in the cycle.

7. Conclusion

In this paper we have presented an overview and compilation of methods for finding the slip behaviour and shear traction distribution for incomplete contacts under various paths in $P - \sigma$ space. These solutions are applied to a number of novel load paths which have desirable properties when used in fretting fatigue experiments. By using both sequential and proportional load paths it is possible to set up two tests with the same start and end points, but where in one load cycle the contact remains fully stuck and the other experiences partial slip; this allows the effect of slip to be largely decoupled from the remotely applied loads and the stress field within the body of the specimen. The triangular load paths presented experience slip in only one direction, so that by using combinations of clockwise and anticlockwise load cycles the effect of slip direction and the difference between unidirectional and reversing slip can be isolated and studied. Combined, load paths of these forms provide a useful toolbox for investigating the fundamental causes of fretting fatigue and investigating what effect slip has on the life of the contact.

8. Acknowledgements

James Truelove acknowledges with thanks the award of an iCASE award ref 17000027 from Rolls-Royce plc which has enabled him to carry out this work.

David Hills and Luke Blades acknowledge Rolls-Royce plc and the EPSRC for their support under the Prosperity Partnership Grant "Cornerstone: Mechanical Engineering Science to Enable Aero Propulsion Futures", Grant Ref: EP/R004951/1.

References

[1] J. Barber, M. Davies, and D. Hills, "Frictional elastic contact with periodic loading," *International Journal of Solids and Structures*, vol. 48, no. 13, pp. 2041–2047, 2011.

[2] D. Hills, M. Davies, and J. Barber, "An incremental formulation for half-plane contact problems subject to varying normal load, shear, and tension," *The Journal of Strain Analysis for Engineering Design*, vol. 46, no. 6, pp. 436–443, 2011.

[3] D. Nowell and D. Hills, "Mechanics of fretting fatigue tests," *International Journal of Mechanical Sciences*, vol. 29, no. 5, pp. 355–365, 1987.

[4] M. Ciavarella and G. Macina, "New results for the fretting-induced stress concentration on hertzian and flat rounded contacts," *International Journal of Mechanical Sciences*, vol. 45, no. 3, pp. 449–467, 2003.

[5] R. Ramesh, J. Barber, and D. Hills, "Plane incomplete contact problems subject to bulk stress with a varying normal load," *International Journal of Mechanical Sciences*, vol. 122, no. January, pp. 228–234, 2017.

Statement of Authorship for joint/multi-authored papers for PGR thesis

To appear at the end of each thesis chapter submitted as an article/paper

The statement shall describe the candidate's and co-authors' independent research contributions in the thesis publications. For each publication there should exist a complete statement that is to be filled out and signed by the candidate and supervisor **(only required where there isn't already a statement of contribution within the paper itself).**

Title of Paper	Frictional Half Plane Contacts Subject to Varying Normal Load and Bulk Tension Under Various Load Paths with Application to Fretting Fatigue Experiments
Publication Status	☑Published □ Accepted for Publication □Submitted for Publication □Unpublished and unsubmitted work written in a manuscript style
Publication Details	Truelove, J. P. J., Blades, L. E., Hills, D. A., & Paynter, R. J. H. (2023). Frictional half plane contacts subject to varying normal load and bulk tension under various load paths with application to fretting fatigue experiments. Tribology International, 185, 108563.

Student Confirmation

Student Name:	James Truelove		
Contribution to the Paper	Analysis, Design of Load Paths, Writing of MATLAB scripts, Writing of manuscript, Production of figures.		
Signature	James P J. Truelove	Date	17/07/23

Supervisor Confirmation

By signing the Statement of Authorship, you are certifying that the candidate made a substantial contribution to the publication, and that the description described above is accurate.

Supervisor name and title: Prof D A Hills		
Supervisor comments James writes the truth. His contribution to this work was Very significant. Paynter and Blades were guiding postdocs, but the work was James'.		
Signature	Date	19th July 2023

This completed form should be included in the thesis, at the end of the relevant chapter.

9 The State of Stress Under P-Sigma Loading

While finding the slip zone size and shear traction distribution for a contact following a multi stage load path is useful for designing experiments with a variety of slip behaviour many other factors are crucial in determining fretting fatigue life. Some of these include the stress parallel to the surface, which propagates any cracks that initiate in the contact, and the slip displacements, which under many wear laws would control the rate of material removal.

In order to fully characterise the experiments and investigate all possible factors that could be contributing to a change of fatigue life knowledge of the state of stress in both bodies is required. During the initial series of experimental investigations a finite element model was used to find the state of stress within the body, but modelling the slip behaviour within the contact with a high resolution was found to be challenging.

In this paper we therefore model the state of stress in the bodies during these fretting fatigue experiments within half plane theory, by using Muskhelishvili complex potentials. The solution is built up by considering the potential functions corresponding to each component of the applied loading and contact traction, therefore allowing, via superposition, the full state of stress in the specimen and pad to be found. Using these stress fields a number of extra properties are derived, including the slip displacements and the distribution of energy dissipated per cycle in slip.

Comparisons are drawn between pairs of tests, and it is shown how varying the load path can cause significant differences in the state of stress and slip behaviour of the contact while the external load state remains the same. Of particular note here are the isosceles load paths, for which it is shown that it is possible to reverse the order of loading while maintaining a match for a number of parameters, allowing the effect of slip direction to be uncoupled from other properties of the contact.

The results described in this paper offer several new potential paths for investigations into the fundamental causes of fretting fatigue. This includes a method of uncoupling the effect of slip from the applied loads allowing for isolated investigation of the effect of slip direction and reversal.

The State of Stress in Fretting Contacts Under Varying Load Paths

James Truelove, Luke Blades, David Hills

June 13, 2023

Abstract

Fretting fatigue employing a number of novel load paths having useful properties for experiments are discussed. For each of these the full state of stress is found, and a number of further properties derived including steady state slip/stick pattern and slip displacements. It is shown that by careful control of the load path it is possible to design fretting fatigue experiments where the slip behaviour of the contact differs, but other properties of the contact remain relatively unchanged. This provides the means of conducting an experimental fretting fatigue study in which the effect of slip is isolated.

1 Introduction

Fretting fatigue is a form of damage that occurs when two bodies in notionally stationary contact are subjected to oscillating tangential loads. Experimental investigations into fretting fatigue failures typically involve attempting to match the loads and contact geometry present in the prototype components to a contact formed in a geometrically simpler test specimen, usually a dog bone tensile test specimen in contact with a pair of pads.

The loads applied to the test specimen normally vary sinusoidally in time, with all load components in phase, so that the path through load space is simply a straight line. These tests are simple to perform experimentally and in many cases it is possible to analyse the steady state behaviour of the contact in closed form, though with the disadvantage that it is not possible to adjust properties of the fretting contact (such as the slip zone size) without changing the range of the applied loads and hence the state of stress.

Recently a number of experiments have been performed in the Fretting fatigue laboratories at the University of Oxford [1] indicating that the order in which the loads are applied and the path taken through load space plays a critical role in determining the fatigue life of a contact. In a previous paper we analysed load paths of various forms to find the contact pressure and shear traction distributions [2]. Here we extend that work to investigate the effect of varying load paths on the state of stress in the bodies. Using the state of stress some further properties are derived, such as the slip displacements and frictional dissipated energy.

While we have investigated the state of stress in these experiments numerically using finite element models [1] here we instead use Muskhelishvili Complex Potentials to find the stress state in closed form, but modelled within half plane theory.

2 Stress from Muskhelishvili Complex Potentials

To find the state of stress in both bodies we employ Muskhelishvili Complex Potentials, which allow us to represent the state of stress in terms of analytical functions of complex variables. In our previous paper [2] we built up solutions for tractions for contacts undergoing multi-step but simple load paths via superposition of solutions. Here we apply the same principles to finding the complete state of stress.

We take, as an example, a Hertzian contact.

The Muskhelishvili Complex Potential for a Hertzian contact pressure distribution, $p(x) = \frac{2P}{\pi a}\sqrt{1-\left(\frac{x}{a}\right)^2}$,

is given by [3]

$$\phi(z) = \frac{zi}{2E^*R} - \frac{ip_0}{2a}\sqrt{z^2-a^2} \qquad x<0 \tag{1}$$

$$\phi(z) = \frac{zi}{2E^*R} + \frac{ip_0}{2a}\sqrt{z^2-a^2} \qquad x>0 \tag{2}$$

where a is the half width of the contact, R is the radius of curvature, E^* is the plane strain elastic modulus, p_0 is the peak contact pressure (given by $p_0 = \frac{2P}{\pi a}$), P is the applied normal load and $z = x + iy$.

The complex potential for a partial slip shear traction for a Hertzian contact where the shear traction is excited by purely bulk tension loading was found by Cwiekala [4] for a contact under constant normal load following the method devised by Vázquez et al [3] and is given by

$$\phi(z) = -\frac{\sigma_0}{8} + \frac{2}{\pi}\frac{fp_0 z}{a^2}\sqrt{z^2-c^2}[\Pi(n,k) - K(k)] \qquad x<0 \tag{3}$$

$$\phi(z) = -\frac{\sigma_0}{8} - \frac{2}{\pi}\frac{fp_0 z}{a^2}\sqrt{z^2-c^2}[\Pi(n,k) - K(k)] \qquad x>0 \tag{4}$$

where

$$k = \sqrt{1-\left(\frac{c}{a}\right)^2} \tag{5}$$

$$n = \sqrt{\frac{a^2-c^2}{a^2-x^2}} \tag{6}$$

c is the half width of the stick zone, σ_0 is the change in applied bulk tension and K and Π are complete elliptic integrals of the first and third kind, respectively. Ramesh et al [5] showed that the solution for a sequentially loaded contact can be used to find the solution for a contact fallowing any arbitrary load path, so these potential fields can be applied to the study of complex load paths.

Under full stick, proportional loading, $\frac{d\sigma}{\sigma} = \frac{dP}{P}$ the shar traction is given by $q(x) = \frac{\pi x}{4}\frac{\sigma}{P}p(x)$, and the complex potential is

$$\phi(z) = -\frac{\sigma_0}{8} + \frac{\sigma_0 z}{4a^2}\left(z + \sqrt{z^2-a^2}\right) \qquad x<0 \tag{7}$$

$$\phi(z) = -\frac{\sigma_0}{8} + \frac{\sigma_0 z}{4a^2}\left(z - \sqrt{z^2-a^2}\right) \qquad x>0 \tag{8}$$

$$\tag{9}$$

Finally, in some load paths employed in the set of tests a uniform bulk tension is present within the half space *before* the contact is formed. This has has a potential field simply given by

$$\phi(z) = -\frac{\sigma_0}{8}. \tag{10}$$

Having found the complex potentials the stress fields can be found using the expressions derived by Vázquez et al [6], where for the complex potentials associated with a contact pressure the stress components are given by

$$\sigma_{xx}(x,y) = -\phi(z) + \phi(\bar{z}) - iy\left[\frac{\delta}{\delta z}\phi(z) + \frac{\delta}{\delta \bar{z}}\phi(\bar{z})\right] \tag{11}$$

$$\sigma_{yy}(x,y) = -\phi(z) + \phi(\bar{z}) + iy\left[\frac{\delta}{\delta z}\phi(z) + \frac{\delta}{\delta \bar{z}}\phi(\bar{z})\right] \tag{12}$$

$$\sigma_{xy}(x,y) = y\left[\frac{\delta}{\delta z}\phi(z) - \frac{\delta}{\delta \bar{z}}\phi(\bar{z})\right], \tag{13}$$

and for the complex potentials associated with a shear traction the stress components are given by

$$\sigma_{xx}(x,y) = 2\left[\phi(z) + \phi(\bar{z})\right] + iy\left[\frac{\delta}{\delta z}\phi(z) - \frac{\delta}{\delta \bar{z}}\phi(\bar{z})\right] \tag{14}$$

$$\sigma_{yy}(x,y) = -iy\left[\frac{\delta}{\delta z}\phi(z) - \frac{\delta}{\delta \bar{z}}\phi(\bar{z})\right] \tag{15}$$

$$\sigma_{xy}(x,y) = i\left[\phi(z) - \phi(\bar{z})\right] - y\left[\frac{\delta}{\delta z}\phi(z) - \frac{\delta}{\delta \bar{z}}\phi(\bar{z})\right] \tag{16}$$

where $\bar{z}$ is the complex conjugate of z.

2.1 Slip Displacement

Having found the state of stress in both bodies it becomes possible to find the slip displacements in the regions where there is slip. Knowing the slip displacement is essential to characterise several other relevant physical quantities, such as the frictional work done per unit area and other damage mechanisms, such as wear. Using the stress field it is trivial to find the strain parallel to the surface, ϵ_{xx}. From Hooke's law in plane strain this is simply given by.

$$\epsilon_{xx} = \frac{1-\nu^2}{E}\left(\sigma_{xx} - \frac{\nu}{1-\nu}\sigma_{yy}\right) \tag{17}$$

From compatibility considerations it is clear that during an increment of load any regions of the contact which are stuck, if they continue to stick, must experience the same change in ϵ_{xx}, as coincident points on the contacting surface of each body must displace, tangential to the surface, by the same amount. In regions of the contact which are slipping, however, the change in surface strain in each body will be different, with the integral of the difference in surface strain over the slip zone giving the slip displacement during the increment of loading. The slip displacements, denoted $d(x)$, are given by [7]

$$d(x) = \int_c^x [\epsilon_{xx1}(x,0) - \epsilon_{xx2}(x,0)]dx \qquad a < x < c \tag{18}$$

where a is the width of the contact, ϵ_{xxi} is the strain in body i parallel to the surface, and $a > x > c$ where c is the edge of the slip zone. For load paths with multiple stages of loading or reversing slip the slip displacements can be found by considering the change in strain over each slipping step of loading individually, and summing the results.

2.2 Dissipated Energy

From the slip displacement and the surface traction it is possible to determine the energy dissipated within the cycle, via

$$W = Fs \tag{19}$$

where W is the work done, F the applied force and s the displacement in the direction of the force. Given the slip displacements we can use this expression to find the energy dissipated in the slip zones

$$W = \int_c^a q(x)d(x)dx \tag{20}$$

where $q(x)$ is the shear traction (in the slip zone equal to $fp(x)$), d(x) is the slip displacement, and the integral is evaluated over the slip zone. Note that this integral may have to be evaluated at multiple points in the load history, as slip displacements in each direction need to be handled separately and the edge of the contact and slip zone (and hence the limits of intergration) change over the loading cycle.

3 Proportional and Sequential Loading

One of the simplest ways of demonstrating the importance of load history on the behaviour of a fretting contact is to compare the behaviour of a contact following proportional and sequential load paths between the same end states. As demonstrated in our previous papers [1, 2] by careful choice of the end points of the load cycle it is possible to design a test so that following the proportional load path the contact remains stuck, while following the sequential load path the contact slips.

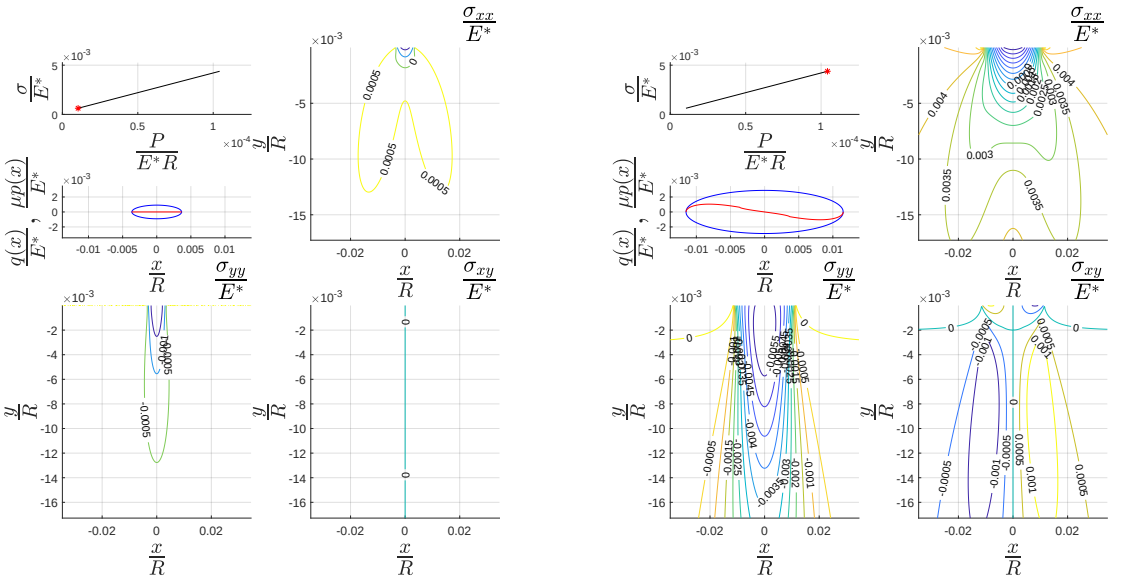
3.1 Proportional Loading

Let us begin by finding the state of stress in the half plane following a proportional load path. The contact is loaded along a straight line in load space between two points, (P_1, σ_1) and (P_2, σ_2), with the gradient of loading chosen so that at no point during the cycle does any slip occur. At point (P_1, σ_1) the contact interface is assumed to be free from shear traction. As shown in [2] the shear traction solution consists of a superposition of two full stick shear traction distributions, one extending over the complete contact and one extending over the region which was initially stuck. The potential field therefore has four components: two potential fields arising from proportional full stick shear traction distributions, as

given by equation 7, a contact pressure distribution given by equation 1 and a constant stress field over the body equal to σ_1 given by equation 10.

Note that in this and subsequent sections the plots here will only show the state of stress in the lower half plane, in this model representing the dogbone. The state of stress in the upper half plane can be found using the same method, the main differences being that the shear traction in the contact will be of opposite sign, and the remotely applied bulk tension will be zero.

Plots of the shear traction distribution and stress components are given in figure 1 at various points during the loading portion cycle. As there is no slip or non-linear effects the state of stress during unloading is identical to the state of stress during loading. Each contour in the plot represents an increment of $\frac{\sigma}{E^*}$ equal to 0.0005



(a) The state of stress at the minimum load point of the proportional load cycle.

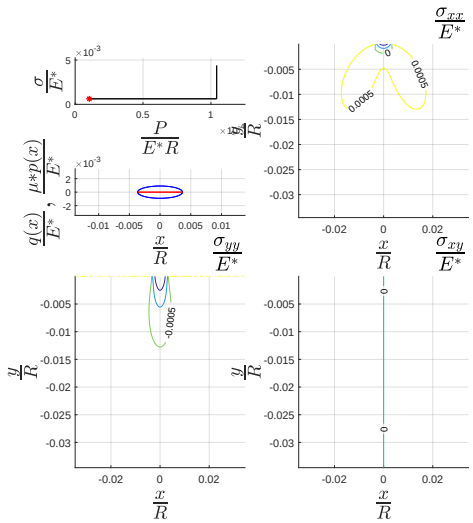
(b) The state of stress at the maximum load point of the proportional load cycle.

Figure 1: The state of stress and surface traction at various points in a proportional loading cycle.

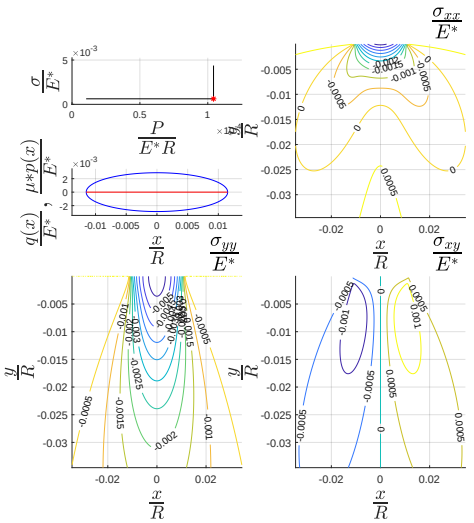
3.2 Sequential Loading

Let us now consider a sequential loading history. In this cycle we move between the same points in load space, (P_1, σ_1) and (P_2, σ_2), but in four distinct steps. First the contact is loaded from (P_1, σ_1) to (P_2, σ_1), that is the normal load is increased at a constant bulk tension. During this stage of loading the contact interface remains traction free, so the potential field consists of a term associated with the contact pressure term given by equation 1 and a term associated with a constant stress field, given by equation 10. During the second stage of loading the contact is loaded from (P_2, σ_1) to (P_2, σ_2), that is, bulk tension is applied at a constant normal load. This causes no change in the normal solution, but a partial slip shear traction distribution is created, with associated potential function 3. The third step of this load cycle involves unloading to (P_2, σ_1), so that the bulk tension is removed at a constant normal load. During this stage of the load cycle a reverse slip zone is developed where the slip zone size is smaller than that developed during loading, so that the shear traction solution consists of two partial slip stress fields superimposed, one caused by the reverse slip during unloading, the other due to the forward slip during loading being preserved over the unloading stick zone. The final stage of the load cycle consists of unloading from (P_2, σ_1) to (P_1, σ_1), i.e. the normal load is removed at a constant bulk tension. This stage of unloading has itself two steps: while the size of the contact is larger than the loading slip zone reverse slip will continue to occur and the shear traction solution will be the two partial slip distribution solution discussed previously. Once the contact is smaller than the loading slip zone the contact will be traction free.

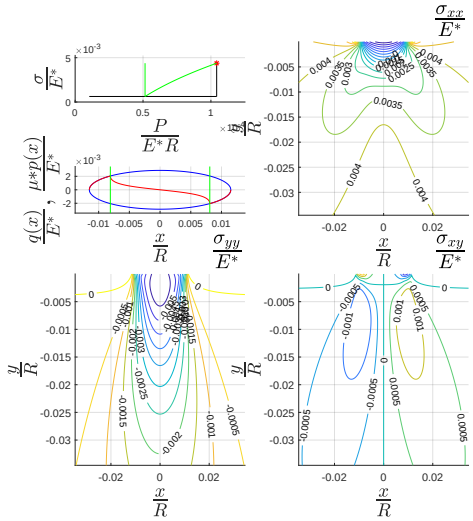
Plots of the stress fields at various points around the load cycle are show in in figure 2, with figures 2a being at the start of the first stage of loading, 2b being the second stage, 2c being the third stage and 2d being the final stage of loading.



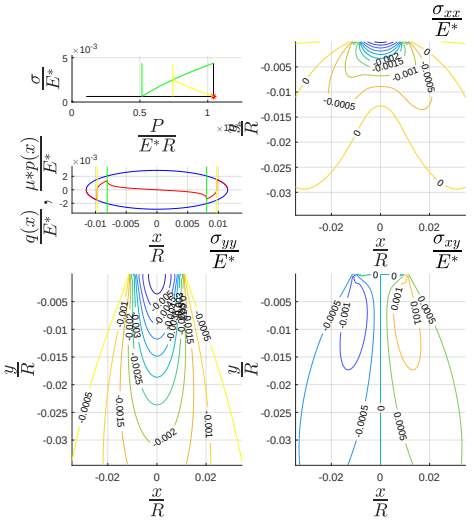
(a) The State of stress at the start of the sequential load cycle.



(b) The state of stress at the start of the second stage of loading.



(c) The state of stress at the start of the third stage of loading.

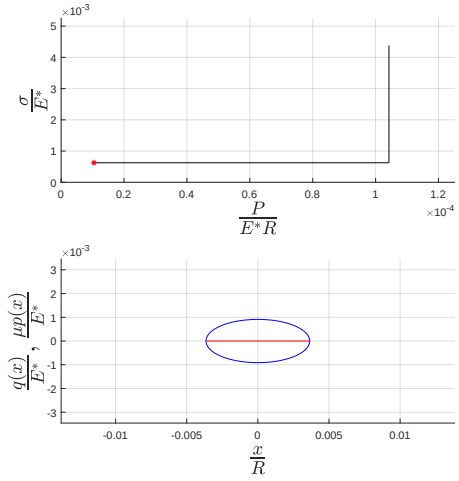


(d) The state of stress at the start of the fourth stage of loafing.

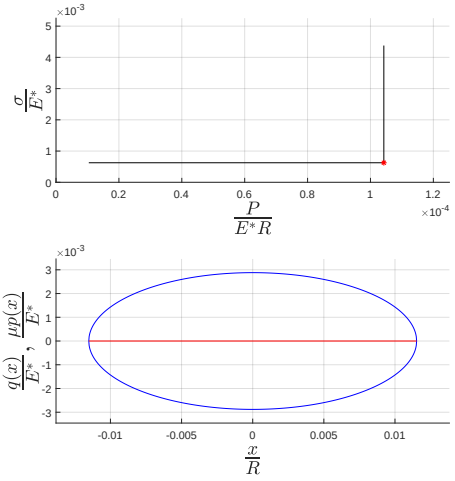
Figure 2: The state of stress at various points around the sequential loading cycle.

Having found the state of stress in the half planes we can now use equation 18 to find the slip displacements present within the slip region. In this load cycle slip occurs in both directions, with slip being locked into the contact when the direction of loading reverses. To account for this the slip displacements during the initial, forward slip loading phase are found, then subtracted from the overall state of slip during unloading to find the reverse slip displacements.

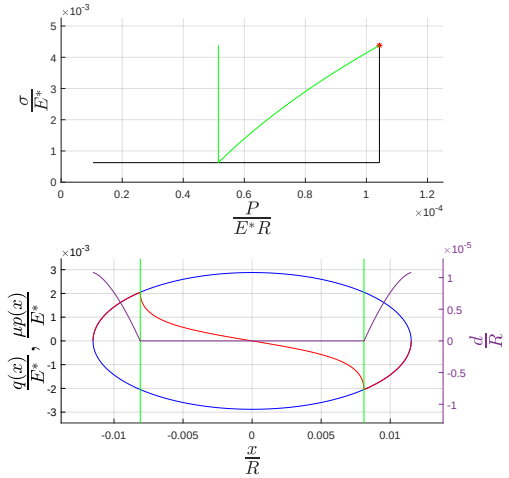
Figure 3 shows the slip displacements at the same points in the load cycle used in figure 2, overlaid on the contact pressure and shear traction distribution. The slip displacements are shown in purple, with the forward slip displacement from loading shown in solid line, and the reverse slip displacements from unloading shown in dashed lines. The blue lines show the contact pressure distribution, the red lines show the shear traction distribution, and the green and yellow markers show the extent of the loading and unloading slip zones respectively. Note that the slip displacement during loading is not the same as the slip displacement during unloading, in constant normal load cycles this condition is required to prevent accumulation of material. In this cycle, however, particles in the interface return to their original position while out of contact, therefore reducing the amount of reverse slip.



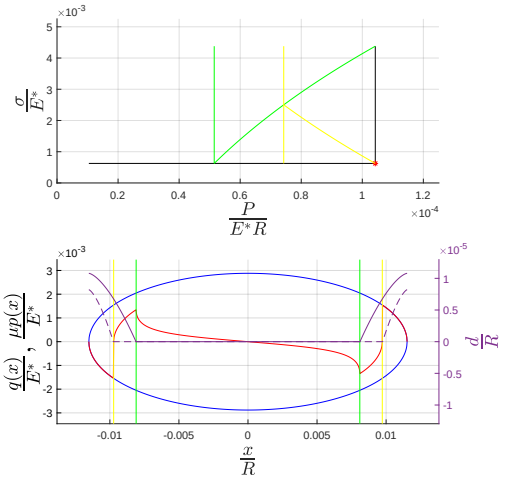
(a) The slip displacements at the start of the sequential load cycle, no slip present.



(b) The slip displacements at the end point of the first step of the sequential load cycle, no slip present.



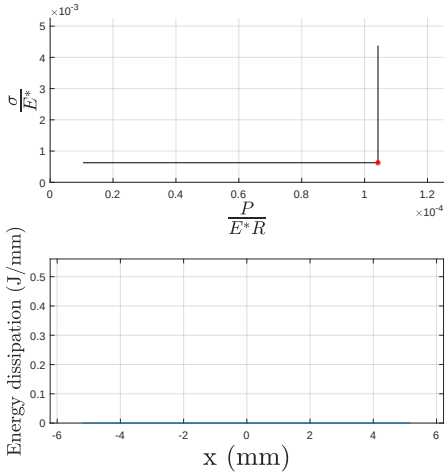
(c) The slip displacements at the end of the second step of the sequential load cycle, forward slip present.



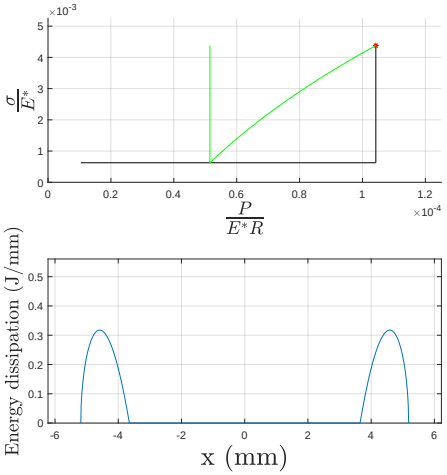
(d) The slip displacements at the end of the third step of the sequential load cycles, forward and reverse slip present.

Figure 3: The slip displacements in the contact at various points in the load cycle for a contact following a sequential load path. For clarity each direction of slip is shown separately.

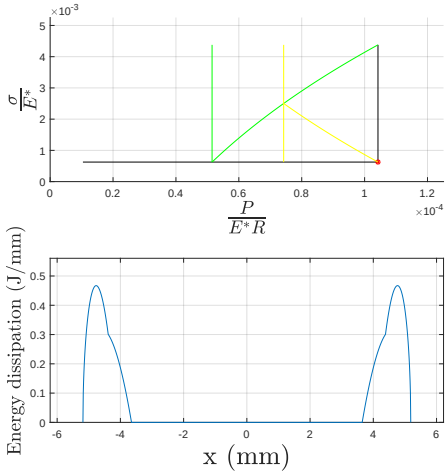
The final quantity to calculate is the dissipated energy, using equation 20. The dissipated energy at various points around the cycle is shown in figure 4. As slip occurs in both directions during this loading cycle we must once again handle each loading step separately.



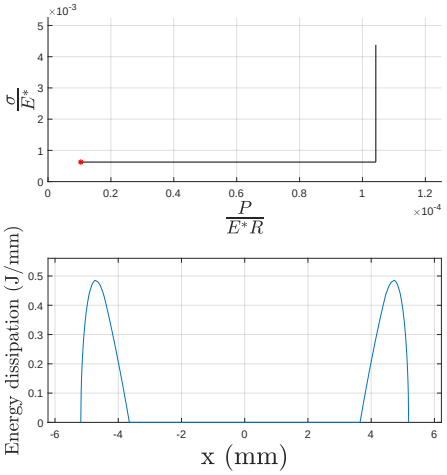
(a) The dissipated energy at the end of the first stage of the sequential load cycle.



(b) The dissipated energy at the end of the second stage of the sequential load cycle.



(c) The dissipated energy at the end of the third stage of the sequential load cycle.



(d) The dissipated energy at the end of the fourth stage of the sequential load cycle.

Figure 4: The cumulative dissipated energy during one cycle of loading, illustrated at various points around the load path.

3.3 Comparison and Commentary

We have now found the complete state of stress for two load cycles moving between the same two points in load space, but with drastically different behaviour. Some of the differences are obvious: the proportional load cycle remains fully stuck throughout the entire load path while the sequential load path experiences reversing slip, for example.

Drawing direct comparisons between the state of stress is only possible at the end points of the load cycle, as these are the only points in the two load cycles where the force states are coincident. Furthermore, at load point (P_1, σ_1) the state of stress is identical in both load paths, as the shear traction and contact pressure is identical, so no meaningful comparison can be made.

Figure 5 shows the difference in the state of stress at point (P_2, σ_2). The two figures in the top left show a comparison of the shear traction and σ_{xx} stresses along the surface, with the stresses field shown in red, the proportional stresses shown in blue, and the difference between them shown in dashed black. The three other plots in the figure show contours of the difference in stress in the half plane, with the

state of stress from the proportional load cycle having being subtracted from the state of stress from the sequential load cycle. In these plots each contour represents an increment of normalised bulk load, $\frac{\sigma}{E^*}$, equal to 0.0002. It is apparent that the variations in the full stress field are small, and confined primarily to a small region near the edge of contact.

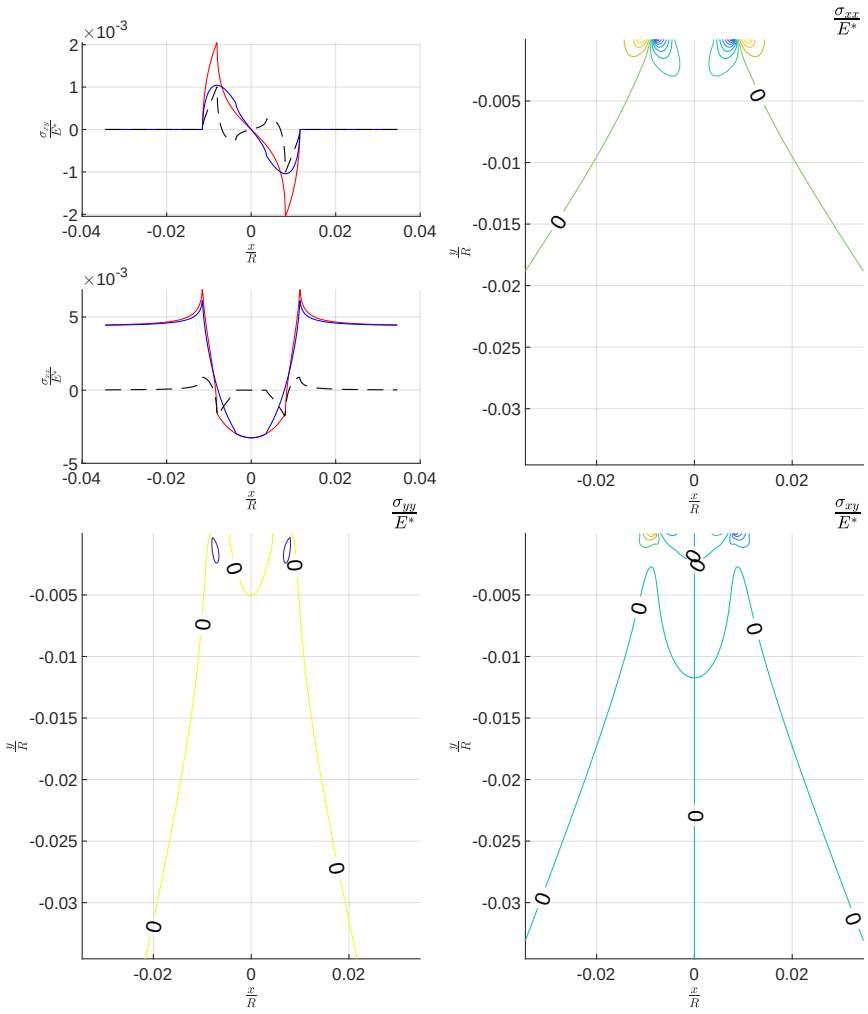


Figure 5: The difference in the stress components between a proportional and sequential load path at point (P_2, σ_2).

It is worth considering the behaviour of the σ_{xx} stress on the surface in more detail, as it is believed that the stress parallel to the surface of the half plane is responsible for driving crack propagation, by causing any cracks which initiate on the surface to open. Figure 6 contains two plots, the top one shows the maximum and minimum values of σ_{xx} at each point in space throughout the load cycle, with the proportional load path in red and the sequential in blue. The bottom plot shows the range of σ_{xx} within a load cycle for each point in space – this is the difference between the top two plots.

The maximum σ_{xx} plots are similar, with the major difference being in the region between the maximum and minimum extent of the contact. In the sequential load case the maximum value of σ_{xx} in this area is zero, as the compressive component of stress due to the contact pressure is applied *before* the tensile component due to the bulk tension. In the proportional load case, however, the maximum σ_{xx} is positive during the simultaneous application of normal load and bulk tension. A peak of tensile

σ_{xx} tension due to the bulk tension follows the edge of contact.

The plots of the minimum σ_{xx} show significant differences, with the sequential load case having much more negative σ_{xx} than the proportional case. In the proportional case the shear tractions are always of the same sign, so the corresponding component of σ_{xx} is always tensile. The sequential load path, in contrast, features shear traction reversal: during the unloading portion of the load path shear tractions having opposite sign are created, resulting in compressive σ_{xx} stresses. This therefore makes the minimum value of σ_{xx} much more negative than in the proportional load case.

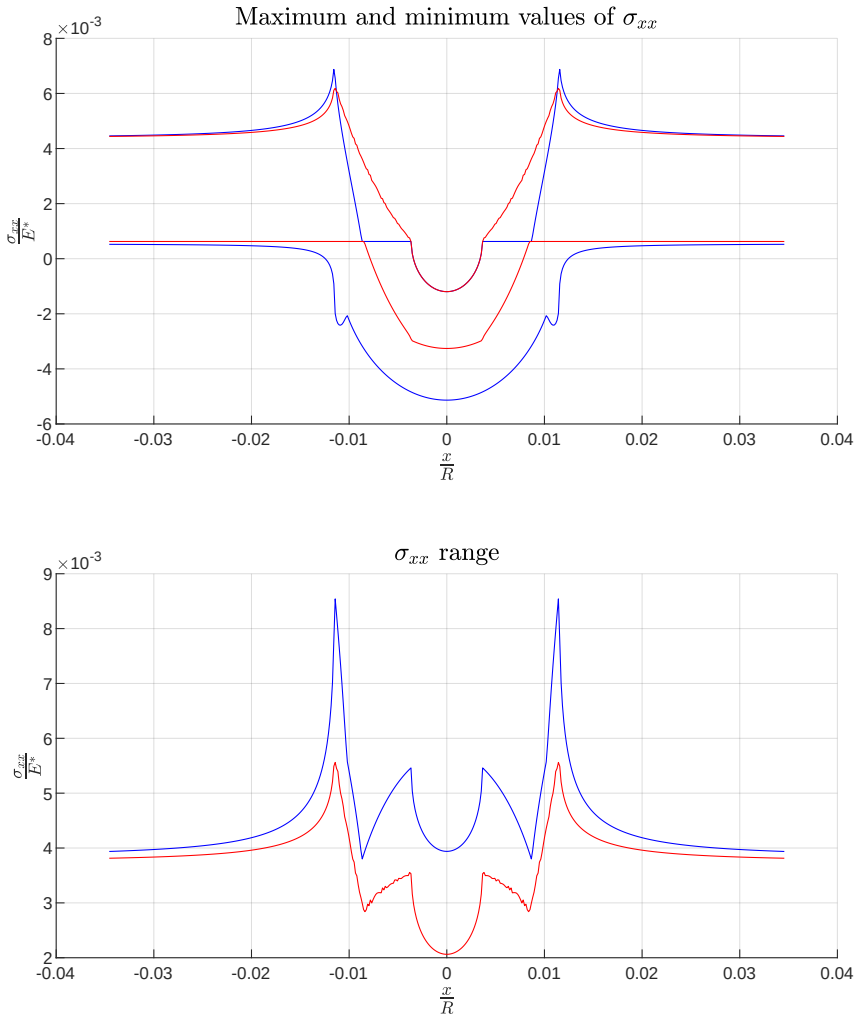


Figure 6: The maximum and minimum values of σ_{xx} along the surface (top), and the range of σ_{xx} throughout the cycle (bottom). The proportional cycle is shown in red, the sequential in blue.

4 Triangular Loops

In the first section of this paper we studied the proportional and sequential loading cycles, and where, in each case, the unloading path is the same as the loading path. We now wish to extend the analysis to cover load paths where the unloading portion of the cycle is different from the loading portion, so that the load path takes the form of an enclosed loop. As discussed in our previous paper [2], these load paths have a number of features which make them illuminating to use in fretting fatigue experiments.

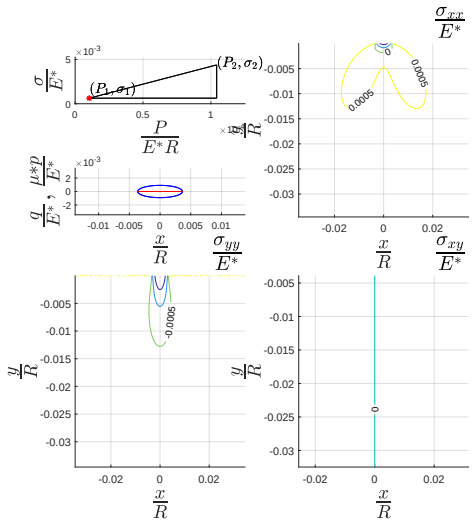
4.1 Right angled Loops

Having compared the behaviour of the proportional and sequential load paths we now wish to combine them, forming a load path consisting of either a sequential loading followed by proportional unloading, or a proportional loading followed by sequential loading. We previously found the shear traction solution for these load paths in [2], where we showed that they experienced slip in only one direction. Experimentally these load paths are therefore valuable for studying the effects of slip directionality and slip reversal on fatigue life.

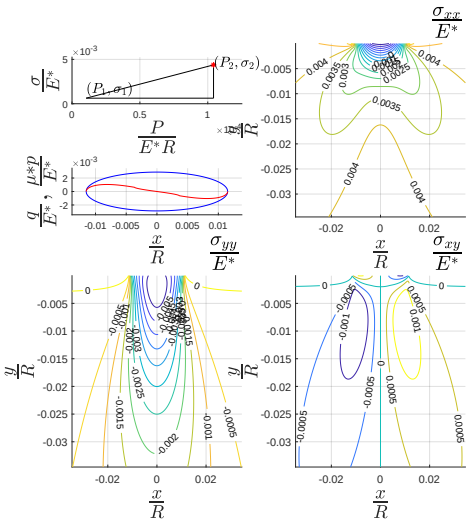
4.1.1 Clockwise

First let us consider this load path in a clockwise direction, so that the contact is first loaded proportionally from (P_1, σ_1) to (P_2, σ_2), then unloaded sequentially, from (P_2, σ_2) to (P_2, σ_1) to (P_1, σ_1). The gradient of loading during the proportional step is chosen so that the contact remains fully stuck. The full stress field solution consists of a contact pressure potential field and a superposition of two full stick shear tractions, as described in section 3.1. During the second step of loading the bulk tension is removed, and a reverse slip zone develops at the edge of contact. The solution during this step therefore consists of a partial slip solution, as given by equation 3, with the stuck shear tractions from the previous loading step preserved only over the stick zone. During the third and final stage of loading the normal load is itself removed, during which a small reverse slip zone follows the edge of contact. The shear traction distribution during this phase of the cycle therefore has the same components as in the second step.

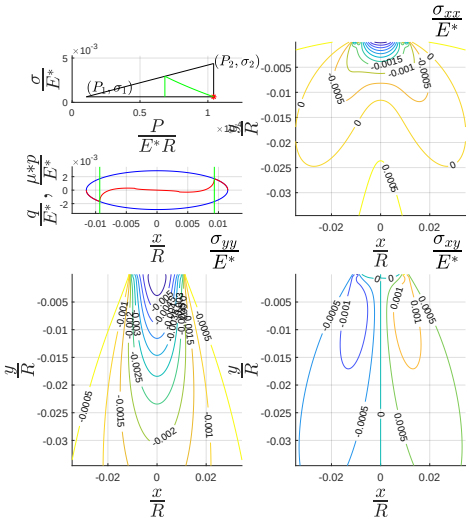
The state of stress in the half plane is plotted in figure 7 at various points around the load path. The plots in the top left show the location in the load path with the construction used to find the slip zone size and the surface traction components. The contact pressure is in blue, the shear traction in red. The remaining plots show contours of the σ_{xx} (top right), σ_{yy} (bottom left) and σ_{xy} (bottom right) stress fields.



(a) The state of stress at the start of the clockwise right angle load path



(b) The state of stress at the end of the first step of the clockwise right angle load path



(c) The state of stress at the end of the second step of the clockwise right angle load path

Figure 7: The state of stress and surface tractions at various points along the clockwise right angled load path.

Having found the state of stress in the half plane it is possible to find the slip displacements throughout the load cycle. An example of these is plotted in figure 8, the upper figure showing the current position within the load path, the lower figure showing the contact pressure in blue, shear traction in red and slip displacement in purple. Within a complete cycle all particles in the bodies must return to their original location to prevent accumulation of material. In this load path slip occurs in only one direction, with the reverse motion of the bodies occurring when the two components are out of contact.

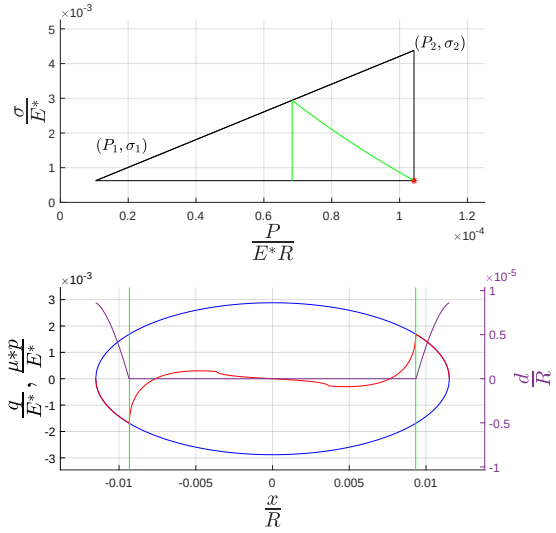
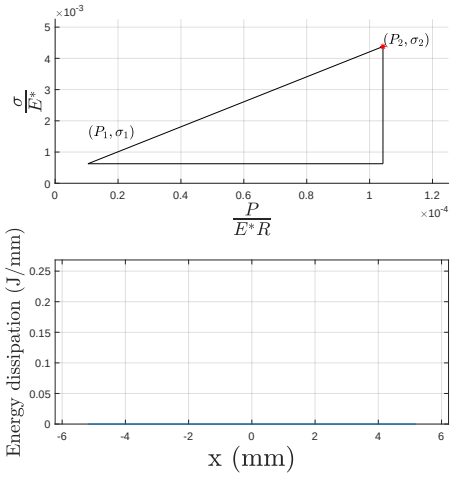


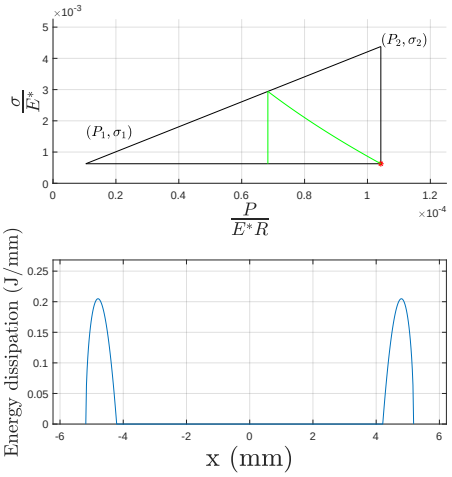
Figure 8: The Slip displacements during the clockwise right angled load path

The final step in the analysis, here, is calculating the dissipated energy per cycle, using the slip displacements and equation 19. The dissipated energy at the end of each step of the loading cycle is plotted in figure 9. During the first load step the contact is loaded proportionally - there is no slip, and therefore no energy dissipation. The second step of the loading cycle consists of unloading the bulk tension at a fixed normal load the product of the contact pressure and the slip displacements produce

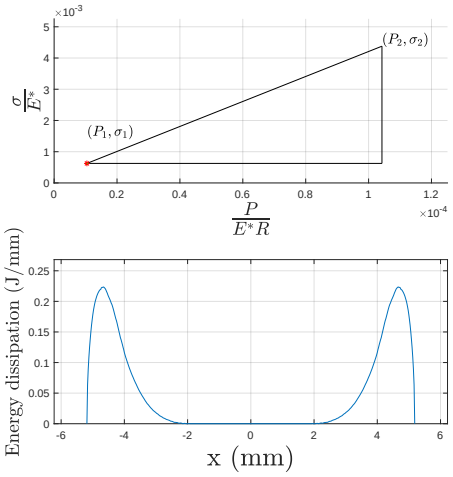
the energy distribution shown, with the energy tending smoothly to zero at both the inner and outer edges of the slip zone. During the final stage of the cycle the normal load is removed at a constant bulk tension. This causes a small slip zone to follow the edge of the contact creating the "tail" of the energy distribution, as shown.



(a) The cumulative dissipated energy at the end of the first step of the right angled clockwise loop



(b) The cumulative dissipated energy at the end of the second step of the right angled clockwise loop



(c) The cumulative dissipated energy at the end of the third step of the right angled clockwise loop, showing the total energy dissipation in a cycle

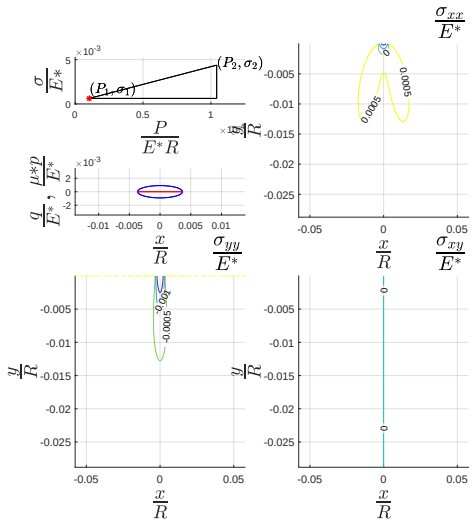
Figure 9: The cumulative dissipated energy dissipated energy at various points in the right angled clockwise loading path

4.1.2 Anticlockwise

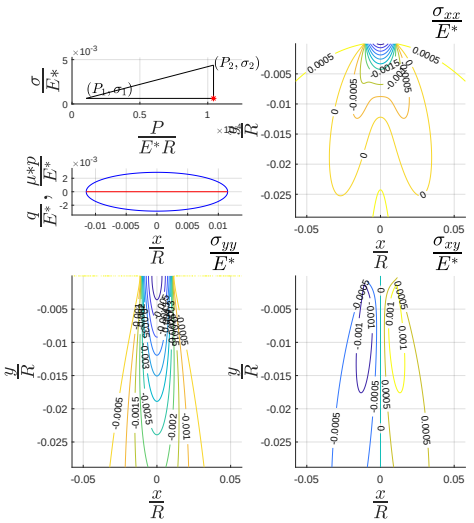
Let us now consider the behaviour of the contact when we follow the same load path, but in the opposite direction - first loading the contact sequentially from (P_1, σ_1) to (P_2, σ_2), then unloading the contact proportionally. During the first stage of this load cycle the normal load is applied at a constant bulk tension, the contact is loaded from (P_1, σ_1) to (P_2, σ_1), with the contact interface remaining shear traction free. The second stage of this load cycle is the application of the bulk tension at a fixed normal load,

the contact is loaded from (P_2, σ_1) to (P_2, σ_2). As discussed in [2] during this step slip will occur, as the gradient of loading exceeds the maximum to maintain stick. The slip zone size here is larger than that found during the clockwise case, as in this load path the slip zone is growing into a traction free interface, while in the clockwise load path the slip zone grows into an interface with a pre-existing shear traction distribution which opposes the slip, and the slip displacement is in the opposite direction. The final step of this load path is a proportional unloading from (P_2, σ_2) to (P_1, σ_1). As the loads are removed the slip-stick transition point moves towards the centre of the contact, just as it did in the clockwise load path.

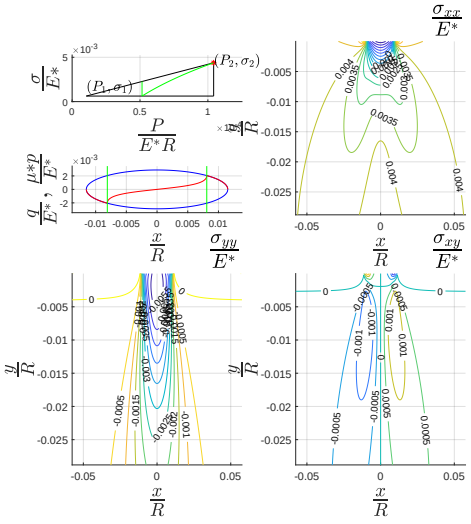
The full state of stress at various points around this load cycle is shown in figure 10, in an identical format to the plots given in the clockwise load cycle. The pair of plots in the top left of the figure show the position in load space and the shear traction distribution, the remaining three figures show (clockwise from top right) the σ_{xx}, σ_{xy} and σ_{yy} stress fields.



(a) The state of stress at the start of the anticlockwise right angle load path



(b) The state of stress at the start of the second step of the anticlockwise right angle load path



(c) The state of stress at the start of the third step of the anticlockwise right angle load path

Figure 10: The state of stress and surface tractions at various points along the anticlockwise right angled load path.

Although figure 10 shows the stress fields in the lower half plane only, the stress fields in the upper half plane can be found using the same method. Having found the full state of stress it is possible to use equation 18 to calculate the slip displacements, these are shown in purple at a location in the load path in figure 11.

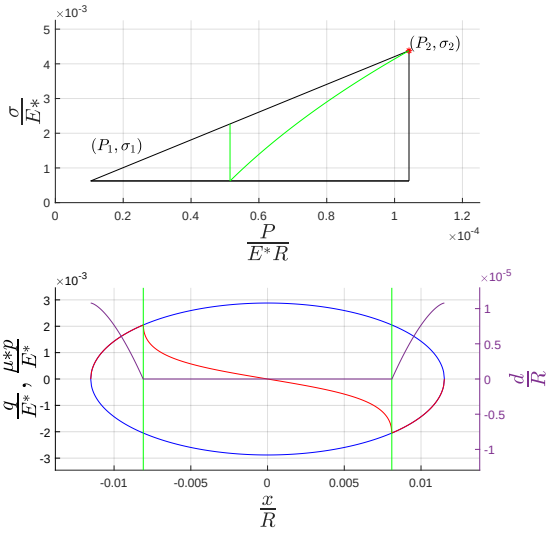
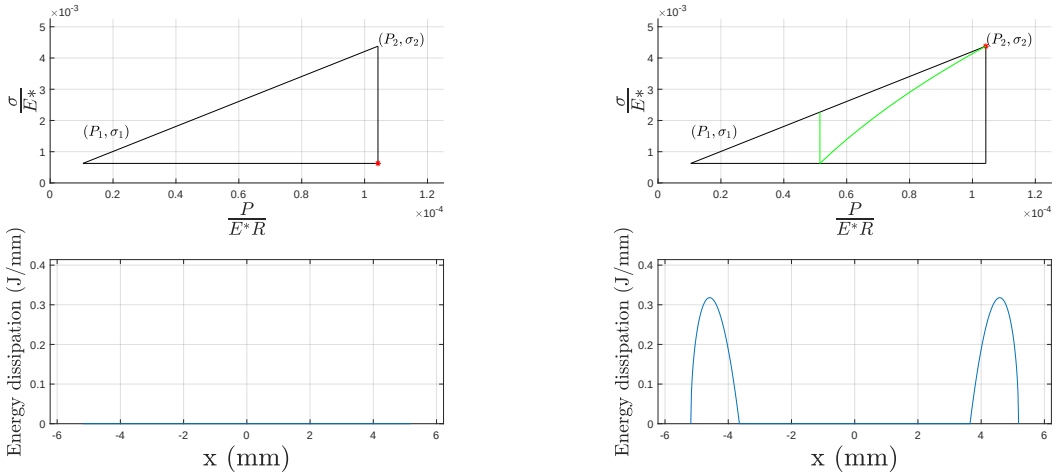


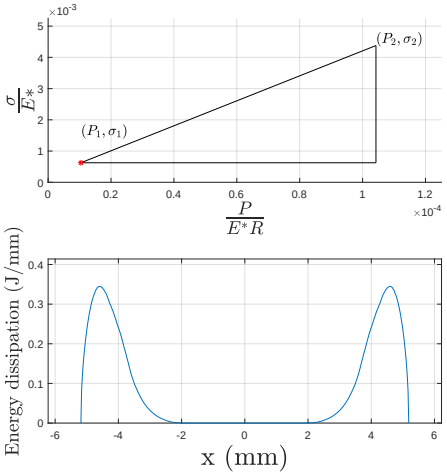
Figure 11: The slip displacements at a point in the anticlockwise right angled load path

Finally it is possible to calculate the dissipated energy, shown in figure 12. During the first step of the load cycle there is no shear traction and no slip, so there is consequently no dissipated energy. During the second step of loading bulk tension is applied at a constant normal load, and a slip zone is formed. The product of the shear traction (bounded at the edge of contact) and the slip displacements (bounded at the slip-stick transition point) produce the energy distribution shown, bounded at both ends. During the final stage of this load cycle the contact is unloaded proportionally, and a slip zone follows the edge of the contact. This results in the "tail" of the energy distribution, extending towards the initial size of the contact.



(a) The cumulative dissipated energy at the end of the first step of the right angled anticlockwise loop

(b) The cumulative dissipated energy at the end of the second step of the right angled anticlockwise loop



(c) The cumulative dissipated energy at the end of the right angled anticlockwise loop

Figure 12: The cumulative dissipated energy at various points in the anticlockwise right angled load path

4.1.3 Comparison and Commentary

In the previous sections a pair of load paths having the form of a right angled triangle were described, both having the useful property that slip occurs in only one direction. Load paths of this form therefore have great utility in fretting fatigue experiments, as by using them in combination they allow investigation of the effect of slip direction and reversal. To characterise fully these experiments it is necessary to compare how properties of the contact change when the order of loading is reversed.

The stress parallel to the surface, σ_{xx} is one such property – it's presence is thought to be responsible for propagating cracks once they initiate at the surface, which leads to the eventual failure of the component.

Figure 13 compares the σ_{xx} stress for the clockwise and anticlockwise right angled loops, the clockwise direction being plotted in red, the anticlockwise plotted in blue. The upper figure shows the maximum and minimum values of σ_{xx} at each location in the contact over the course of a cycle, while the lower figure shows the range in σ_{xx} at each location.

It is immediately apparent that simply reversing the direction of loading results in a significant difference in the σ_{xx} stresses due to the difference in the shear traction distribution along the interface. In the clockwise direction the shear traction reverses sign during the load cycle whereas in the anticlockwise direction the shear tractions are always of the same sense. Due to this shear traction reversal the slip zones in the clockwise load cycle are smaller than those in the anticlockwise load cycle – following the clockwise path the slip zone has to grow into a region of the contact with a pre-existing shear traction that opposes the slip, whereas in the anticlockwise case the slip zone grows into a traction free interface. These factors combined result in the clockwise load path experiencing a larger range of σ_{xx} stresses, but over a smaller area.

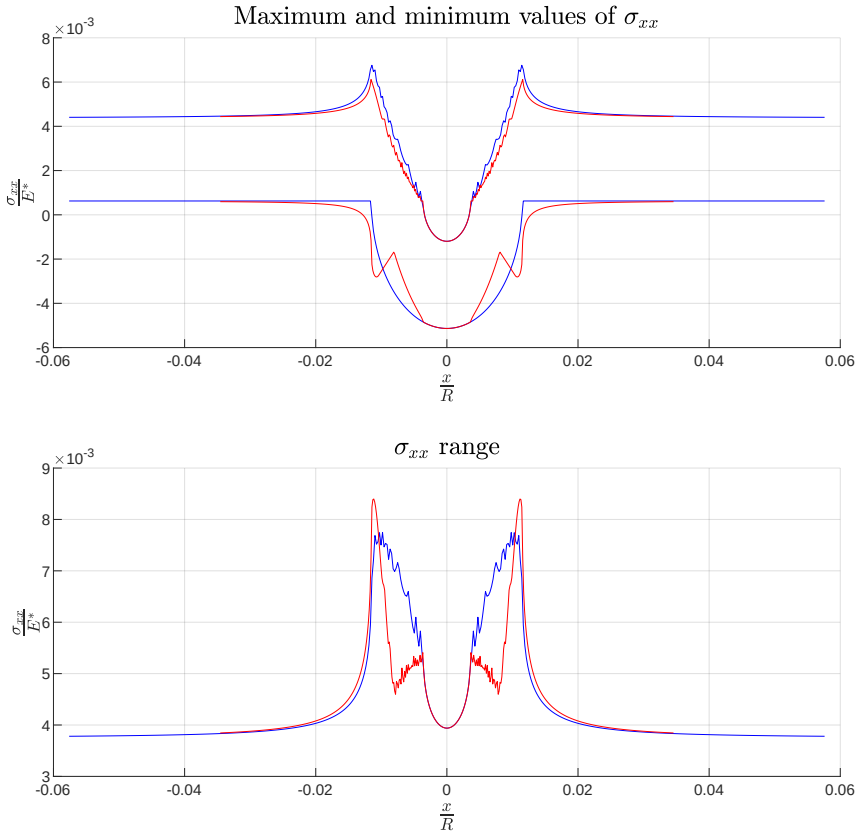


Figure 13: The difference in the σ_{xx} stresses along the surface of the dog bone for the right angled load path for the clockwise (red) and anticlockwise (blue) loading directions. The top plot shows the maximum and minimum values of σ_{xx} at each location along the surface of the half plane, the bottom figure shows the range of σ_{xx} at each location over a cycle.

We continue the analysis by again calculating the slip displacements. Figure 14 shows the maximum slip displacement at each location in the contact, with the clockwise load path shown in red and the anticlockwise load path shown in blue.

It can clearly be seen that while slip occurs over the same regions of the contact the slip displacements differ significantly in each direction, with the anticlockwise load path having larger slip displacements at all locations within the contact. This is expected: as previously mentioned in one direction the slip extends into a traction free interface, while in the other it extends into a pre-existing shear traction field which opposes the slip. With this difference in the slip zone size it is reasonable to assume a corresponding increase in the slip displacement.

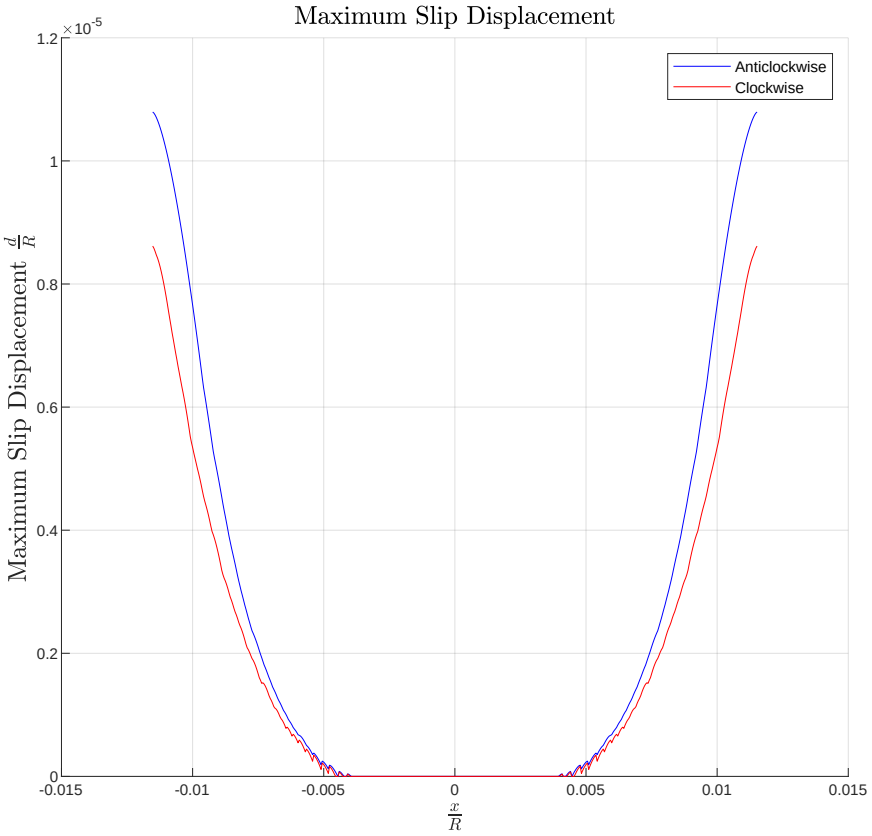


Figure 14: The maximum slip displacements at each point in the contact over the complete load cycle, for the clockwise (red) and anticlockwise (blue) right angled triangular load paths.

Finally we calculate the energy dissipated within the cycle, this is plotted for one complete load loop in figure 15. Once again, the anticlockwise loop is plotted in blue, the clockwise loop in red.

It is apparent that the dissipated energy in the anticlockwise direction is significantly higher than that in the clockwise direction. It is already known that reversing the direction of loading results in a significant difference in the slip displacements, so it is unsurprising that there is a corresponding difference in the dissipated energy. It is worth noting, however, that the result is not simply scaled by the difference in slip displacement, as the shear traction in the slip zone depends upon the applied load when the contact slips, which itself depends on the load path.

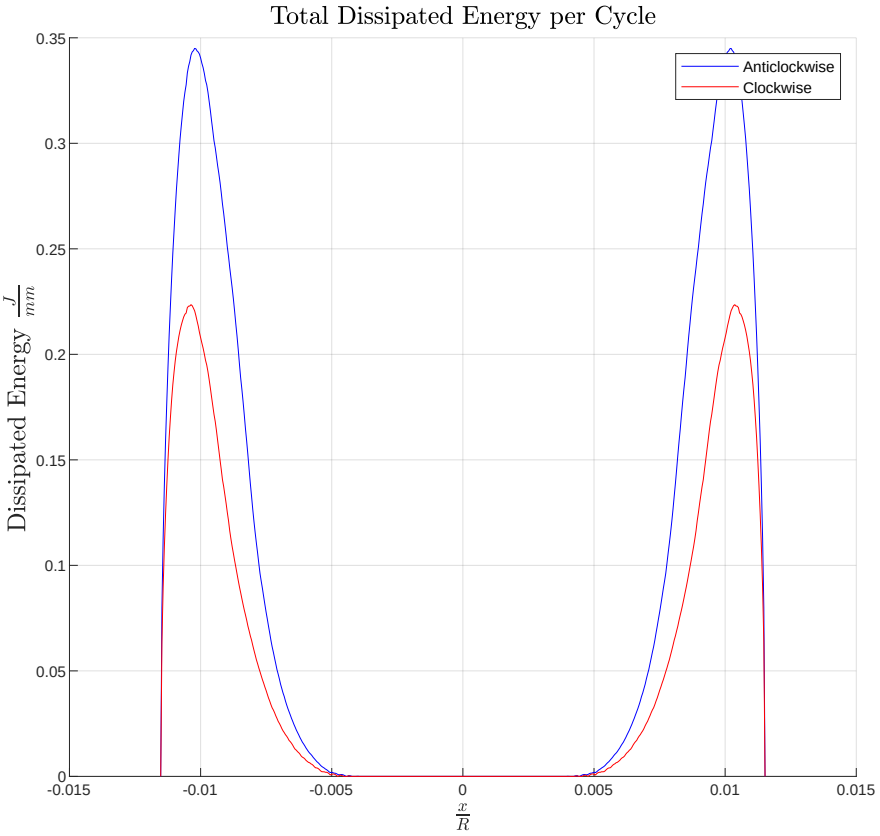


Figure 15: The difference in total dissipated energy per cycle for the clockwise (red) and anticlockwise (blue) right angled load paths.

While the load paths as described do allow for investigation of slip directionality there are a number of major differences between them which limit the extent to which it is possible to isolate the effect of slip direction from other tribological effects.

The σ_{xx} stresses change significantly when the direction of loading is reversed, especially at the very edge of the contact where fretting fatigue cracks are likely to initiate, so the crack propagation behaviour may vary significantly. The slip displacements and dissipated energy also change drastically if the direction of the load path is swapped, which implies that the wear and surface damage will change significantly.

4.2 Isosceles Loops

The right angled load path discussed in the previous section has the very useful property that slip occurs in only one direction during the loading cycle, allowing for experimental investigation of the effect of slip directionality and reversal, but it has a number of major shortcomings, primarily based around the slip and stress behaviour being significantly different when the direction of loading is reversed. In order to address these an alternative load path having the form of an isosceles loop is proposed. This load path is symmetrical in P, σ space, which means that the slip zone constructions are identical in each loading direction and therefore the slip zone sizes are the same.

The three corners of the load path are located at load coordinates (P_1, σ_1), (P_2, σ_{max}) and (P_2, σ_{min}), where to maintain symmetry one of the load points is fixed in relation to the other two, via $\sigma_{max} = \sigma_1 + (\sigma_1 - \sigma_{min})$.

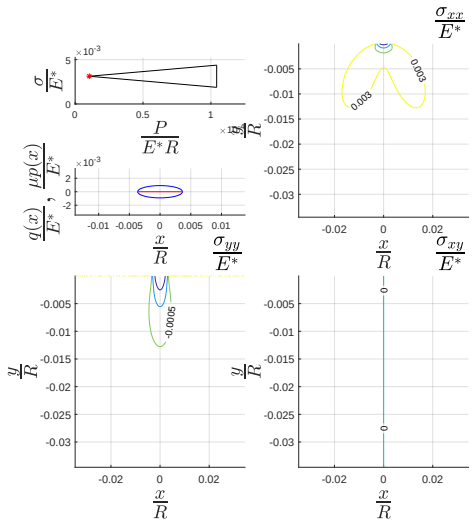
4.2.1 Clockwise

Let us start by considering the behaviour of the contact when the load path follows a clockwise direction. It has three parts, in the first of which the contact is loaded proportionally from the minimum load point (P_1, σ_1) to the maximum load point (P_2, σ_{Pmax}), the gradient of loading being chosen so that during this stage of loading the contact remains fully stuck. The full stress field solution during this stage of loading therefore consists of a pair of potential fields associated with two fully stuck shear traction distributions, as given by equation 7, in an identical manner to the proportional and clockwise right angled load path.

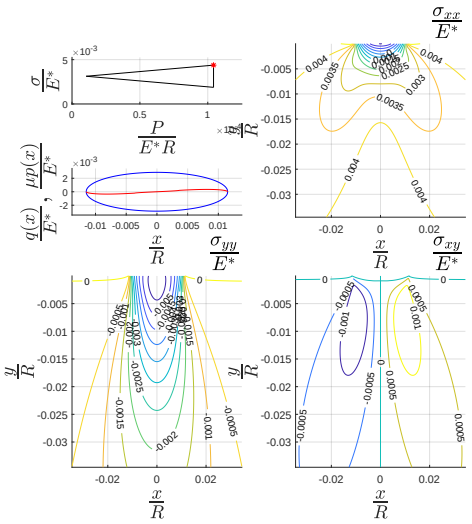
The second step of this load path involves the unloading of the bulk tension at a fixed normal load, the contact is unloaded from (P_2, σ_{max}) to (P_2, σ_{min}). During this stage of unloading a slip zone is created, with the shear traction distribution from the slip being of opposite sign to the shear tractions locked in during the proportional loading. The full stress field solution therefore consists of the pair of full stick shear traction distributions from the first step of the load cycle, but preserved only over the region of the contact that does not slip, and a potential field associated with the partial slip shear traction distribution, given by equation 3.

The final stage of the load path is a proportional unloading from (P_2, σ_{min}) to (P_1, σ_1). During this the slip will continue, following the edge of the contact, while the shear traction from the proportional loading will be preserved over the shrinking stick zone. The full stress field solution therefore has the same three components as the second stage of loading.

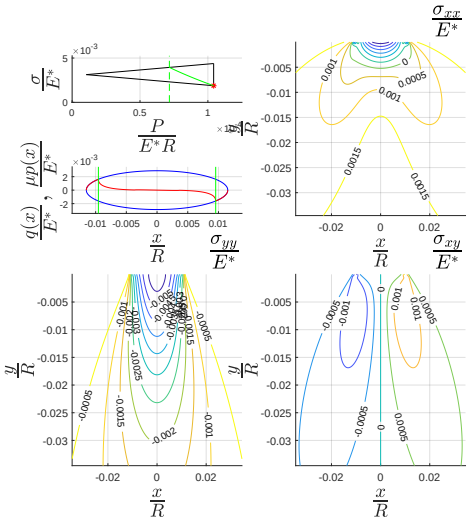
Figure 16 shows plots of the full stress field in the lower half plane at various points around the load path. These figures are in the same format as the plots in the previous sections. The upper left plots show the position in load space and the contact pressure envelope (blue) and shear traction distribution (red). The remaining three plots show (going clockwise from the top left) contours of the σ_{xx}, σ_{xy} and σ_{yy} stress fields.



(a) The state of stress at the start of the clockwise isosceles load path



(b) The state of stress at the start of the second step of the clockwise isosceles load path



(c) The state of stress at the start of the third step of the clockwise isosceles load path

Figure 16: The state of stress at various points around the clockwise isosceles load path

Once we have found the stress σ_{xx} parallel to the surface we can once again find the slip displacements throughout the load cycle, by using equation 18. Figure 17 shows an example plot of the slip displacements (in purple) overlaid on the shear traction (red) and contact pressure envelope (blue) at a point in the load history.

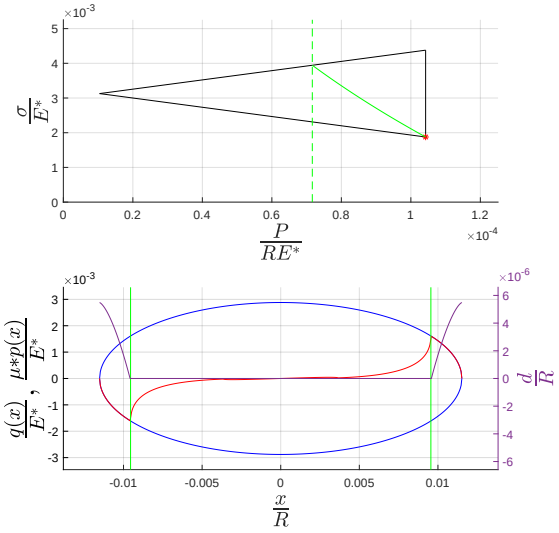
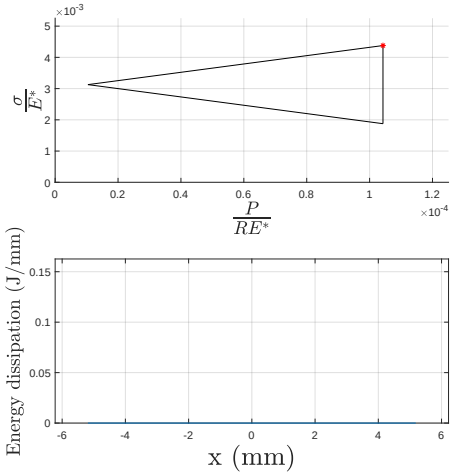
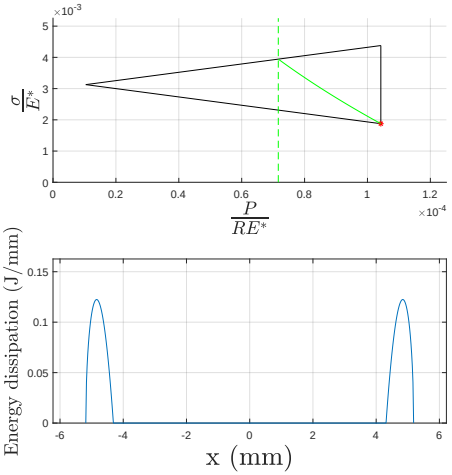


Figure 17: The slip displacement at a point in the clockwise isosceles load path

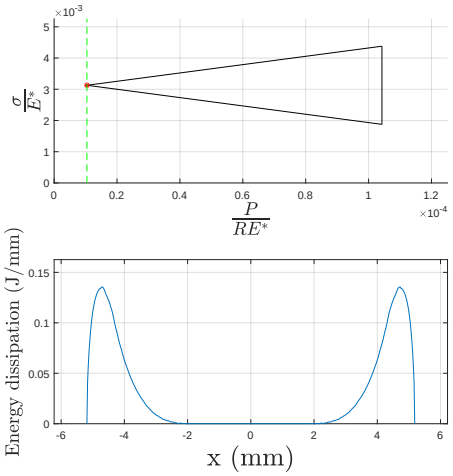
Finally we can use the slip displacements to find the dissipated energy per cycle, using equation 20. The distribution of dissipated energy at various points around the cycle are plotted in figure 18.



(a) The cumulative energy dissipation at the end of the fist step of the clockwise isosceles load path



(b) The cumulative energy dissipation at the end of the second step of the clockwise isosceles load path



(c) The cumulative energy dissipation at the end of the third step of the clockwise isosceles load path

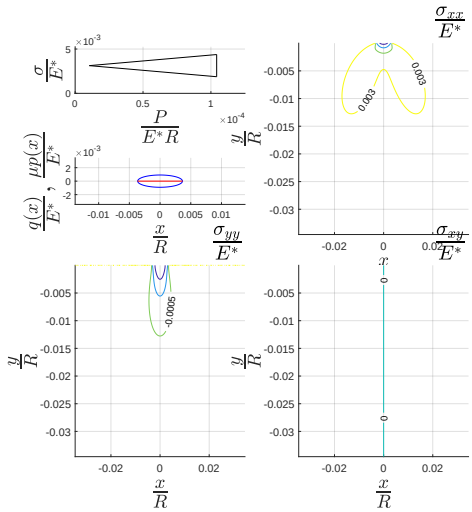
Figure 18: The cumulative energy dissipation at various points around the clockwise isosceles load path

4.2.2 Anticlockwise

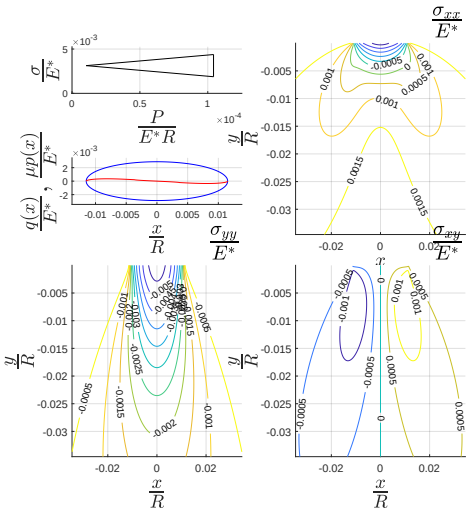
Lastly consider the behaviour of the contact when the direction of the load path, so that the order of loading is (P_1, σ_1), (P_2, σ_{min}), (P_2, σ_{max}), (P_1, σ_1). As the load path is symmetrical the shear traction produced has the same form as that produced during the clockwise load path, but with opposite sign.

The shear traction components during each step of the load path are the same as those described in section 4.2.1, the only difference being a change of sign, and therefore the corresponding potential field components during each stage of the load path are likewise similar.

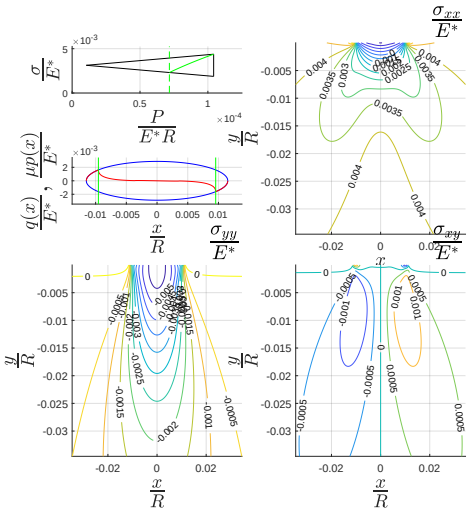
Plots of the state of state of stress in the lower half plane at various points around the load path are given in figure 19. The top left plots show the location in the load cycle and the shear traction distribution (red) and contact pressure envelope (blue). The remaining three plots show (clockwise from top right) contour plots of the σ_{xx}, σ_{xy} and σ_{yy} stress fields.



(a) The state of stress at the start of the anticlockwise isosceles load path



(b) The state of stress at the start of the second step of the anticlockwise isosceles load path



(c) The state of stress at the start of the third step of the anticlockwise isosceles load path

Figure 19: The state of stress at various points around the anticlockwise isosceles load path

Once again we can use the stress parallel with the surface to find the slip displacements, via equation 18. Figure 19 shows an example plot of the slip displacements at a given point in the load cycle.

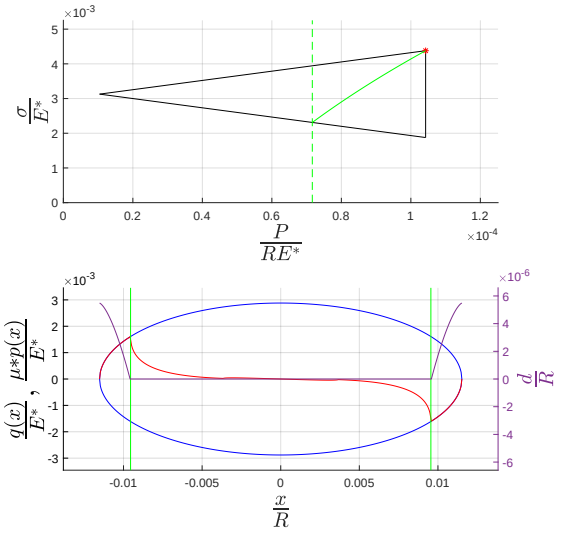
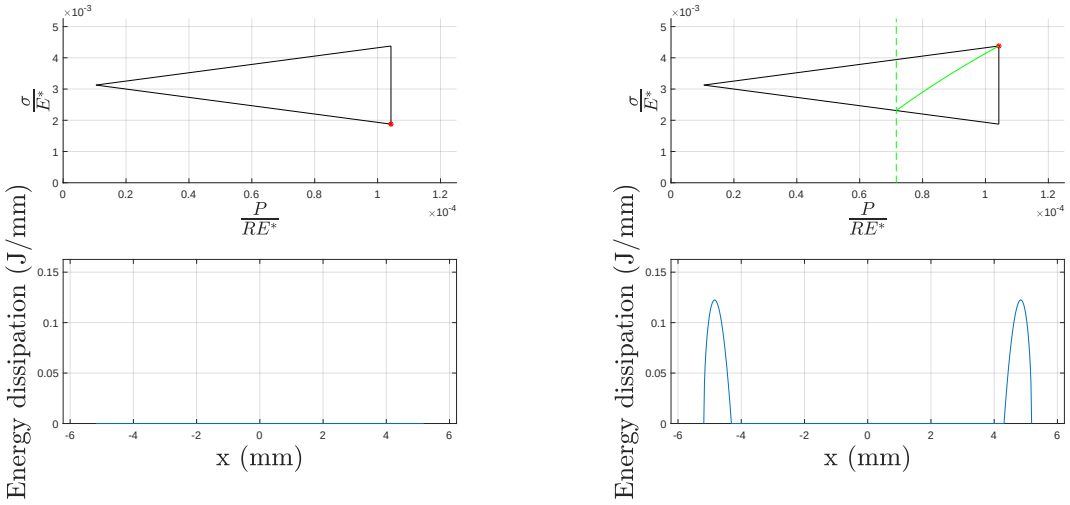


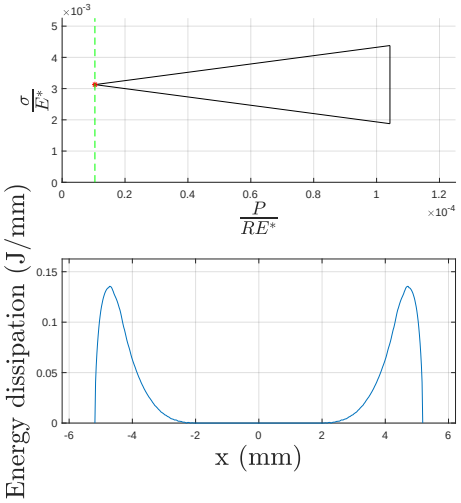
Figure 19: The slip displacement at a point in the anticlockwise isosceles load path

Finally we can once again find the dissipated energy by evaluating equation 20. The dissipated energy distribution at various points around the load path is plotted in figure 20.



(a) The cumulative dissipated energy at the end of the first step of the anticlockwise isosceles load path

(b) The cumulative dissipated energy at the end of the second step of the anticlockwise isosceles load path



(c) The cumulative dissipated energy at the end of the third step of the anticlockwise isosceles load path

Figure 20: The cumulative dissipated energy at various points around the anticlockwise isosceles load path

4.2.3 Comparison and Commentary

By using the isosceles load path we are able to design a pair of fretting fatigue experiments in which reversal of the loading direction creates shear traction distributions which are identical in form but opposite in sign. This has the potential to be extremely useful in the design of fretting fatigue experiments for investigating the effect of slip reversal. In order to characterise fully experiments using these load paths it is important, however, to consider how other properties of the contact vary as the loading is reversed

First let us consider the stress parallel to the surface, σ_{xx}. This stress component is responsible for propagating any cracks which initiate in the contact, and therefore controls whether a surface crack arising from fretting damage will result in failure of the component and how many load cycles that failure will take.

Figure 21 shows two plots comparing the range of σ_{xx} stresses for loading in both the clockwise and anticlockwise direction. The top plot shows the maximum and minimum values of σ_{xx} at each location in the contact over a clockwise (red) and anticlockwise (blue) cycle, the bottom plot shows the range of σ_{xx}.

It can clearly be seen that despite the two directions of loading producing identical shear traction distributions the σ_{xx} distributions produced have major differences. This is because the σ_{xx} has contributions from the contact pressure, remotely applied bulk tension and shear traction, the combination of those combinations depends upon the load path.

It is worth noting that in the region around the edge of the contact at its maximum extent ($\frac{a}{R} \approx 0.1$) the range of shear stresses over a complete cycle are similar, and from experimental measurements [1] it is known that this is the location where cracks initiate during testing. This suggests that the propagation life for a newly initiated crack would be similar.

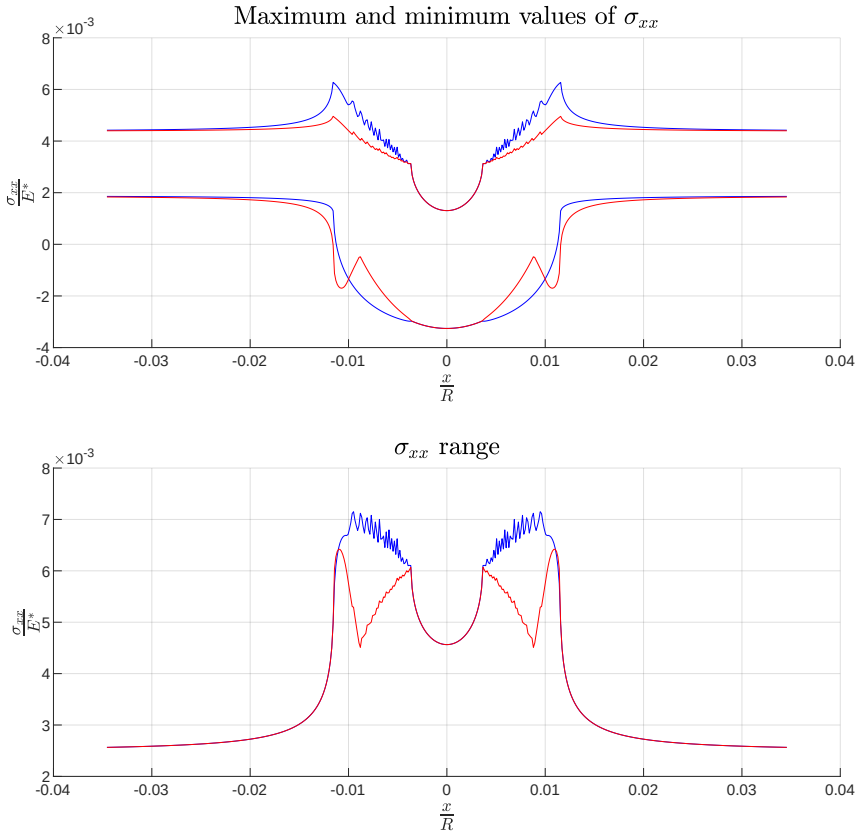


Figure 21: The difference in the σ_{xx} stresses along the surface of the dog bone for the isosceles load path for the clockwise (red) and anticlockwise (blue) loading directions. The top plot shows the maximum and minimum values of σ_{xx} at each location along the surface of the half plane, the bottom figure shows the range of σ_{xx} at each location over a cycle.

Next let us consider the effect of reversing the loading direction on the slip displacements in the contact. Figure 22 shows plots of the maximum slip displacements at each location in the contact for the clockwise (red, dashed) and anticlockwise (blue) loading directions. The slip displacements are found to be identical, which when combined with the knowledge that the shear tractions and contact pressures are also identical would lead some wear laws to imply that the wear to the surface should also be identical.

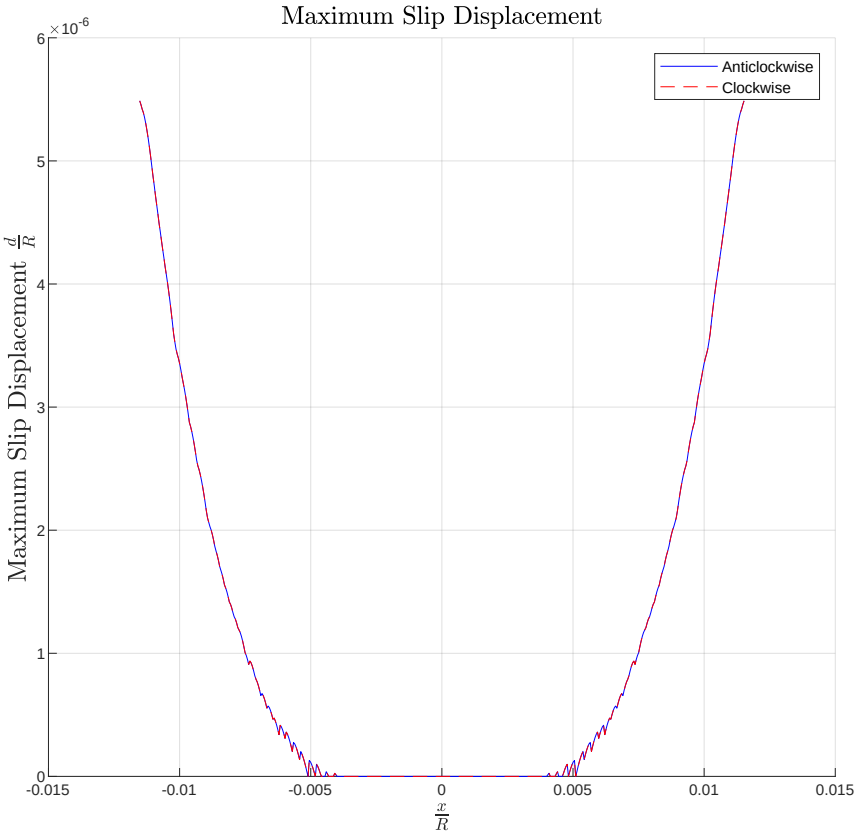


Figure 22: The maximum slip displacements at each point in the contact over the complete load cycle, for the clockwise (red, dashed) and anticlockwise (blue) isosceles triangular load paths.

Finally Figure 23 shows plots of the dissipated energy per cycle in the clockwise (dashed, red) and anticlockwise loading directions. As expected the dissipated energy per cycle is identical: this is because the slip displacements and shear tractions were already known to be the same in both loading directions and the dissipated energy is simply the integral of their product.

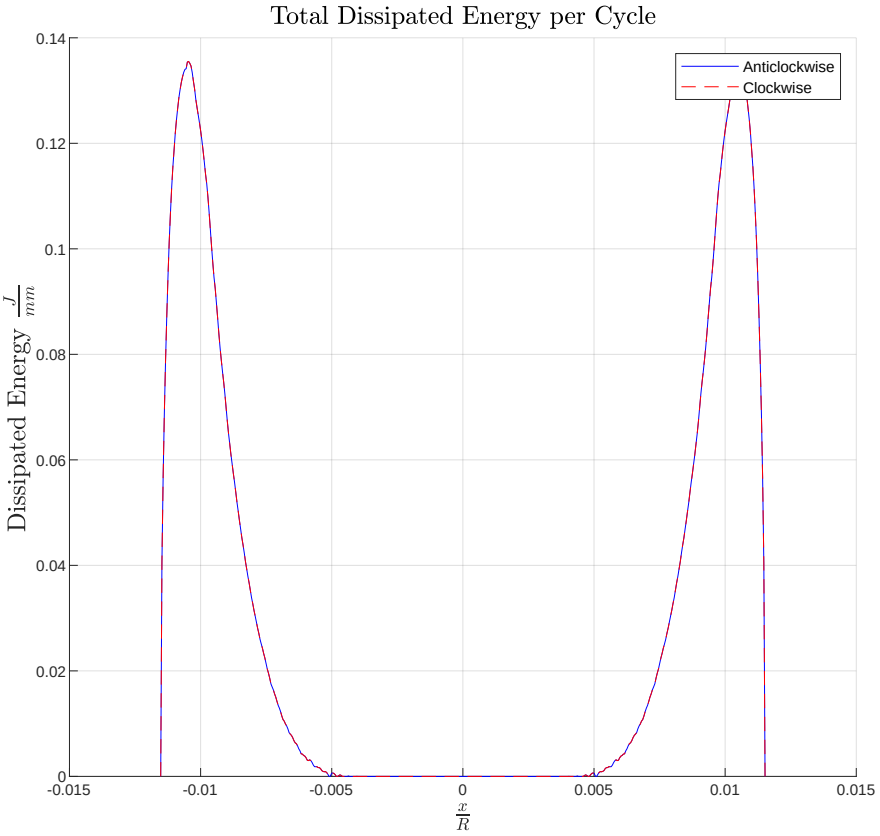


Figure 23: The difference in total dissipated energy per cycle for the clockwise (red, dashed) and anticlockwise (blue) isosceles load paths.

By using these isosceles load paths we have therefore arrived at a pair of tests in which slip occurs in only one direction. The slip displacements and dissipated energy per cycle are identical when the direction of loading reverses, and where the σ_{xx} stresses in the region around the edge of the contact are similar.

5 Conclusion

Throughout this paper we have found the full state of stress for contacts following complex bulk tension-normal load paths via the use of complex potentials. A number of further properties have been derived from these stress fields, specifically the slip displacements and dissipated energy.

The first pair of load paths discussed were proportional and sequential in form, it was demonstrated that by changing the order in which the loads are applied and removed it is possible to design a pair of fretting fatigue experiments moving between the same points in load space, but where the shear traction distributions, presence of slip and dissipation of energy are drastically different. By performing fretting fatigue experiments using these load paths it is possible to begin identifying which properties of the contact problem contribute to fretting fatigue failures.

The proportional and sequential load paths were then combined, creating a right angled load path where the contact slips in one direction only. These load paths have great potential to be used experimentally to investigate the effect of unidirectional vs reversing slip, as well as the effect of slip direction, but investigation shows that the behaviour of these load paths diverges in a number of other ways, with there being significant differences in slip displacements, dissipated energies and the underlying stress field.

To address the shortcomings in the right angled load path an isosceles load path is developed. This also has the useful property that slip occurs in only one direction, but the slip displacements and dissipated energy is identical in each loading direction. Additionally the stress parallel to the surface is almost identical in each loading direction in the region adjacent to the edge of the contact.

Together these solutions provide a comprehensive set of tests that make possible new experimental investigations into the failure of fretting contacts.

6 Acknowledgements

James Truelove acknowledges with thanks the award of an iCASE award ref 17000027 from Rolls-Royce plc which has enabled him to carry out this work.

David Hills and Luke Blades acknowledge Rolls-Royce plc and the EPSRC for their support under the Prosperity Partnership Grant "Cornerstone: Mechanical Engineering Science to Enable Aero Propulsion Futures", Grant Ref: EP/R004951/1.

References

[1] L. Blades, J. Truelove, R. Paynter, and D. Hills, "Experimental investigation of the effects of load path on the life of fretting fatigue contacts," *Tribology International*, 2023.

[2] J. Truelove, L. Blades, D. Hills, and R. Paynter, "Frictional half plane contacts subject to varying normal load and bulk tension under various load paths with application to fretting fatigue experiments," *Tribology International*, 2023.

[3] J. Vázquez, C. Navarro, and J. Domínguez, "A new method for obtaining the stress field in plane contacts," *International Journal of Solids and Structures*, vol. 49, no. 26, pp. 3659–3665, 2012.

[4] N. Cwiekala and D. A. Hills, "Half-plane contacts subject to remote tension," *The Journal of Strain Analysis for Engineering Design*, vol. 56, no. 8, pp. 539–547, 2021.

[5] R. Ramesh, J. Barber, and D. Hills, "Plane incomplete contact problems subject to bulk stress with a varying normal load," *International Journal of Mechanical Sciences*, vol. 122, no. January, pp. 228–234, 2017.

[6] J. Vázquez, C. Navarro, and J. Domínguez, "Explicit equations for sub-surface stress field in plane contacts," *International Journal of Mechanical Sciences*, vol. 67, pp. 53–58, 2013.

[7] J. R. Barber, *Contact mechanics*. Springer, 2018.

Statement of Authorship for joint/multi-authored papers for PGR thesis

To appear at the end of each thesis chapter submitted as an article/paper

The statement shall describe the candidate's and co-authors' independent research contributions in the thesis publications. For each publication there should exist a complete statement that is to be filled out and signed by the candidate and supervisor **(only required where there isn't already a statement of contribution within the paper itself).**

Title of Paper	The State of Stress in Fretting Contacts Under Varying Load Paths
Publication Status	□Published □ Accepted for Publication ☑Submitted for Publication □Unpublished and unsubmitted work written in a manuscript style
Publication Details	

Student Confirmation

Student Name:	James Truelove		
Contribution to the Paper	Analysis, Writing of MATLAB code, Writing of manuscript, Production of Figures.		
Signature	James P J. Truelove	Date	17/07/23

Supervisor Confirmation

By signing the Statement of Authorship, you are certifying that the candidate made a substantial contribution to the publication, and that the description described above is accurate.

Supervisor name and title: Prof D A Hills		
Supervisor comments The innovation behind some of the load paths studied here is 100% James' effort. Therefore the whole of most inventive part of this is his. In addition he, of course, did the work he cites as a contribution.		
Signature	Date	19th July 2023

This completed form should be included in the thesis, at the end of the relevant chapter.

10 Future Work

10.1 Design of Additional Load Paths

One potential area for further work involves the design and analysis of additional load paths. The load paths presented in the last two papers of the thesis allow for isolation of the effect of slip direction, but there are other possible experiments which may be valuable to perform.

The full stick change in shear traction under combined P, σ loading along a straight line segment is given by

$$\Delta q(x) = \frac{\pi x}{4} \frac{\sigma_2 - \sigma_1}{P_2 - P_1} \left[p(x; P_2) - p(x; P_1) \right]$$

It is therefore possible to recreate a shear traction distribution under conditions of full stick by following load paths with specifically chosen gradients.

One such experiment could involve exactly recreating the shear traction distribution that arises after slip in the isosceles load path (i.e. the shear traction distribution at one of the corners of the load path), but under conditions of full stick. To do this we would follow a load path having two parts, the first being a straight line following the first part of the path taken during the isosceles experiments up to the point where the size of the contact is equal to the size of the stick zone in the slipping contact, the second being a curve with gradient defined by the no-slip condition under bulk tension loading,

$$\frac{d\sigma}{dP} = \frac{4\mu}{\pi a(P)}$$

The first part of the load path recreates the tangential surface displacements locked into the contact during the first step of the isosceles load path that are preserved when the contact slips, the second part of the load path recreates the shear traction and surface displacements that would arise in the isosceles load path due to slip. This load path is shown in figure 1, the contact is first loaded from (P_1, σ_1) to (P_2, σ_2) along a straight line, then is further loaded to (P_3, σ_3) along a curve defined by the frictional limit condition, recreating the shear traction distribution present at the bottom right corner of the isosceles path under full stick. In order for the contact to remain stuck the contact must be unloaded following the same path.

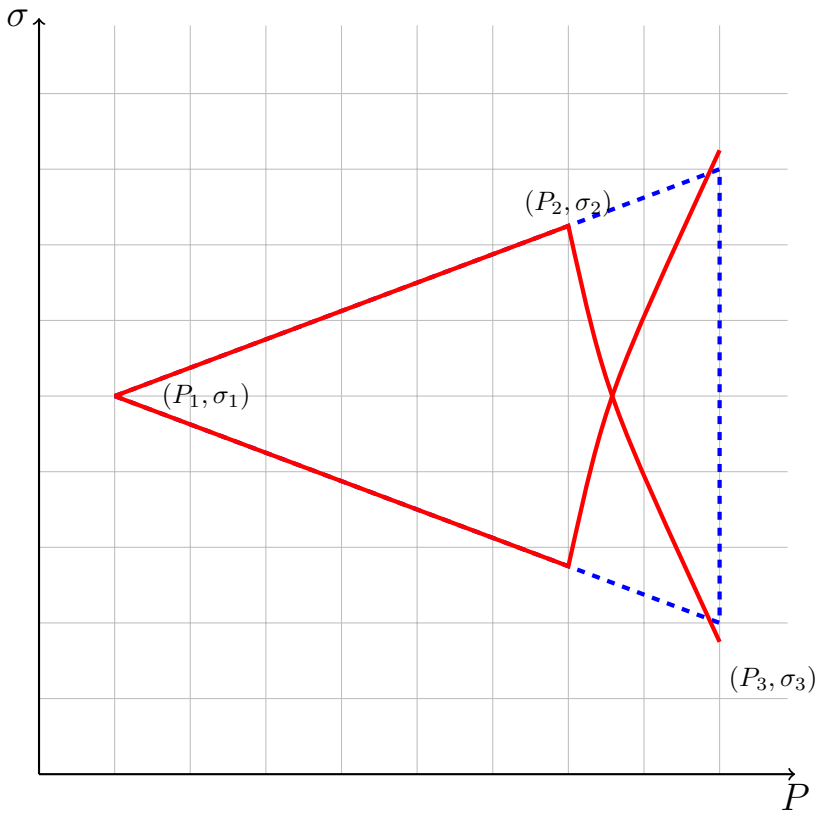


Figure 1: The form of load path required to recreate the shear traction distribution from the isosceles load path under conditions of full stick.

By comparing a contact following this load path to one following the isosceles load path it is possible to perform two experiments where the shear traction distribution at the maximum load point is the same, but where only one experiences slip. Using load paths of this form would therefore make it possible to investigate whether differences in fretting fatigue life when comparing slipping and stuck contacts are the result of differences in shear traction distribution, or whether they arise from the action of the slip.

10.2 Finding the Shear Traction Solution Under Conditions of Full Stick

Another area where there is potential for expansion involves alternate methods of finding the slip and shear traction behaviour of the contact. While the work, as presented, allowed for a variety of useful experiments to be designed and analysed it was somewhat restricted with regards to the contact geometries and load space it is possible to investigate. The papers included here consider the solution for a normal load – shear force loading with any contact geometry, and the solution for a normal load – bulk tension loading on a Hertzian geometry. While it is possible to design innovative load path based experiments within these constraints, as demonstrated in the included

papers, being able to study contacts under a combination of bulk tension and shear loading and with a wider range of geometries would open up a number of additional possibilities, both for experimental work and for being able to model contacts in prototypical engineering assemblies.

There are two methods of solving partial slip contact problems. The first, based on the Cattaneo-Mindlin solution, takes the fully sliding solution and applies a corrective term over the region which remains stuck. The second method involves finding the shear traction distribution under conditions of full stick, then using dislocations or some similar method to introduce slip into regions of the contact where the shear traction violates the frictional slip limit. The papers presented in this thesis are based around solutions using the first method. Use of the second method may expand the range of load paths that can be studied.

In order to use the dislocation based solution the shear traction distribution under conditions of full stick must be found. Hills and Davies [18] produced an incremental method of finding the shear traction distribution under combined normal, shear, bulk tension and moment loading, but only for the case where both edges of the contact are advancing, i.e. monotonically increasing load. In order to apply the method to load paths as described in this thesis the change in shear traction during a fully stuck unloading step would also be needed.

For an incomplete contact under a combination of normal force and shear force the solution when the normal force is reduced can be found by considering the surface displacements and horizontal equilibrium. Under conditions of full stick, points on the surface within the contact cannot move tangentially relative to each other once they come into contact, so that the relative tangential surface displacements within the region of the contact that remains after the load is reversed must therefore be the surface displacements that were locked into the contact at an earlier point within the loading step.

Given that we know the form of the relative surface displacements we can therefore calculate the shear traction distribution they imply. By inspection it can be seen that this is equivalent to the shear traction distribution at the point during the loading cycle where the contact has the same size as it had at the end of the unloading step. It is possible, however, for the applied shear force at the end of the unloading cycle to be different from the shear force at the equivalent normal load in the loading cycle. Since no slip is permissible the two surfaces cannot displace relative to each other. This implies that the solution for the additional shear traction term arising from the difference in the applied shear force is equivalent to the solution for a shear loaded fully stuck sharp edged punch, i.e. a shear traction distribution with square root singularities at each end.

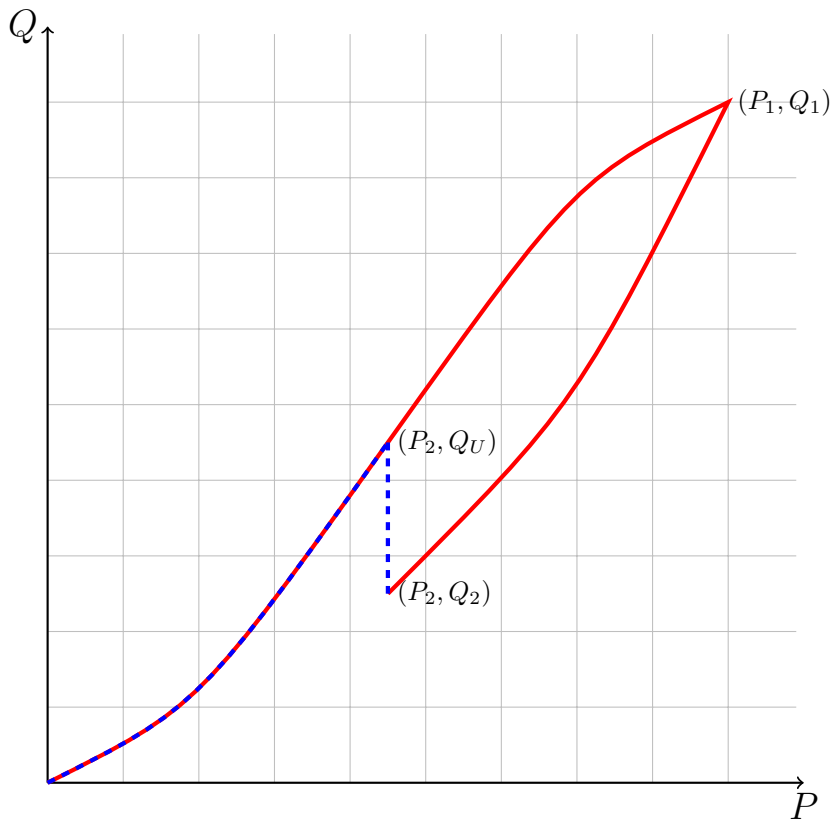


Figure 2: Under conditions of full stick loading first to (P_1, Q_1) then unloading to (P_2, Q_2) is equivalent to loading along the fist to (P_2, Q_U) then unloading at a fixed normal force to (P_2, Q_2)

Arguments following a similar line apply to the study of a fully stuck contacts loaded with a combination of normal forces and bulk tensions, the surface displacements from the loading stage of the load cycle are only preserved over the region of the contact that remains following unloading. The tangential surface displacement distribution within the contact is therefore the same as the tangential surface displacement from the loading part of the cycle, at the normal load the contact is unloaded to, allowing the shear traction distribution to be found. An additional shear traction distribution will arise due to the difference in bulk tension at the same normal load during loading and unloading, this will likely be given by the solution for a fully stuck punch loaded with bulk tension, i.e. a singular at each end shear traction distribution.

When considering problems including a combination of Normal force, Shear force and bulk tension undergoing unloading it is possible that the arguments from the bulk tension alone and shear force alone load path can be applied, with the relative surface displacements within the contact being preserved from the loading step. The arguments for finding the additional term for the change in applied loads needs revision, however as it must account for both a change in applied bulk tension, in addition to a change in shear force and the requirement for equilibrium.

The addition of a moment to the problem adds extra complications in that it is possible for one edge of the contact to advance while the other recedes. Finding the behaviour of the contact when unloaded with a varying moment would therefore require significant work.

11 Conclusion

Experimental investigation remains an important way of exploring fretting fatigue and predicting the failure of components. The papers presented here discuss a range of work related to the analysis of fretting fatigue experiments, produced with the aim of improving experimental practice.

In the paper 'A Comparison of the State of Stress at an Incomplete Fretting Contact Edge with a Crack Tip' an investigation was performed into whether analogies existed between the state of stress at a crack tip and the state of stress at the edge of a fretting contact. Such analogies have been previously proposed in the literature and offer a potential method of modelling the failure of contacts where a significant amount of plasticity is present. It was shown that, in order for the plastic zone around the edge of the contact to resemble the plastic zone at the edge of a crack tip, a coefficient of friction much greater than 1 would be required, a situation that does not occur using realistic combinations of materials and surface finishes. The analogy is therefore shown not to hold for the situation being investigated, implying that modelling the edge of contact as a shear loaded crack would be inappropriate.

The paper 'Measurement of Moment Coupling in Fretting Fatigue Experiments' described a method of measuring the magnitude of moment coupling present in fretting fatigue experiments using digital image correlation, moment coupling being the generation of unwanted moments due to the design of the test apparatus resulting in lever arms being present in the load path for the shear force. It was shown, for our test rig, that the coupled moment varies linearly with applied shear force and is essentially independent of the applied normal load. It was shown that, by varying the normal load, it is possible to cancel out the effect of the moment at one edge of the contact. An iterative solver was used to find the load paths required and digital image correlation was used to verify that the moment had been cancelled out at one edge of the contact.

Building on the work on the measurement of moment coupling, the paper 'Flat and rounded contacts - modelling the effect of a moment with application to fretting fatigue tests' discusses a method of modelling the effect of a moment on a flat and rounded contact in an asymptotic framework. It was shown how, by modelling the punch as sharp ended, a very simple expression for equivalent pairs of Pressure-Moment loading can be found, which can be easily applied in either experimental design or experimental control. A study was performed over a range of geometries

and load conditions, and the results were shown to apply well over a wide range of conditions, even when the corner radius is large compared to the size of the flat or where the moment loads are very large. The results found can be used for a range of purposes, it is possible to use this method to either remove a coupled moment, or to simulate the effect of a moment on a test rig that does not have independent moment control.

'Fretting Fatigue Experiments with Single Crystal Pads' describes a series of experiments designed to investigate the effect of crystal orientation in single crystal pads on the fretting fatigue life of a polycrystaline specimen. Previous experimental investigation had indicated that the orientation of the crystal structure played a crucial, perhaps dominant, role in determining the life of such a contact, with the results by Sarsfield [28] and Fleury [29] showing significant variance in life between tests using different single crystal pads. The experiments performed in this paper failed to show any correlation between the orientation of the crystal structure and the resulting life of the contact, it was noted, however, that pads manufactured from the same specimen of single crystal material tend to show similar fatigue lives.

The first part of the load path work is contained in the paper 'Half-Plane Contact Problems in partial Slip with varying Normal and Tangential Loads', which discusses the effect of load path on the behaviour of contacts under combined normal load-shear loading. A review of various solutions was given, and it was shown how by varying the order in which the loads are applied it is possible to create load paths where the remotely applied loads are the same, but the slip behaviour and shear traction distribution varies. While it is not practical to use these load paths experimentally this paper presents a number of ideas and principles which were applied to more experimentally feasible load paths in the following papers.

The paper 'Frictional Half Plane Contacts Subject to Varying Normal Load and Bulk Tension Under Various Load Paths with Application to Fretting Fatigue Experiments' built on the work in the previous paper, instead considering load paths using combinations of bulk tension and normal force loading. It was shown how varying the load path can result in contacts having the same externally applied loads at the ends of the load cycle, but differing slip and shear traction behaviour. A number of load paths having novel features with application to fretting fatigue tests were derived, such as comparing slipping contacts to those with no slip, varying the slip zone sizes when moving between the same points in load space, and having a load cycle where slip occurs in only one direction. Each of these load paths was illustrated with plots of the shear traction distribution at various points around the cycle.

The final paper, 'The State of Stress in Fretting Contacts Under Varying Load Paths', directly extends the work performed in the previous paper, 'Frictional Half Plane Contacts Subject to

Varying Normal Load and Bulk Tension Under Various Load Paths with Application to Fretting Fatigue Experiments'. Muskhelishvili complex potentials were used to find the full state of stress in both contacting bodies, and a number of properties were derived. The stress parallel to the surface, slip displacements and dissipated energy were all calculated, and it was demonstrated how via careful design of experimental load paths it is possible to match certain parameters while varying others. The isosceles load paths in particular are shown to make it possible to create load paths which slip in only one direction, which also have the property that reversal of the direction of loading does not change the slip displacements or dissipated energy, and does not drastically change the range of stress parallel to the surface.

Together these papers represent a body of work covering a number of aspects of fretting fatigue experiments, and provide several refinements to the process of designing experiments. The work presented offers a number of new possibilities for investigating fretting fatigue and related phenomena.

References

[1] J. R. Barber, *Contact mechanics*. Springer, 2018.

[2] H. Hertz, "Ueber die berührung fester elastischer körper," *Journal für die reine und angewandte Mathematik*, vol. 92, pp. 156–171, 1881.

[3] A. Flamant *et al.*, "Sur la répartition des pressions dans un solide rectangulaire chargé transversalement," *CR Acad. Sci. Paris*, vol. 114, no. 1892, pp. 1465–1468, 1892.

[4] J. Boussinesq, *Application dès potentiels a l'étude de l'équilibre et du mouvement des solides élastiques*. Gauthier-Villars, 1885.

[5] V. Mossakovskii, "Application of the reciprocity theorem to the determination of the resultant forces and moments in three-dimensional contact problems," *PMM*, vol. 17, pp. 477–482, 1953.

[6] M. R. Moore and D. A. Hills, "Extending the mossakovskii method to contacts supporting a moment," *Journal of the Mechanics and Physics of Solids*, vol. 141, p. 103989, 2020.

[7] C. Cattaneo *et al.*, "Sul contatto di due corpi elastici: distribuzione locale degli sforzi," *Rend. Accad. Naz. Lincei*, vol. 27, no. 6, pp. 342–348, 1938.

[8] R. D. Mindlin and H. Deresiewicz, "Elastic spheres in contact under varying oblique forces," *Journal of applied mechanics*, vol. 20, no. 3, pp. 327–344, 1953.

[9] M. Ciavarella, "The generalized cattaneo partial slip plane contact problem. i—theory," *International Journal of solids and structures*, vol. 35, no. 18, pp. 2349–2362, 1998.

[10] J. Jager, "A new principle in contact mechanics," *Journal of applied mechanics*, vol. 120, no. 4, pp. 677–864, 1998.

[11] J. Barber, M. Davies, and D. Hills, "Frictional elastic contact with periodic loading," *International Journal of Solids and Structures*, vol. 48, no. 13, pp. 2041–2047, 2011.

[12] R. Fleury, D. Hills, R. Ramesh, and J. Barber, "Incomplete contacts in partial slip subject to varying normal and shear loading, and their representation by asymptotes," *Journal of the Mechanics and Physics of Solids*, vol. 99, pp. 178–191, 2017.

[13] D. Nowell and D. Hills, "Mechanics of fretting fatigue tests," *International Journal of Mechanical Sciences*, vol. 29, no. 5, pp. 355–365, 1987.

[14] M. Ciavarella and G. Macina, "New results for the fretting-induced stress concentration on hertzian and flat rounded contacts," *International Journal of Mechanical Sciences*, vol. 45, no. 3, pp. 449–467, 2003.

[15] C. Navarro, A. Mugadu, D. Hills, and J. Dominguez, "The influence of underlying tension on partial slip in complete and nearly complete contacts," *International journal of mechanical sciences*, vol. 45, no. 4, pp. 757–773, 2003.

[16] R. Ramesh, J. Barber, and D. Hills, "Plane incomplete contact problems subject to bulk stress with a varying normal load," *International Journal of Mechanical Sciences*, vol. 122, pp. 228–234, 2017.

[17] D. Spence, "An eigenvalue problem for elastic contact with finite friction," in *Mathematical Proceedings of the Cambridge Philosophical Society*, vol. 73, pp. 249–268, Cambridge University Press, 1973.

[18] D. Hills, M. Davies, and J. Barber, "An incremental formulation for half-plane contact problems subject to varying normal load, shear, and tension," *The Journal of Strain Analysis for Engineering Design*, vol. 46, no. 6, pp. 436–443, 2011.

[19] M. Williams, "Stress singularities resulting from various boundary conditions in angular corners of plates in extension," *Journal of applied mechanics*, vol. 19, no. 4, pp. 526–528, 1952.

[20] J. Dundurs and M. Lee, "Stress concentration at a sharp edge in contact problems," *Journal of elasticity*, vol. 2, no. 2, pp. 109–112, 1972.

[21] M. Comninou, "Stress singularity at a sharp edge in contact problems with friction," *Zeitschrift für angewandte Mathematik und Physik ZAMP*, vol. 27, pp. 493–499, 1976.

[22] A. Mugadu, D. Hills, and L. Limmer, "An asymptotic approach to crack initiation in fretting fatigue of complete contacts," *Journal of the Mechanics and Physics of Solids*, vol. 50, no. 3, pp. 531–547, 2002.

[23] D. Dini and D. A. Hills, "Bounded asymptotic solutions for incomplete contacts in partial slip," *International journal of solids and structures*, vol. 41, no. 24-25, pp. 7049–7062, 2004.

[24] D. Dini, A. Sackfield, and D. Hills, "Comprehensive bounded asymptotic solutions for incomplete contacts in partial slip," *Journal of the Mechanics and Physics of Solids*, vol. 53, no. 2, pp. 437–454, 2005.

[25] A. Giannakopoulos, T. Lindley, and S. Suresh, "Aspects of equivalence between contact mechanics and fracture mechanics: theoretical connections and a life-prediction methodology for fretting-fatigue," *Acta materialia*, vol. 46, no. 9, pp. 2955–2968, 1998.

[26] A. Giannakopoulos, T. Lindley, S. Suresh, and C. Chenut, "Similarities of stress concentrations in contact at round punches and fatigue at notches: implications to fretting fatigue crack initiation," *Fatigue & fracture of engineering materials & structures (Print)*, vol. 23, no. 7, pp. 561–571, 2000.

[27] L. Chambon and B. Journet, "Modelling of fretting fatigue in a fracture-mechanics framework," *Tribology international*, vol. 39, no. 10, pp. 1220–1226, 2006.

[28] H. Sarsfield, "Fretting fatigue tests on udimet 720li with single crystal cmsx-4 pads," UTC Report 250, University of Oxford, 2008.

[29] R. Fleury, *Investigation of fretting fatigue in turbine fir tree blade to disc joints at high temperature*. PhD thesis, University of Oxford, 2015.

[30] X. Huang, T. Gibson, M. Zhang, and R. Neu, "Fretting on the cubic face of a single-crystal ni-base superalloy at room temperature," *Tribology International*, vol. 42, no. 6, pp. 875–885, 2009.

[31] R. Fleury, R. Paynter, and D. Nowell, "The influence of contacting ni-based single-crystal superalloys on fretting fatigue of ni-based polycrystalline superalloys at high temperature," *Tribology International*, vol. 76, pp. 63–72, 2014.